# Distinct focal adhesion protein modules control the adhesion site segregation and cell migration behavior

Technische Universität Dortmund
Fakultät für Chemie

Dissertation

Zur Erlangung des akademischen Grades eines
Doktors der Naturwissenschaften
(Dr. rer. Nat.)

vorgelegt von
Master of Biochemistry
aus Lahore, Pakistan

Sarah Imtiaz

November 2017

Erstgutachter: Prof. Dr. Philippe Bastiaens
Zweitgutachter: PD Dr. Leif Dehmelt

# Summary

Cell-matrix adhesion sites are multi-protein complexes, which regulate cell adhesion and migration. These complex processes require a tightly regulated organization of the adhesion sites and cytoskeleton. Contrary to the extensively studied assembly of focal adhesions (FA), there is little known about the segregation of adhesion sites and their functional relevance in cell motility. A multi-scale combinatorial RNAi screen was employed to address two important questions: how do core FA proteins mediate the adhesion segregation process and how do they regulate the migration behavior of the cell?

The localization of tensin-1 is partially mediated by its interaction with integrins whereas phosphorylation of tensin-1 and cytoskeletal tension is involved in the fibrillar adhesion (FB) complex formation. However, the exact role of focal adhesion proteins in this process remains to be identified. Based on fixed cell imaging, we recognized distinct proteins involved in the FA segregation process. p130CAS in association with tln1, VASP, α-actinin-1 and zyxin functionally relates with the well-known signaling protein FAK to regulate the localization of tensin-1 in FA. In addition to the known function of actin in mediating the binding with tensin-1, our studies identified a new set of actin-regulatory proteins (VASP, α-actinin-1, zyxin) involved in the recruitment of tensin-1 in FA. Structural proteins including kindlin-2, ILK and talin-1 in combination with other FA proteins modulate the translocation of tensin-1 to form FB. The results of this study provide a foundation for further characterization of molecules putatively linking core FA proteins to the adhesion segregation process.

Two integrin binding proteins, talin-1 and kindlin-2, are independently implicated in the regulation of cell survival, proliferation and migration. Co-depletion of talin-1 and kindlin-2 adversely affected these cellular processes as compared to the individual knockdowns of these proteins. These adverse effects included failure of adhesion sites assembly, drastic reduction in cell survival and proliferation as well as impaired motility.

Cell-matrix adhesions, in cooperation with Rho-Rac signaling, mediate different modes of cell migration. Using a live-cell imaging screening, the missing FA

components involved in the regulation of modes of migration in a two-dimensional (2D) flat surface were identified. Co-depletions of signaling proteins (FAK, CAS) resulted in a peripheral organization of FA and fast migrating cells, which failed to form cellular protrusions. This mode supported the amoeboid type of migration. Impaired migration upon depletion of structural proteins (talin-1, kindlin-2 and ILK) gave rise to heterogeneous cellular phenotypes: (i) immobile, round shaped cells with several FA in contrast to (ii) elongated, randomly moving cell with few FA. In contrast, elongated cells, which migrate quickly, generated blunt protrusions and few FA. This lamellipodia-based locomotion was specifically associated with the depletion of actin-regulatory proteins (α-actinin-1, zyxin and VASP).

Notably the same set of proteins, which were involved in the adhesion segregation process, were also associated with specific modes of migration. This suggests a role for FB in shaping cell motility. Failure to form FB complexes is linked to enhanced cell migration (amoeboid and lamellipodial modes), whereas the inability to translocate tensin-1 is related to impaired migration (confined mode). Taken together, this study has shown that FA are composed of different functional modules that distinctly control different stages of the adhesion transformation process and the migration behavior. Furthermore, we found that functional modules of canonical FA proteins are related to their known functional and spatial organization in compartments of focal adhesions.

# Zusammenfassung

Zell-Matrix-Adhäsionsstellen sind Multi-Protein-Komplexe, welche die Zelladhäsion und -migration regulieren. Diese komplexen Prozesse erfordern eine streng regulierte Organisation der Adhäsionsstellen und des Zytoskeletts. Im Gegensatz zu der ausgiebig untersuchten Anordnung fokaler Adhäsionen (FA) ist über die Segregation von Adhäsionsstellen und ihre funktionelle Relevanz in der Zellmotilität wenig bekannt. Ein kombinatorisches RNAi-Screening, welches sich auf zehn FA-Proteine und deren 45 paarweisen Kombinationen konzentrierte, wurde verwendet, um zwei wichtige Fragen zu beantworten: Wie vermitteln FA-Kernproteine den Adhäsionssegregationsprozess und wie regulieren sie das Zellmigrationsverhalten?

Die Phosphorylierung von Tensin-1 vermittelt die fibrilläre Adhäsion (FB) - Komplexbildung, während die Spannung des Zytoskeletts an der Translokation von Tensin-1 zu FB beteiligt ist. Der exakte Modulator dieses Prozesses ist jedoch noch nicht identifiziert. Durch Mikroskopie fixierter Zellen haben wir verschiedene Proteine identifiziert, die am FA Segregationsprozess beteiligt sind. CAS in Verbindung mit Tln1, VASP, α-Aktinin-1 und Zyxin steht funktionell mit dem bekannten Signalprotein FAK, welches die FB-Komplexbildung vermittelt, in einer Tensin-1-Phosphorylierungs-abhängigen Weise in Beziehung. Zusätzlich zu der bekannten Funktion von Actin bei der Vermittlung der Bindung von Tensin-1 an FAs haben wir einen neuen Satz von Aktin-regulatorischen Proteinen (VASP, α-Actinin-1, Zyxin) identifiziert, welche Tensin-1 in die FA rekrutieren. Strukturproteine, einschließlich Kindlin-2, ILK und Talin-1 in Kombination mit anderen FA-Proteinen wurden als Modulatoren der Tensin-1-Translokation zu FB identifiziert. Die Ergebnisse dieser Studie liefern eine Grundlage für die weitere Charakterisierung von Molekülen, welche möglicherweise die Kern-FA-Proteine mit dem Adhäsionssegregationsprozess verknüpfen.

Zwei Integrin-bindende Proteine, Talin-1 und Kindlin-2, sind unabhängig von einander an der Regulation des Überlebens, der Proliferation und der Migration von Zellen beteiligt. Im Gegensatz zu den separaten *Knock-downs* dieser Proteine, beeinträchtigte der gleichzeitige *Knock-down* die oben genannten zellulären Prozesse.

Die beobachteten Effekte waren die Beeinträchtigung der Bildung von Adhäsionsstellen, drastische Reduktion des Zellüberlebens / der Proliferation und eine beeinträchtigte Motilität.

Der Rho-Rac-Signalweg steuert in Kooperation mit Zellmatrix-Adhäsionen verschiedene Arten der Zellmigration. Mithilfe eines *Live-Cell*-Mikroskopiescreenings wurden weitere FA-Proteinen identifiziert, die an der Regulation von Migrationsmoden in einer zweidimensionalen, flachen Oberfläche beteiligt sind. Der gleichzeitige *Knock-Down* von Signalproteinen (FAK, CAS) führten zu einer peripheren Organisation von FA in schnell wandernden Zellen, die keine zellulären Fortsätze bilden konnten, ein Modus, der die amöboidartige Migration unterstützt. Im Gegensatz dazu erzeugen schnell migrierende, langgestreckte Zellen stumpfe Fortsätze und wenige FA. Diese Lamellopodia-basierende Fortbewegung war spezifisch mit dem *Knock-down* von Aktin regulatorischen Proteinen (α-Actinin-1, Zyxin und VASP) assoziiert. Beeinträchtigte Migration bei dem *Knock-down* von Strukturproteinen (Talin-1, Kindlin-2 und ILK) führte zu heterogenen zellulären Phänotypen: (i) Immobile, runde Zellen mit mehreren FA im Gegensatz zu (ii) verlängerten, sich zufällig bewegenden Zellen mit wenigen FA.

Interessanterweise waren dieselben Proteine, die an dem Adhäsionssegregationsprozess beteiligt waren, auch mit spezifischen Migrationsmoden assoziiert, was die Rolle von FB bei der Zellmotilität zeigt. Die fehlende Bildung von FB-Komplexen ist mit einer verstärkten Zellmigration (amöboide und lamellipodiale Modi) verbunden, während die Beeinträchtigung der Tensin-1 Translokation, mit der beeinträchtigten Migration zusammenhängt (eingeschränkter Modus). Diese Arbeit hat gezeigt, dass FA aus verschiedenen funktionalen Modulen zusammengesetzt sind, welche die unterschiedlichen Stadien des Adhäsions-Transformationsprozesses und des Migrationsverhaltens steuern. Darüber hinaus fanden wir, dass funktionelle Module von kanonischen FA-Proteinen mit ihrer bekannten funktionellen und räumlichen Organisation in Kompartimenten fokaler Adhäsionen verwandt sind.

# Table of contents

# 1. Introduction

## 1.1 Cell-matrix adhesion sites

The extra cellular matrix (ECM) serves as a substrate for cell attachment and plays an important role in defining the cell behavior[6,7]. The complex ECM is composed of several proteins like collagens, fibronectin, vitronectin and growth factors[8]. The precise organization of these components governs the functions of ECM. Slight changes in the molecular contents of ECM result in different cell-matrix interactions and cellular phenotypes[6]. ECM conveys environmental signals to the cells, indicating its important role in modulating cellular processes such as morphogenesis, migration, embryogenesis, differentiation and cell attachment[9].

Attachment of the cell to the ECM is initiated by integrins. Integrins are the major cell surface transmembrane receptors present in all metazoans[10] and are composed of non-covalently coupled heterodimers of 18α and 8β subunits. The selective combinations of these subunits result in the formation of 24 distinct integrin receptors[10]. Extracellular domain binds with ECM ligands whereas intracellular domain binds with adhesion site (AS) proteins and actin cytoskeleton, thereby integrin mediates downstream signaling pathways[11]. In addition to integrins, transmembrane proteins such as growth factor receptors, proteoglycans, tetraspannins and metalloproteases are also involved in the organization of adhesion sites[12].

Integrins provide a central mechanism to integrate the intracellular and extracellular compartments by cell-matrix adhesion sites[9,13]. There are two major signaling modes of integrins as shown in Figure 1.1. In the first mode also referred as outside-in signaling, integrins convey signals into the cell by transferring information about microenvironment, location and composition of the matrix. For example, exogenous tension generated by the matrix rigidity is transmitted inside of the cell by the integrin receptor. This signaling mode takes place during the processes such as cell migration, growth and survival. The second mode of signaling is termed as inside-out signaling in which intracellular signals stimulate changes in integrins. The endogenous tension produced by the actin cytoskeleton arrangement and actomyosin contractility regulates the interaction of integrins with ECM and directly or indirectly

modifies the activation of integrin receptors[13]. Overall changes in tension level regulate inside-out and outside-in signaling. In the current work, I examined the perturbation of adhesion site proteins that mainly affect the inside-out signaling.

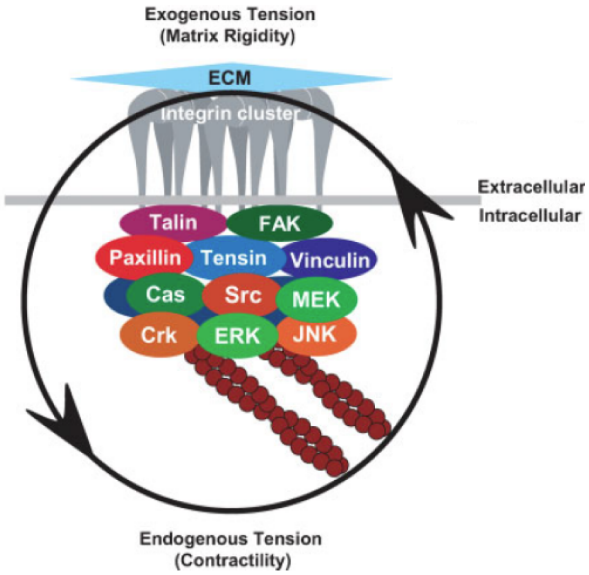


**Figure 1.1 Different modes of integrin signaling.** Integrin receptors are responsible for bi-directional transfer of informations between the extracellular and intracellular compartments of the cell. This figure is acquired from Berrier and Yamada, 2007[9].

Cell-matrix adhesion sites were first identified in 1971 as electron-dense plaques in the plasma membrane of the cultured cells[14]. Soon after identification, the question arose whether they are merely artificial structures or exist *in-vivo* as well. Later on, immunoelectron microscopy discovered focal contacts in epidermis of the cells and validated their presence *in-vivo*[15]. Subsequently, prominent adhesions sites were visualized in a variety of cells[16-18]. The possibility of tagging fluorescent proteins with cDNA led to the identification of numerous components of adhesion sites[19].

The molecular complexity of adhesion sites is larger than what we know to-date. Many aspects such as unknown components, post-translational modifications, proteolytic cleavage, splice variants and conformational changes feature this complexity[19]. Approaches ranging from traditional biochemical assays to microscopic studies and functional genomics identified several protein-protein interactions of the integrin adhesome. By combining the data from these approaches, integrin adhesome was delineated with 90 core components that are physically present in adhesion sites

and 66 peripheral components which interact with core components thus affecting the activity of integrin adhesome[20]. Recently a core consensus adhesome including 60 proteins was proposed, based on the combination of mass-spectometeric analysis of integrin adhesion complexes and literature curated data. The core consensus adhesome is comprised of four theoretical signaling modules: (i) α-actinin–zyxin–VASP (ii) talin–vinculin, (iii) FAK–paxillin (iv) ILK–PINCH–kindlin as major units of the cell adhesion network[21].

## 1.2 Types of cell-matrix adhesion sites

There are three types of commonly observed adhesion sites in the cells that spread on rigid substrates: (i) Nascent adhesions (ii) Focal adhesions and (iii) Fibrillar adhesions[22]. Distinguishing features of adhesion sites are summarized in Table 1.1. **Nascent adhesions (NA)** or focal complexes are the best-studied classical adhesion sites. Nascent adhesions are transient dot-like structures which interact with matrix and provide the primary cell attachment[22]. They are rapidly formed at front of the cell in filopodia and lamellipodia during migration[23].

| Property/ structure | Focal complexes | Focal adhesions | Fibrillar adhesions |
|---|---|---|---|
| **Location** | Edge of lamellipodium | Cell periphery | Central region of the cells |
| **Morphology** | Dot-like | Elongated, oval | Fibrillar or beaded |
| **Size (long axis)** | 1 μm | 2 – 5 μm | Variable 1 – 10 μm |
| **Typical constituents** | Paxillin<br>Vinculin<br>Tyrosine-phosphorylated proteins | $\alpha_v$ integrin<br>Paxillin<br>Vinculin<br>α-actinin<br>Talin<br>FAK | $\alpha_5$ integrin<br>Tensin |
| **Induced by** | Rac | Rho | Rho(?) |

**Table 1.1 Characteristic features of three distinct adhesion sites.** This table is acquired from Geiger et al., 2001[22].

**Focal adhesions (FA)** are elongated or oval shaped structures, located at the cell periphery (Table 1.1). FA mediate the strong attachment with the substrate, mainly via $\alpha_v\beta_3$ integrins and proteins such as talin-1[24], connects it to the actin microfilament bundles. Depending on the force experienced by the integrins and the

substrate rigidity, focal adhesions transform into fibrillar adhesions. The adhesion sites formed by $\alpha_v\beta_3$ integrins attach primarily with ECM protein vitronectin while the adhesion sites formed by $\alpha_5\beta_1$ integrins associate with the fibronectin. Each of them attach with a specific proteins cluster associated with the actin cytoskeleton and is regulated by the contractility driven by myosin-II[25]. Due to the rigid substrate provided by vitronectin, $\alpha_v\beta_3$ integrins experience more force generated by actin cytoskeleton resulting in the recruitment of more adhesion site proteins and maturation of focal adhesions. Integrins $\alpha_5\beta_1$ most commonly bind with fibronectin, which provide flexible and movable substrate. In this case, the force experience by $\alpha_5\beta_1$ integrins results in its translocation to the cell center. Tensin also translocates with $\alpha_5\beta_1$ integrins and takes part in fibrillar adhesions formation[26] (Figure 1.2).

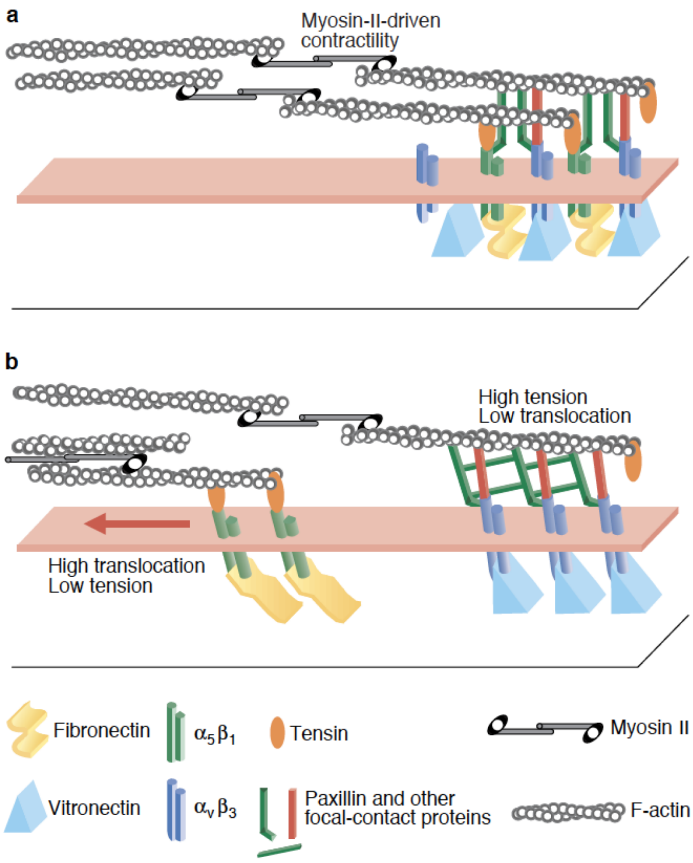


**Figure 1.2 Segregation of cell-matrix adhesion sites.** (a) The adhesion sites formed by αvβ3 and α5β1 integrins attach with ECM proteins vitronectin and fibronectin, respectively. (b) The soft substrate of α5β1 integrins experiences less force generated by cytoskeleton and translocates to the cell center. In contrary, the rigid substrate of αvβ3 integrins experiences strong forces and forms mature focal adhesions at cell periphery. This figure is acquired from Zamir et al., 2000[26].

**Fibrillar adhesions (FB)** are dot-like or elongated structures ranging from 1-10 µm (Table 1.1). Intracellular tension is the critical regulator for the formation, localization and signaling of FA and FB. Focal adhesions are comprised of higher levels of phosphorylated proteins such as FAK and paxillin. They are comprised of actin-binding proteins such as vinculin and α-actinin. Conversely, fibrillar adhesions have less phosphorylated FAK and paxillin but higher level of tensin. Owing to their specific molecular composition, both adhesion types give rise to different signaling pathways designated as signal A and signal B in Figure 1.3.

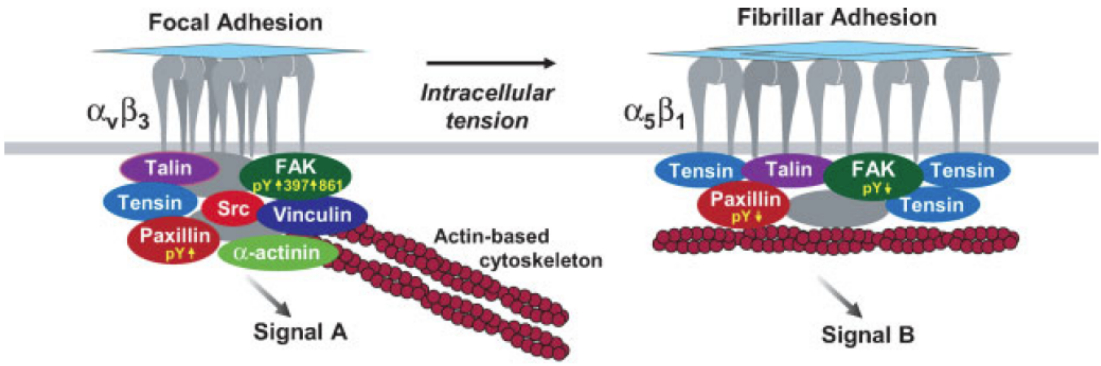


**Figure 1.3 A comparison between focal and fibrillar adhesions.** Integrins αvβ3 adhere to the rigid substrate and form FA with higher level of phosphorylated proteins. FB are produced due to α5β1 integrins with higher levels of tensin protein. The particular molecular composition of both adhesion sites plays an important role in activating different signaling pathways as illustrated. This figure is acquired from Berrier and Yamada, 2007[9].

## 1.3 Assembly and maturation of cell-matrix adhesion sites

During migration, cells develop cellular protrusions known as lamellipodia or filopodia due to the extending actin network[27]. Rho-GTPase such as Rac1 or Cdc42 and phosphatidylinositol (3,4,5)-trisphosphate (PIP3)[28] create a cellular protrusion (lamellipodium) linked with the extending actin network and the protrusion is stabilized by nascent adhesions[29]. The Arp2/3 complex induces further branching of actin to formulate the actin cytoskeleton which induces the extension of the lamellipodia[30,31]. Interestingly, initiation of nascent adhesions is mediated by crosslinking of actin and integrins instead of motor activity of the myosin. Depending on the actomyosin contractility, nascent adhesions either develop into FA or disassembled rapidly (turnover). RhoA signaling is involved in the disassembly of mature FA in the rear edge of the cell[28].

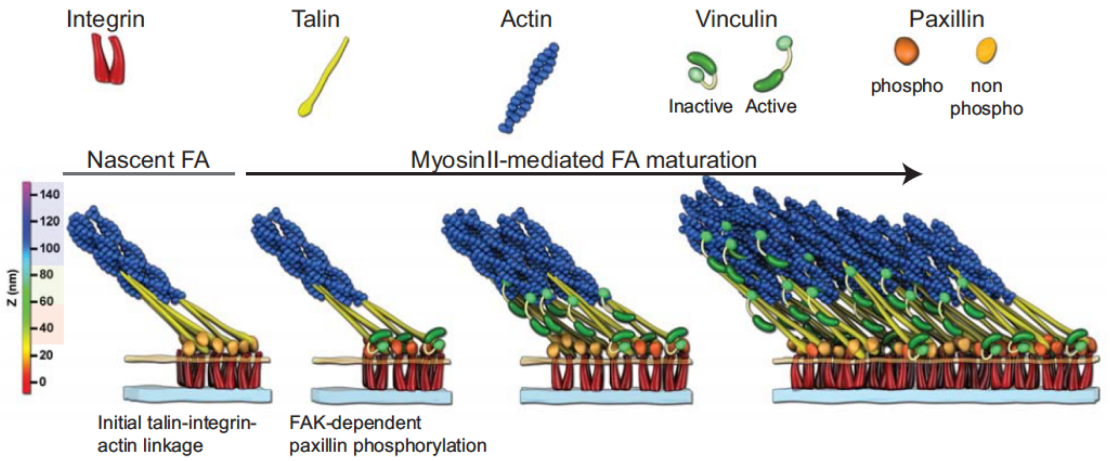


**Figure 1.4 Maturation of adhesion sites.** The initial link of talin-integrin-actin formulates the nascent adhesions. Paxillin is localized to the nascent adhesion. Afterwards, FAK-dependent phosphorylation recruits more paxillin. FAK and paxillin offer interaction sites for other adaptor proteins whereas myosin-II-mediated actomyosin contractility promotes the maturation of nascent adhesion into focal adhesions. The model of maturation of adhesion sites is adopted from Case et al., 2015[32].

Maturation of NA into focal adhesion is a multistep process (Figure 1.4), involving the initial talin-integrin-actin link, combined activity of Rho-GTPases (including Rho, Rac and Cdc42)[33], FAK-dependent recruitment of phosphorylated paxillin[34], talin-induced recruitment of vinculin[35], mechanical state of the underlying actin cytoskeleton and myosin-II-mediated actomyosin contractility[36-38]. Theodosiou *et al.,* 2016 have shown the co-operative function of kindlin-1/2 and talin-1/2 to activate the integrins in fibroblasts[2]. Talin and vinculin are essential adaptor proteins to facilitate the force transduction in adhesion sites[35]. The actin fibers develop into a dense network, facilitated by the axial organization of VASP and zyxin[39] and by the interaction of α-actinin-actin[40]. Focal adhesions typically disrupt within 10-20 minutes or transform into fibrillar adhesions[26].

## 1.4 Disassembly of cell-matrix adhesion sites

The disassembly of adhesion sites is observed in two different scenarios; (i) disruption of mature focal adhesions in the rear edge of the cell and (ii) turnover of nascent adhesions at the front of protruding lamellipodium. In both cases, disassembly is facilitated by changing cytoskeletal forces and tyrosine phosphorylation events in FA[41]. Disruption of mature focal adhesions in migrating cells is synchronized process and is reviewed by Broussard *et al.*, 2008[42]. Contrary to the very well-known

mechanism of focal adhesion assembly, there is not even one complete model that explains the disassembly of focal adhesions. However, there are factors such as Rho GTPases[43], microtubules[44] and calpain proteases[45] which are known to regulate the disassembly in mature focal adhesions.

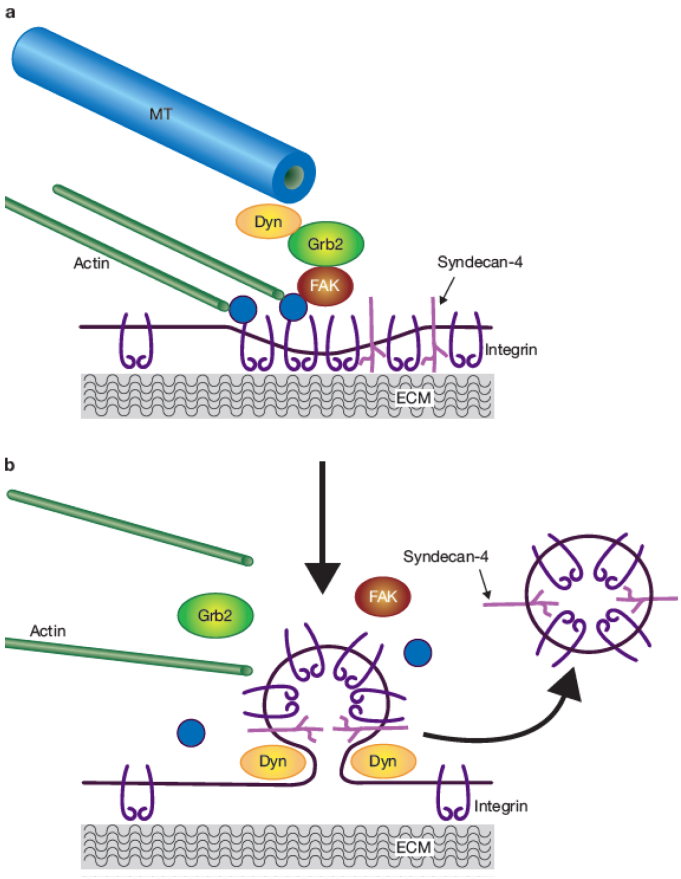


**Figure 1.5 Microtubule-induced disassembly of focal adhesions.** (a) A microtubule is represented, locally targeting a focal adhesion. The blue circles depict the integrin adhesome, connecting to the integrins and actin cytoskeleton. Microtubule-induced disassembly is facilitated by the combined action of FAK and dynamin with the help of adaptor protein Grb2. (b) The proposed disassembly of FA is due to the dynamin localization at the collar of endocytic vesicle, disintegration of actin (green fibers) and adhesion site plaque proteins (blue circles). The vesicle triggers the disassembly of focal adhesion structure, which leads to the integrins internalization. This model is adopted from Burridge, 2005[46].

Microtubules negatively regulate the cell contractility by indirectly sequestering the signaling molecules in the cytoplasm, thereby triggering the dissociation of focal adhesions[47]. Kaverina and colleagues showed that microtubules-dependent local delivery of relaxing factors instigates the disassembly of FA by inhibition of Rho GTPases and actomyosin contractility[48]. Furthermore, Ezratty *et al.,* 2005 elucidated the combined effect of microtubules and endocytosis in disruption of

adhesion sites, involving FAK, Grb2 and dynamin in Rac and Rho independent-manner[49] as shown in Figure 1.5. The endocytic vesicle resulted in the localized removal of integrin receptors from the membrane, causing the dissociation of actin filaments and plaque proteins (Figure 1.5). Calpain proteases suggest another possible mechanism to destabilize the FA by proteolytic cleavage of FA proteins[50] such as $\beta_3$-integrin[51], FAK[52] and talin[53].

## 1.5 Nano scale organization of focal adhesions

Super-resolution fluorescence microscopy revealed the nanoscale architecture and axial positioning of proteins in focal adhesions[24,54] (Figure 1.6). The nanoscale architecture implies the significance of highly organized arrangement of the proteins to build a functional focal adhesion unit. Kanchanawong *et al*., 2010 demonstrated that focal adhesions are orthogonally separated from integrins and actin by approximately 40 nm. The core region of FA have different layers: (i) signaling layer includes paxillin and FAK; (ii) force transduction layer comprises the talin and vinculin and (iii) the actin-regulatory layer contains the vasodilator-stimulated phosphoprotein (VASP), zyxin and α-actinin (Figure 1.6). In the current study, proteins from different signaling layers were selected to correlate their role with their position-specific function in FA.

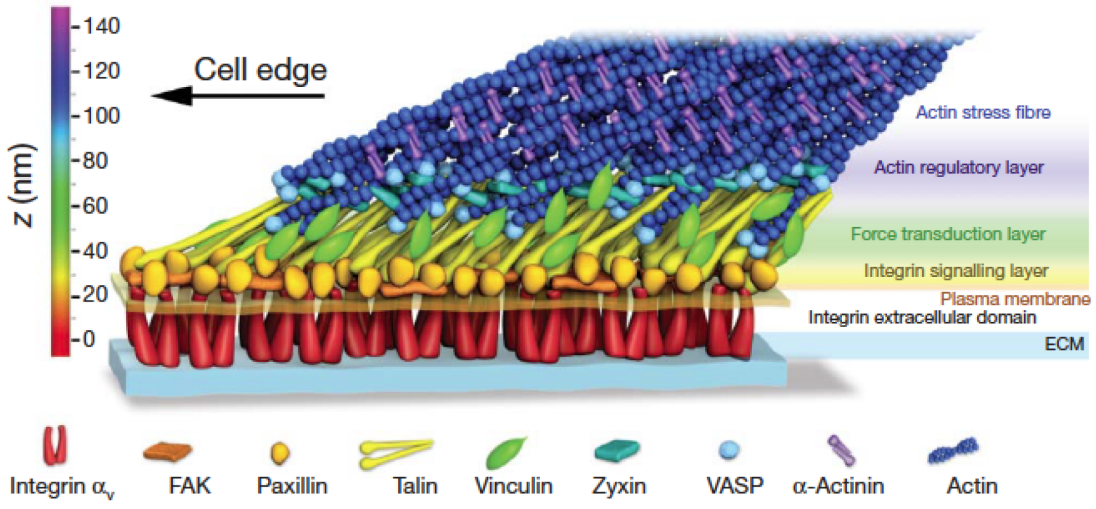


**Figure 1.6 Nanoscale organization of focal adhesions.** Focal adhesions are arranged in three different signaling layers. Each layer has its characteristic components, labeled in different colors. The color bar on the left side indicates the distance in z-direction in nm. This figure is acquired from Kanchanawong et al., 2010[24].

## 1.6 Cell-matrix adhesion sites regulate cell survival and proliferation

The significance of cell adhesion for survival was first identified when cells, in normal serum conditions, underwent apoptosis after detachment from ECM[55,56]. Few years later, Frisch *et al.,* 1996 showed that FAK was involved in the adhesion-dependent cell survival. Integrins interacts with ECM proteins to activate FAK to suppress apoptosis in epithelial and endothelial cells. This adhesion-dependent cell death was termed as anoikis[57].

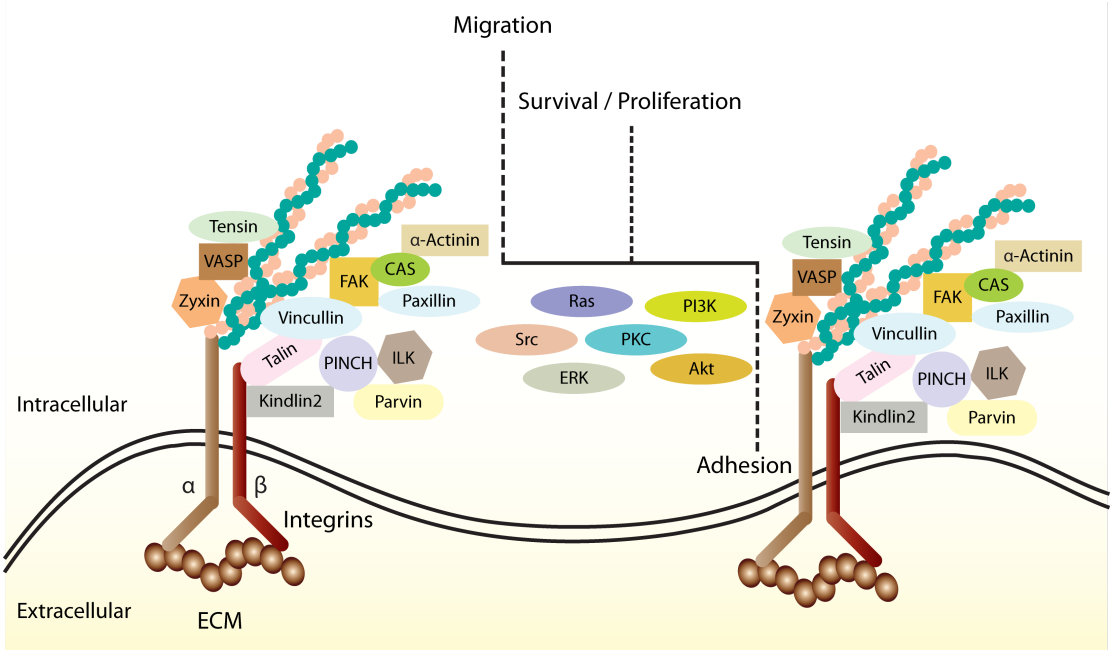


**Figure 1.7 Integrin signaling and crosstalk with other cascades.** The cytoplasmic domains of integrins are associated with FA proteins, while the extracellular domain attach to ECM proteins. Integrin-linked non-receptor kinases such as FAK, Src and ILK interact with other signal transduction pathways, including PI3/Akt, MAPK and PKCs. Integrins also interact with cytoskeleton proteins. Collectively, integrin crosstalk regulates the cell shape, survival, adhesion and migration. This figure is modified from Ozaki *et al.*, 2011[58].

Cell attachment via adhesion sites regulate cell survival and proliferation due to the crosstalk of integrins with growth factor receptor signaling, partly due to the physical association between these receptors[59-61]. However, integrins also directly signal through the non-receptor tyrosine kinases Src and FAK, leading to the activation of several pathways such as phosphoinositide-3-kinase (PI3K)[62,63] and mitogen-activated protein kinase (MAPK) pathway[64,65] (Figure 1.7). The consequent downstream signals from these pathways are critical for the regulation of cyclin-

dependent kinases (CDKs) and cell cycle progression. The disruption of CDK signaling causes cell cycle arrest that leads to the apoptosis (reviewed in Giancotti and Ruoslahti, 1999[66]) which shows integrin-mediated cell cycle signaling is an essential mechanism by which integrins promote cell survival and proliferation[65,67].

Many adhesions site proteins have been identified in regulation of survival, proliferation and anoikis such as CAS[68,69], vinculin[70], talin-1[71] and kindlin-2[72]. The exact mechanistic role of cell-matrix adhesion sites in adhesion-dependent cell survival and proliferation is not fully understood, although integrin-mediated adhesion prevents the cell death or anoikis[62]. This motivated us to design a screen with pairwise depletion of FA proteins to understand their functions in these essential cellular processes.

## 1.7 Cell-matrix adhesion sites and cell migration

Cell migration is an essential process during embryonic development, mitosis and wound healing[73]. The abnormalities in cell migration lead to the diseased conditions such as cancer[74]. Uncontrolled migration or migration into non-targeted tissues promotes the tumor growth and cancer metastasis[73]. In many cancers, higher levels of ILK were observed, the reason that the inhibition of ILK activity is antitumorigenic, suggesting ILK an attractive target for cancer therapeutics[75]. Thus, studies investigating those adhesion site proteins which critically regulate the migration *in-vitro* might identify the candidate targets to block tumor metastasis.

The process of cell migration in 2D environments is regulated by the tight coordination of cell-matrix adhesion sites and the cytoskeleton[42,76]. Adhesion-mediated signaling crosstalk with MAPK[77], Akt[78], Erk and PKC[58] to govern the coordinated migration of the cells (Figure 1.7). Migration process is highly synchronized and can be considered as cyclic in nature. It starts in response to external stimuli by the formation of a protrusion, driven by actin polymerization in the leading edge of the cell[43]. Subsequently, cell-matrix adhesion sites are formed to attach with the substrate as anchoring points of migration. In the next step, forces generated by the actomyosin contractions cause the cell body and nucleus to move forward. The last step is the disassembly of adhesion sites in rear edge of the cell[73,79], possibly due to the microtubule signaling[80]. The coordinated function of microtubules

and actin cytoskeleton is required for cell polarization and migration[81]. Important regulatory mechanisms involved in different steps of migration are summarized in Figure 1.8.

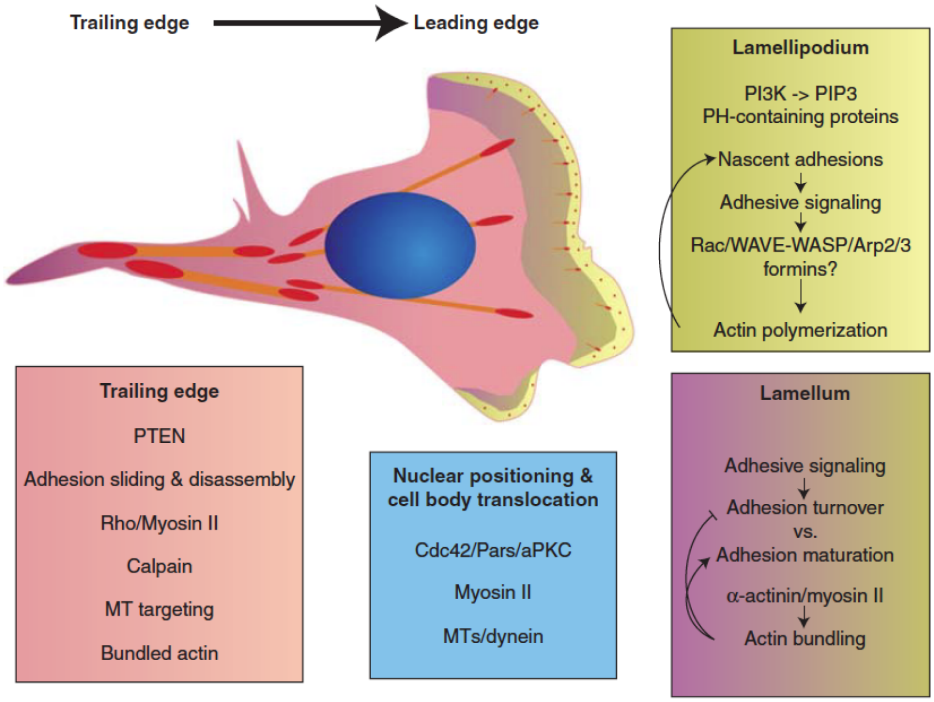


**Figure 1.8 Molecular constituents involved in cell migration.** Migrating cells have a front edge with many small nascent adhesions and rear edge with few focal adhesions. Shown here is the schematic outline of the key processes and their components involved in establishing the cell motility in a polarized cell. This figures is acquired from Huttenlocher and Horwitz, 2011[82].

Cell-matrix adhesion sites and the actomyosin contractility are strong modulators of cell migration in 3D matrices[83]. Lamellipodial mode of fibroblasts migration in 2D (2 dimensional) flat surface is one of the several possible modes of migration observed in 3D (3 dimensional). Tumor cells show high level of plasticity and rapid switching between different modes of migration. There are several factors involved in the regulation of migration in 3D matrices. Cell protrusions define the mode of fibroblast migration such as lobopodia, lamellipodia and amoeboid mode of migration (Figure 1.9). The difference among these modes of migration is based on two features: (1) degree of cell-matrix adhesion and (2) requirement of ROCK, RhoA and myosin-II activity[84].

Another feature of migration is adaptive switching between different modes of migration e.g. lobopodial to lamellipodial, reported for non-cancerous[85] and cancerous fibroblasts[86] respectively. Shafqat-Abbasi *et al.,* 2016 reported the adaptive switching between continuous and discontinuous mode of migration in mesenchymal cells. The cells with continuous mode of migration show minor change in cell shape due to well-established cell-matrix adhesions. Discontinuous mode was associated with dramatic changes in cell shape and direction of movement, characterized by less cell-matrix adhesions. Interestingly, these authors found the involvement of talin, fibronectin and ROCK in producing the two different modes of migration[87].

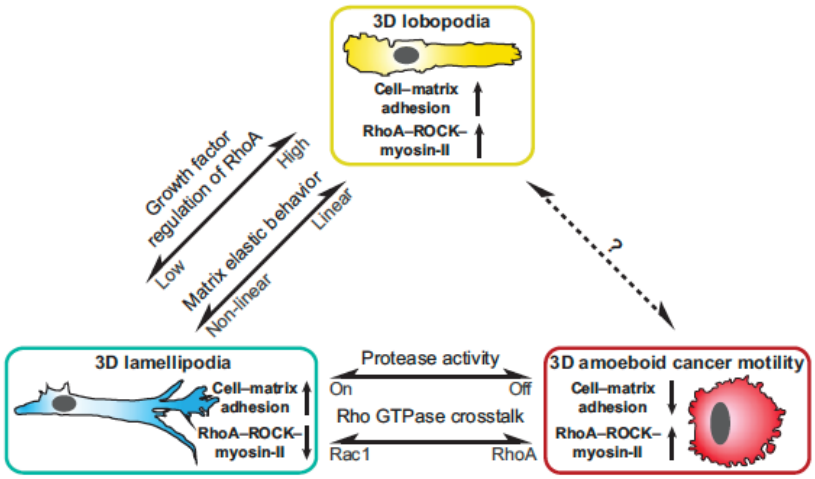


**Figure 1.9 Factors controlling the distinct modes of cell migration in 3D.** Three modes of migrations can be identified in metazoan cells namely lobopodia, lamellipodia and amoeboid, regulated by cell matrix adhesion sites, RhoA, ROCK and myosin-II activity. These figures are acquired from Petrie and Yamada, 2012[84].

Despite the enormous information about the regulation of migration at molecular level in 2D, different modes of migration are not well explored. Moreover, the concerted activity of core FA proteins in the regulation of many aspects of cell migration is still not well understood and has been addressed in this study.

## 1.8 RNAi technology

The development of RNAi technology[88] opened new possibilities to study the gene function[89,90]. Initially, genome wide screens were conducted with the possibility of observing single phenotype such as cell viability[91] and growth rate[92,93] due to the limitations of analytical approaches. Subsequent improvements overcame the

restraints of analyzing high content data provided by multiparameteric imaging screens[94-97]. A step further in RNAi field was taken by the introduction of pairwise gene depletion to examine the genetic interactions. Using these combined approaches, researchers were able to map cell cycle regulators[98] and genetic interactions in healthy[99] as well as in cancerous mammalian cells[100].

Adhesion sites are composed of large number of proteins[101]. Owing to this diversity, it is challenging to study the structure-function relationship of adhesion sites. Comprehensive RNAi screens have identified the genes that regulate migration[102], formation of FA[103], adhesion dynamics and migration[104]. However, understanding the functional relations of canonical FA proteins upon combined perturbations is still lacking. In this study, a combinatorial siRNA screen is devised to uncover the functional epistasis among ten FA proteins to explore the involvement in essential cellular processes.

## 1.9 Functional epistasis

When mutations in two genes give rise to the effect that is different from the effect of individual mutations[105], the phenomenon is known as functional epistasis. This effect can be drastic reduction (more than expected) – synergistic/negative interaction, improvement or control-like behavior (more than expected) – alleviating/positive interaction and effect as expected – proteins are present in a complex[105,106]. Negative interactions are normally associated with severe phenotypes, indicating the involvement of two genes in independent cellular pathways. While less severe positive interactions suggest both genes are the component of a common cellular pathway or a protein complex[107]. The disruption of particular functions of genes or proteins reveal the nature of the epistatic interaction and functional relationship between genes and the pathways[108,109].

## 1.10 Proteins studied during this work

To date, more than 180 proteins are involved in assembling the adhesion sites[101]. In this study, we aimed to develop a pilot screen focusing on a subset of 10 adhesion sites proteins (Figure 1.10) and their combinations (Figure S1a). Based on their major functions, these proteins are categorized into 5 groups: (i) Integrin binding proteins: talin-1, kindlin-2; (ii) Kinases: FAK, ILK; (iii) Adaptor proteins: p130CAS;

(iv) Force modulators: talin-1, vinculin and zyxin; and (v) Modulators of actin cytoskeleton: Zyxin, Ena/VASP (Enabled/Vasodilator Stimulated Phosphoprotein), α-parvin and α-actinin-1. Due to their known overlapping functions, some of them are included in more than one group. In this section, I will discuss the characteristic features of each protein to give an overview about their significance in the formation of adhesion sites. More detailed information about the protein functions could be obtained from Wozniak *et al.,* 2004, Zaidal-Bar and Geiger *et al.,* 2010 and Lo *et al.,* 2006[7,101,110].

### 1.10.1 Integrin Binding proteins

Talin-1 (tln1) is one of the integral adhesion site proteins, which plays an important role in the initiation of adhesion sites. The FERM domain of this protein is β-integrin-binding site which activate the integrins by inside-out signaling[111,112]. Nanoscale architecture of FA revealed the central role of talin in the organization of adhesion sites by directly linking integrins and actin cytoskeleton[24] (Figure 1.6). Kindlin family proteins, also have talin-like FERM domain, were recently identified to participate in bi-directional signaling of integrin[113]. There are three members in kindlin family namely kindlin-1, kindlin-2 and kindlin-3[114]. I have selected kindlin-2 (kin2) as it is an essential protein for bidirectional integrin signaling, controlling the cell adhesion and spreading[113]. As shown in Figure 1.10, tln1 and kin2 both are localized in adhesion sites in REF52 cells.

### 1.10.2 Kinases

Focal adhesion kinase (FAK) is a non-receptor tyrosine kinase and is one of the earliest identified components of FA[17] (Figure 1.10). This universally expressed, integral protein has a focal-adhesion-targeting (FAT) domain which interact with paxillin and talin[115]. FAK is a multifunctional protein and is responsible for the activation of Rho-family GTPase[116], cell migration[34], regulation of downstream signaling by phosphorylation[117], adhesion turnover and crosstalk between integrins and growth factors[34,118].

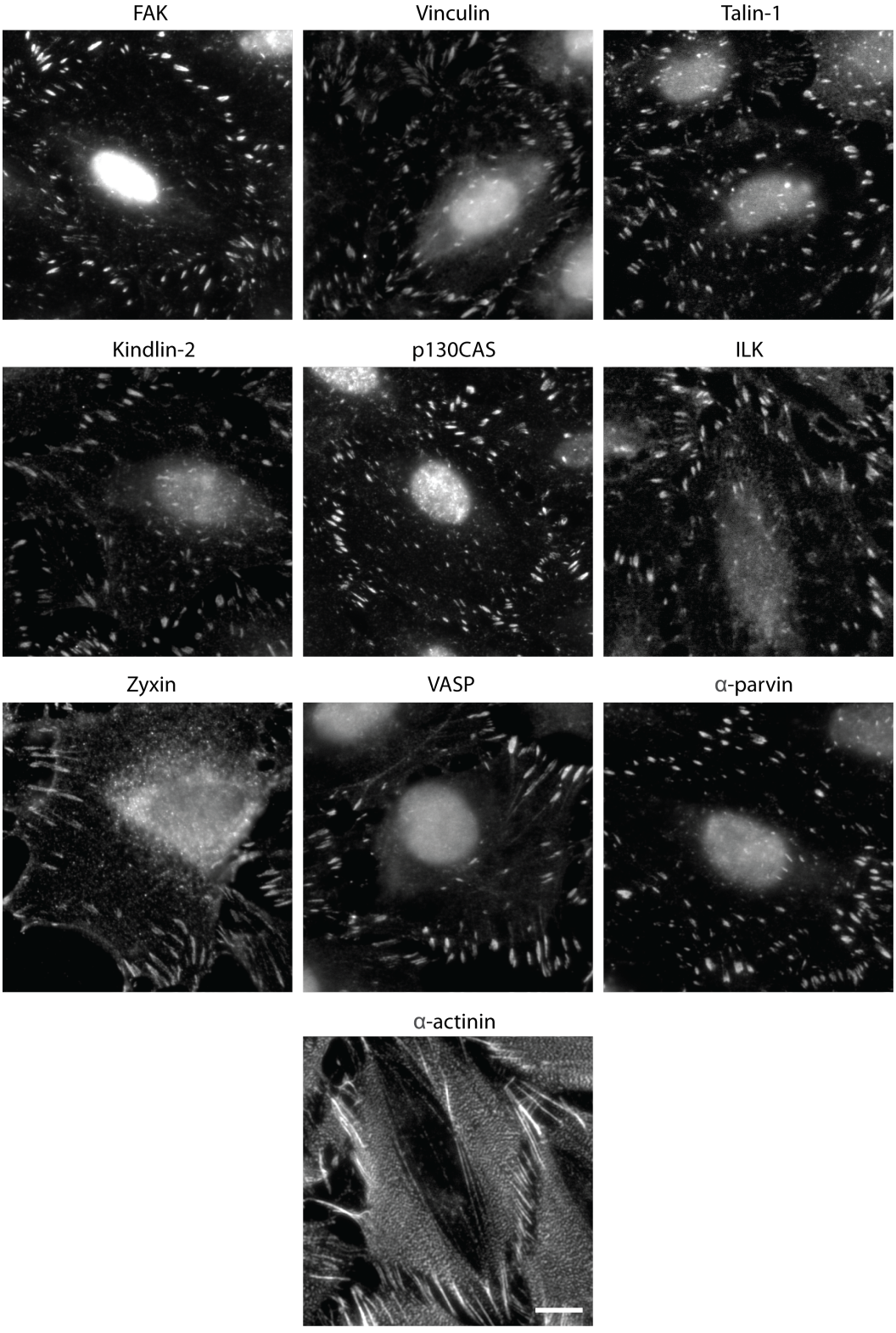


**Figure 1.10 Immunostaining of FA proteins examined in this study.** REF52 YFP-paxillin cells were fixed with 3% paraformaldehyde (PFA), permeabilized with 0.2% triton and incubated with primary antibodies, as indicated. The cells were stained with Alexa 568 and Alexa 647 secondary antibodies (depending on the specie of primary antibody) and visualized under the microscope using 40x objective. Scale bar is 20 μm.

Integrin-linked kinase (ILK); an essential kinase and adaptor protein provides a signaling hub in the integrin adhesome like FAK[119,120]. ILK is also involved in the activation of integrins by direct interaction[121] and possibly due to its interaction with kindlins[113]. Kinase domain on C-terminus mediate interactions with multiple proteins such as paxillin, α-, β- and γ-parvin and possibly with the cytoplasmic tails of β-integrins[122]. The N-terminus contains ankyrin-repeat domain which is responsible for interactions with PINCH1 and PINCH2. ILK is also an essential component of heterotrimeric ILK-PINCH-parvin complex[119]. Level of ILK is increased in certain types of cancer and inhibition of ILK has been shown to be antitumorigenic[75]. It is responsible for the phosphorylation of Akt[75] which in turn regulates the migration in a variety of cells[78] suggesting the indirect role of ILK in modulating the migration.

### 1.10.3 Adaptor/scaffolding proteins

One important scaffolding protein, p130CAS (CAS), localizes in focal adhesions (Figure 1.10). It interacts with Src and Crk kinases[123] in tyrosine phosphorylation-dependent manner. Besides this, CAS also interact with non-receptor tyrosine kinases such as FAK[124]. Overall, it is a key-signaling node for regulating different cellular pathways such as apoptosis and migration[7,125]. Other scaffolding proteins are FAK[126], ILK[127] and adaptor proteins such as vinculin[128] and ILK[120].

### 1.10.4 Force modulators

Vinculin (vin); a main adaptor protein localizes in focal adhesion (Figure 1.10) and interacts with more than 15 adhesion-site proteins. These proteins include; talin, α–actinin, paxillin, VASP, Hic-5 and others[82]. Vinculin directly interacts with force transducer protein talin and actin, which makes it an important factor to mediate the cell adhesion and FA growth. Vinculin keeps talin in active conformation and provide a platform for talin interactions with other proteins resulting in the growth of FA[129].

Zyxin (zyx) play an important role in regulating the assembly of actin stress fibers in association with multiple interacting partners like α-actinin and VASP[130]. Zyxin has a mechanosensing function due to its association with actin polymerization[131]. Zyxin localizes in FA and stress fibers (Figure 1.10) as well as into the nucleus to regulates the gene expression[132].

### 1.10.5 Modulators of actin cytoskeleton

Enabled/Vasodilator Stimulated Phosphoprotein Ena/VASP (VASP) is predominantly present in focal adhesions (Figure 1.10), in filopodia and lamellipodium of migrating cells. It is an important player in the formation and reorganization of actin stress fiber during migration[133]. VASP binds with FA proteins such as vinculin and zyxin to modulate the force transmitted by actin cytoskeleton[130]. α-parvin (α-par), initially identified and characterized as paxillin-binding protein, co-localizes with paxillin in focal complexes in the leading protrusions during migration, suggesting its important role in cell motility[134]. α-parvin interacts with ILK and forms the important ILK-PINCH-parvin complex[119].

Another critical modulator is α-actinin cytoskeletal protein which has four isoforms named as α-actinin 1-4[135,136]. α-actinin interactions enable crosslinking of actin filaments[137]. In this study, we focused on one isoform of α-actinin-1 (α-act1) which mainly localizes in cytoplasm along the actin stress fibers[138] (Figure 1.10). Upon phosphorylation, α-actinin-1 interacts with Src and FAK thereby enhances the integrin-mediated signaling[139]. The concise introduction of the ten core FA proteins emphasizes on a wide-range of functions, representing the diversity and complexity of integrin adhesome.

## 1.11 Aims of the study

Cell-matrix adhesion sites provide precise communication between cells and their environment, which is required for fundamental cellular processes such as adhesion and cell motility. These complex processes depend on accurate organization of the FA proteins, which is evident by their arrangement in particular compartments of the focal adhesions. While the overall molecular architecture of FA has been established, a little is understood about the functional crosstalk within FA to regulate the adhesion-mediated processes. To explore this, ten core FA proteins were selected and a multi-scale combinatorial RNAi screen was performed.

Earlier studies have revealed that FA assembly is a highly regulated process, driven by adhesion-associated proteins. The role of FA proteins in adhesion segregation process and functional relevance of this process in cell migration is least-studied. First aim of this study is to explore the role of FA proteins in the formation of FB and cell motility.

Fibroblasts on flat 2D surfaces use actin polymerization to initiate the membrane protrusions, which are strengthened by FA leading to lamellipodial mode of migration, the most prevalent mode of fibroblasts locomotion. However, it is not a universal mode of migration. Recent studies have shown that fibroblasts migrate in distinct modes, depending on the degree of adhesion driven by actomyosin contractility and physical properties of the ECM. How FA proteins govern these modes is poorly understood. The second aim of this study is to examine the role of canonical FA proteins in regulating different modes of migration.

FA proteins are involved in cell survival/proliferation via integrins-mediated adhesion. Owing to the regulation by different signaling pathways, these processes are highly robust and efficient. The epistatic interaction of FA proteins to control these regulatory processes is, however, not clear. The third aim of this study is to investigate the concerted function of FA proteins in adhesion-dependent cell survival/proliferation.

# 2. Materials and Methods

## 2.1 Mammalian cell culture

REF52 cells stably expressing YFP-Paxillin were cultured in Dulbecco's modified eagle's medium (DMEM; PAN Biotech GmbH) supplemented with 10% fetal bovine serum (FBS) (Invitrogen), 1% non-essential amino acids and 1% L-glutamine (PAN Biotech GmbH). Cells were maintained at 37°C with 5% $CO_2$ until they were 80-90 % confluent. YFP-paxillin REF52 cell line was selected due to the uniform formation and distribution of focal adhesion in these cells. In order to avoid the variability in measurements, cells were cryopreserved from single passage in multiple aliquots and stored at –150°C. For each experiment, a fresh vial was used and cells were maintained for 8-10 passages before transfection.

### 2.1.1 Passaging of cells

Mammalian cells were grown and maintained at a confluency of 70-80%. For splitting, the cells were washed with PBS and incubated with EDTA and trypsin for 5 min. Afterwards, the cells were resuspended in fresh DMEM media and counted using the cell counter (Beckmann). Approximately $3x10^6$ cells were incubated in 75 $cm^2$ flask for 2 days at 37°C with 5% $CO_2$.

## 2.2 siRNA and controls

In order to avoid off-target effects of siRNA[140], I used ON-TARGETplus siRNA SMARTpools of oligonucleotide sequences that were obtained from Dharmacon for the adhesion site proteins (FAK, Paxillin, Vinculin, Talin-1, α-Actinin-1, α-Parvin, VASP, Zyxin, Kindlin-2 and p130CAS). siCONTROL non-specific siRNA and TOX transfection control were also obtained from Dharmacon. The siCONTROL siRNA was also a pool of siRNA sequences. The siRNAs used for transfection are listed in Table 2.1.

| Genes | Sequence 1 | Sequence 2 | Sequence 3 | Sequence 4 |
|---|---|---|---|---|
| **PTK2** | UGUUAUUGA UCAAGCGAG A | GGACAUUGC UGCACGGAA U | UGGAAAAGG AAGAGCGAU U | CCACACACC UAGCGGACU U |
| **VCL** | GCACAGCGG UGGAUUGAU A | GAGCGAAUC CCAACUAUA A | ACAGAUAAG CGGAUUAGA A | CGAGAUCAU UCGUGUGUU A |
| **TLN1** | CGAGAACUA UGCAGGUAU U | CGAAUGACC AAGGGUAUU A | GUUCGUAGA UUAUCAGAC A | GAGAUGAAG AGUCUACUA U |
| **FERMT2** | UGAUUGGAA UUGCGUACA A | CAAUAUAGA AAUCGGGUC U | GCUUGAAGU UAUCGUUUU A | GUAGUAGGC CAGUCGGGA A |
| **BCAR1** | GGGCAGCUC GGCACGUAA A | GGACUGAGA AACCGAGAU U | AGGGCAACA UCGUGCGAC A | CAACAFAUG GCAAGCGCC U |
| **ILK** | GCCAGAAUC UUAAUCGUA U | GAGCAUCUG UAACAAGUA U | CUCAAUAGC CGUAGUGUA A | GAGCCAAGC UGUAAAGUU U |
| **ZYX** | GGAUGAGAC UGUGCGAGU A | CAGUCUGUG UCUUCCGCU A | GUAUUGACC UGGAGAUCG A | UGGCCACAG CUAAGAUUA U |
| **VASP** | GGAUUCACU UUAACGCUU U | GAAAGAGGA AAUAAUCGA A | GCUGAGAAU AGUCGAGGC A | AAAGUGAAC CUGUGCGAA G |
| **PARVA** | GAGAAUGAG GUGCGGACA A | CCGGAAGGC AUGAACGCG A | GCAUCAAGU GGAACGUAG A | GAUCCAAAC UCACGCAAU G |
| **ACTN1** | GCACUUAUC UUCGACAAU A | AAAAGAGCA UCGUCAAUU A | GGAAGGAUG GUCUUGGUU U | GGCCCGAGU UGAUUGACU A |
| **PXN** | GGAACUUCU UCGAGCGGG A | CCAGAAGGG UUCCACGAG A | GGCAAAGCC UACUGUCGG A | GCGAGGAGG AACACGUCU A |
| **siCONTROL** | UGGUUUACA UGUCGACUA A | UGGUUUACA UGUUGUGUG A | UGGUUUACA UGUUUUCUG A | UGGUUUACA UGUUUUCCU A |

**Table 2.1 siRNA used for transfection (Dharmacon)**

## 2.3 Transient transfection of siRNA

REF52 YFP-Paxillin cells (9 x$10^3$ cells per well) were plated in 24-well plates Next day, cells were transfected using 1.13 µl DharmaFECT 1 (Dharmacon) diluted in optimem media (Gibco), with two different siRNA concentrations, 50 nM (for single KD, 1.5 µl siRNA in 23.5 µl of optimum media) or 100 nM (for double KD, 1.5 µl of each siRNA in 22 µl of optimum media). After 20 min, this transfection mixture was added to the cells. To circumvent the cytotoxicity of DharmaFECT, 6 h post transfection, 300 µl of fresh DMEM was added and cells were incubated for 48 h. Control cells were either untransfected or transfected with siCONTROL non-specific siRNA at two different concentrations i.e. 50 nM and 100 nM.

### 2.3.1 Evaluation of knockdown and transfection efficiency

Western blotting analysis (Figure S1b, c) and quantitative RT-qPCR (Figure S1d, e) for each individually depleted protein were used to evaluate knockdown efficiency. For each protein, sufficient level of KD was achieved ranging from 70-90%. In order to confirm the efficient KD of combined siRNAs perturbations, four combinations were tested using Western blotting (Figure S2a). Quantification of the blots indicates approximately 70-90% KD for double siRNA transfections (Figure S2b). Typically, in large-scale screens, it is almost impossible to determine the KD efficiency of each siRNA. In the current screen, I assessed the level of KD in all combinations for both corresponding siRNAs using RT-qPCR. More than three quarter siRNAs had above 70% KD (Figure S1d). Transfection efficiency was ~ 95% in all experiments (Figure S1f) in which whole cell lysates and RNAs extracts were prepared for Western blotting and RT-qPCR, respectively.

For each experiment, REF52 cells in two wells were transfected with TOX siRNA at two concentrations exactly as query siRNAs i.e. 50 nM and 100 nM. The TOX transfection control is RNA duplex that, when successfully transfected into the cells, causes cell death. After 48 h of transfection, the cells were counted (Vi-Cell XR, Beckman Coulter) and transfection efficiency was determined by comparing the viable cells from TOX and NTC transfected cells. The transfection efficiency was achieved up to 90% as shown in Figure S1f.

## 2.4 Quantification of Knockdown

### 2.4.1 Immunoblotting

Lysates were prepared 48 h after transfection using RIPA buffer (Table 2.2). The concentration of protein was measured using the Bradford assay. The protein samples were mixed with 5x SDS sample buffer and denatured for 5-10 min on 95°C. Equivalent amounts of proteins were loaded on 15% sodium dodecyl sulphate polyacrylamide gels and the electrophoresis was executed under denaturing conditions in gel system (Biorad, München) at 80 V for stacking gel and 120 V for separating gel till the molecular weight marker corresponding to the size of the protein of interest was well separated. The proteins were transferred on nitrocellulose membrane for Western blotting in Mini protean 3 cells (Biorad, München) at 300 mA current. The non-specific binding of primary antibodies on free binding sites on nitrocellulose membrane was prevented by block buffer (LI-COR Bioscience). For immunostaining, the membranes were incubated with primary antibodies (Table 2.3) for 12-16 h at 4°C.

| **Lysis buffer (1x RIPA)** | | |
|---|---|---|
| **Component** | Stock | Amount |
| **Tris-HCl,** | 200 mM, pH 7.5 | 5 mL |
| **NaCl** | 1.5 M | 5 mL |
| **$Na_2EDTA$** | 10 mM | 5 mL |
| **EGTA** | 10 mM | 5 mL |
| **Igepal NP40** | 10% | 5 mL |
| **Na-deoycholate** | 10% | 5 mL |
| **Na-pyrophosphate** | 25 mM | 5 mL |
| **Glycerophosphate (stock: 10 mM)** | 10 mM | 5 mL |
| **Protease inhibitor** | 1 tab | for 50 mL |

| | | |
|---|---|---|
| **Inhibitor cocktail I** | | 500 µL |
| **Inhibitor cocktail II** | | 500 µL |
| **SDS** | 10% | 500 µL |
| **PMSF: Mixed directly before use, $t_{1/2}$ 30 min** | 1 M | 500 µL |
| **Add $H_2O$ up to 50 mL** | | |

**Table 2.2 Components of the RIPA buffer**

| Primary Abs | Catalogue number | Company |
|---|---|---|
| **FAK** | 610088 | BD Bioscience |
| **Paxillin** | 610052 | BD Bioscience |
| **Vinculin** | V9264 | Sigma |
| **Talin-1** | MA1-20231 | Thermo Scientific |
| **α-Actinin-1** | A5044 | Sigma |
| **α-Parvin** | PA5-17185 | Thermo Scientific |
| **VASP** | 3132 | Cell Signalling |
| **Zyxin** | Z4751 | Sigma |
| **Kindlin-2** | K3269 | Sigma |
| **p130CAS** | 610272 | BD Bioscience |
| **ILK** | 611802 | BD Bioscience |
| **GAPDH (Host: Mouse)** | G8795 | Sigma |
| **GAPDH (Host: Rabbit)** | 2118L | Cell Signalling |

**Table 2.3 Antibodies for Western blotting and immunostaining**

After washing the nitrocellulose membrane three times with wash buffer (0.1% Triton X-100 in 1xPBS), host-specific secondary antibodies (Table 2.4) were applied for 1 h. Finally, the blots were washed three times with wash buffer and the proteins were visualized using the Odyssey Imaging System (LI-COR Bioscience). Knockdown efficiency was estimated in four combinations following the same procedure as mentioned above. All immunoblotting experiments were conducted as three independent biological repeats.

| Secondary Abs | Host | Catalogue number | Company |
|---|---|---|---|
| **IRDyes 680** | Donkey anti-mouse | P/N 925-68022 | LI-COR Biosciences |
| **IRDyes 680** | Donkey anti-rabbit | P/N 925-68023 | LI-COR Biosciences |
| **IRDyes 800** | Donkey anti-mouse | P/N 925-32212 | LI-COR Biosciences |
| **IRDyes 800** | Donkey anti-rabbit | P/N 925-32213 | LI-COR Biosciences |

**Table 2.4 Secondary antibodies used for Western blotting**

The blots images were exported as tif files for quantification of the knockdown in Fiji[141]. Images were converted from 8-bit to 32-bit files. To remove the bright particles (if any), images were cropped, background was homogenized and removed by the rolling ball background subtraction with a radius of 50 pixels and a sliding paraboloid. The intensity of remaining background was measured from at least four individual spots and the average value was subtracted from the whole image. Subsequently, images were thresholded to visualize the bands of interest. Finally, a region of interest was drawn to measure the intensity of all the bands. Quantification was done in Excel (Microsoft) where the intensity of each band was divided by its respective loading control (GAPDH). The level of KD was estimated by the following formula:

Ratio of KD condition/ratio of control

The KD level was plotted by using the MATLAB (The MathWorks Inc.).

### 2.4.2 Real time quantitative PCR

RNA was extracted from approximately $7x10^4$ transfected REF52 YFP-Paxillin cells using RNA extraction kit (Zymo research). The amount of RNA obtained was measured using Nano drop spectrophotometer (PeqLab). Using 1-step RT-qPCR kit (Promega), cDNA was reverse transcribed from mRNA (5ng for each RNA template) followed by real time PCR amplification according to the manufacturer's instructions. All qPCR reactions were performed in duplicates. Expression data was first normalized to the loading control (Ldha enzyme), and expression fold changes were calculated by comparison with the cells treated with siCONTROL siRNA using $\Delta\Delta Ct^{-2}$ method[142]. Knockdown of each gene was estimated by using their predesigned primers (Table 2.5) at a concentration of 200nM for each primer. All qPCR experiments were conducted as three independent biological repeats.

| Gene | Primer | Sequence |
|---|---|---|
| | | |
| **PTK2** | Forward | CAAGAGTTTACTGGATTCCG |
| **PTK2** | Reverse | GTCAAATCTGTACACTGGAG |
| **VCL** | Forward | CCTGTTCTCATTTCAGCTATG |
| **VCL** | Reverse | CAGAGCTTCTTCTATTCCTTG |
| **TLN1** | Forward | GCAGATGAGTGAAATTGAGG |
| **TLN1** | Reverse | TCCCCTTCATCTTTTCCTTC |
| **FERMT2** | Forward | CAACAGTGACAAAGAAGTCG |
| **FERMT2** | Reverse | ATTGAAGTAATGTCACCCAG |
| **BCAR1** | Forward | CAACCATCATTCGGTGTATG |
| **BCAR1** | Reverse | GGTACATCATATGTTTCCTCAC |
| **ILK** | Forward | ACAATGTTCTACATGAAGGC |
| **ILK** | Reverse | CTTCATCGATCATTACACTACG |

| | | |
|---|---|---|
| **ZYX** | Forward | TATCACAAGCAATATGCTCC |
| **ZYX** | Reverse | ATGAAAGTTCTTATCCAGCG |
| **VASP** | Forward | AAGTCATCCTCTTCTGTGAC |
| **VASP** | Reverse | CCTCTTTCATTTTCTGTAGCTC |
| **PARVA** | Forward | ATCAAGTGGAACGTAGACTC |
| **PARVA** | Reverse | TATTTCCTCTTGGATTTGCC |
| **ACTN1** | Forward | CCTATGTGTCTAGCTTCTACC |
| **ACTN1** | Reverse | ATCCACTCTAACAGATCACTG |
| **LDHA** | Forward | CTCCAGCAAAGATTATAGTGTG |
| **LDHA** | Reverse | TGTGGACTGTATTTCACAAC |

**Table 2.5 Primers used for RT-qPCR (Sigma-Aldrich)**

## 2.5 Wound healing assay

Transfection reagents were scaled to be compatible for 24 well plates and prepared in the same manner as mention in section 1.3. Two-well inserts (Ibidi) were positioned horizontally in glass bottom 24-well plates (MatTek corporation). The plate with inserts was sterilized with ultraviolet radiations under the laminar flow (NuAire). Before seeding cells, plates were incubated for 20-30 min at 37°C for homogenous distribution of the cells. After 48 h of transfection, cells were trypsinized and re-plated in wound healing assay plates and left for 45 min at RT. After 18 h of incubation, inserts were removed and cells were washed with 1xPBS (PAN Biotech) followed by the addition of imaging media (Thermo Fischer) containing 1:2000 Hoechst (1mg/ml) (Thermo Fischer Scientific, H21491) and 10% FBS to visualize the DNA.

The plate was immobilized on the stage of an inverted wide-field microscope (Cell-R, Olympus) equipped with CCD camera (Orca R2, Hamamatsu Photonics), motorized stage, live-cell imaging chamber and controlled by an in-house software based on LabView (National Instruments). In order to maintain precise *z*-position of the objective, the CCD Laser Displacement Sensor (LK-3100, Keyence) was mounted on the microscope objective revolver. A 3x3 matrix of field of views was acquired,

centered in the middle of each wound area and the stage coordinates were stored (Figure 2.1).

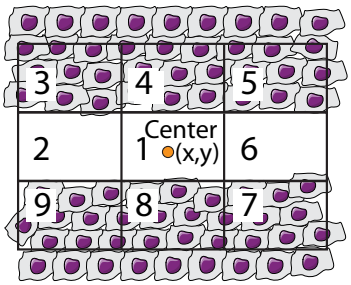


**Figure 2.1 Schematic presentation of 3 x 3 line scan.** x and y coordinates of position one were saved and considered as central position followed by imaging the 9 sub-positions.

Time-lapse image sequences of YFP-paxillin (ex. 510/10, em. 542/27) and DNA (ex. 350/50, em. 440/40) were acquired for the stored positions using a dry 20x/0.75 NA UPLSAPO objective (Olympus, Japan) with an interval of 20 minutes between the frames for a period of about 16 h. Imaging started nearly 70 minutes after insert removal. The cells were maintained at 37°C in the presence of 5% $CO_2$.

### 2.5.1 Analysis of wound healing assay data

For each time point (TP), the acquired 9 images were stitched using the Grid/Collection Stitching Plugin[143] and joined together to create a time-lapse stack file using custom made script in Fiji[141]. Cells were tracked based on DNA staining using TrackMate[144] in Fiji[141] and the tracks coordinates were exported. Only cells that were present in all time points were considered for further processing. Individual tracks were examined and incorrect tracks were removed. In case of fast-migrating cells, an additional manual tracking was performed.

Further the track analysis were performed in modified version of CellTracker[145]. The following parameters were determined for each cell: (b) Total track length – sum of Euclidean distances between coordinates ($x$, $y$) every two consecutive TPs; (c) Median speed of the distribution of instantaneous speeds (distance between two subsequent TPs divided by the time elapsed between their acquisition) (d) Euclidian distance from last TP to origin (position of the cell at TP1) (e) Average angle of direction from origin (Figure 2.2). The obtained parameters of the individual tracks were averaged for each condition.

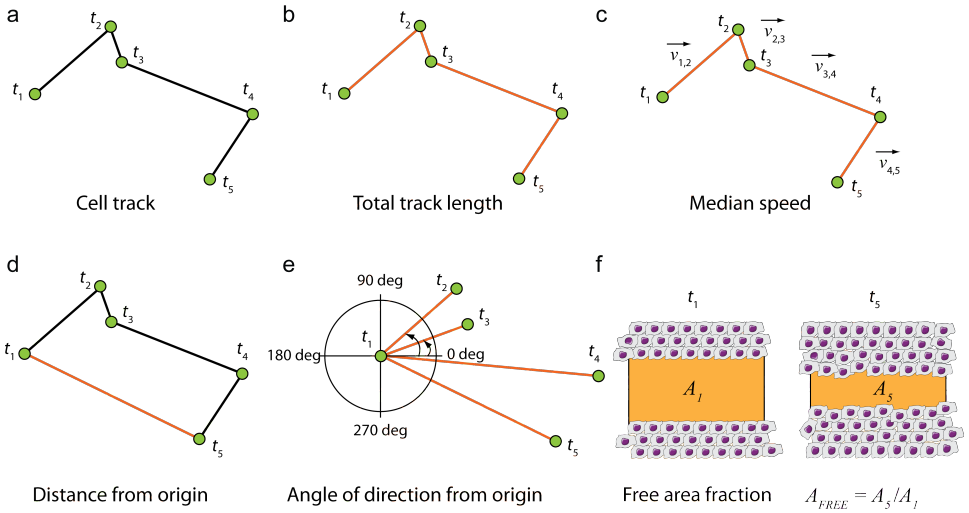


**Figure 2.2 Five parameters characterizing the wound healing assay data.** (a) Cells were tracked at each time point indicated as t1 – t5 and (x, y) coordinates were determined. (b) Total track length. (c) Median speed. (d) Distance from origin indicates distance of the cell in last time point t5 to the first time point t1. (e) Average angle of direction from origin was calculated by averaging the obtained angles for each t2 – t5 in respect of t1. (f) Free area fraction was determined by dividing the free area in last time point (A5) to the free area in the first time point (A1).

Fraction of the free wound area was extracted and it was estimated as:

$$A_{FREE} = A_L/A_F, \qquad \text{Eq. 1}$$

where $A_L$ is the free wound area in the last TP and $A_F$ is the free wound area in the first TP. When the wound was completely closed, the $A_{FREE} = 0$.

The data for all conditions were scaled in the range of [0 1] or standardized (z-scores) for each parameter, creating a unique migration profile.

The obtained z-scores of migration profiles were classified in 9 groups (named MC$i$, $i = 1, \dots, 9$) using $k$-means clustering approach with Manhattan distance measure in Matlab. The Manhattan distance $d$ between two points $a$ and $b$ in $k$-dimensional space is:

$$d(a,b) = \sum_{j=1}^{k} |a_j - b_j|. \qquad \text{Eq. 2}$$

For each group, the average migration profiles were calculated and plotted in polar coordinate system for better visualization, except for cluster 1, which has only one member.

In addition, the Pearson correlation coefficient *rho* was calculated for all pairwise combination of the above-mentioned parameters, except $A_{FREE}$ for each individual condition. The medians of the obtained values were determined for each cluster to evaluate the relationship between migration profiles parameters. Only median speed and total track length were correlated in all pairwise combination. Other parameters were orthogonal (not correlated). The main outcome of the correlation analysis is given in Figure S3.

Image processing and data analysis were performed by Dr. Jana Harizanova (Max Planck Research Institute of Molecular Physiology, Dortmund).

## 2.6 Clonogenic assay

REF52 YFP-paxillin cells, transfected as mentioned in section 1.3, were trypsinized and counted using the cell counter. Equal number of cells (200 cells for each condition) were seeded in 6-well plates in 3ml of DMEM media, in triplicates. The cells were incubated at 37°C in the presence of 5% $CO_2$ for 8 days. Afterwards, plates were washed with 1xPBS, fixed with 4% PFA (Roth) for 10 min and stained with crystal violet (Sigma) for 10 min. The excessive crystal violet solution was removed by washing three times with 1x PBS. The lids were removed for 3-4 h to dry the plates and imaged. Plates were scanned on Typhoon TRIO+ variable mode imager (Amersham Biosciences) with the following settings: Cy5 filter (ex. 633nm, em. 670 band-pass and PMT 530), pixel size 50 microns and focal plane +3 mm. The settings were kept constant for all the measured plates. The data shown is based on three biological repeats of clonogenic assay screens, each repeat containing a sample in triplicates.

### 2.6.1 Image processing and data analysis

Using Fiji[141] based script, plate images were cropped to generate the individual images of each well. Further, the obtained well images were processed by CellProfiler[146] pipeline using Otsu thresholding method to identify the area and number of the individual colonies wherever was possible. Total colony area estimated as in Guzman *et al*., 2014[147] was used to evaluate the proliferation ability in each condition. Based on the colony number, the survival fraction was calculated for all the

conditions. Due to over confluency of some of the samples, the colony number was estimated manually.

The obtained values of colony area of all KD conditions were normalized to the corresponding control and multiplied by 100 in order to obtain the relative change in percentage (e.g. Control = 100%, values < 100% depict decrease in colony area, values > 100% indicate increase in colony area).

The number of colonies or cells survived after seeding represent survival fraction[148]. Plating efficiency (PE)[148] was calculated as

$$PE = \frac{\text{Number of colonies}}{\text{Number of cells seeded}} \times 100 \qquad \text{Eq. 3}$$

The survival fraction (SF)[148] then was defined as:

$$SF = \frac{\text{PE of the treated sample}}{\text{PE of the control}} \times 100 \qquad \text{Eq. 4}$$

The mean value of each triplicate sample was calculated for all conditions. Next, the mean value and standard error of the mean (SEM) from three biological repeats were obtained for both parameters. Image processing and analysis was performed by Dr. Jana Harizanova (Max Planck Research Institute of Molecular Physiology, Dortmund).

## 2.7 Fixation and immunostaining

REF52 YFP-Paxillin cells transfected with siRNA, as explained in the section 1.3, were fixed with 3% PFA (Electron Microscopy Sciences) for 10 min followed by permeabilization with 0.2 % triton X-100 for 5 min, blocked with 5% BSA (Serva) for 30 min and immunostained with primary antibodies (Table 2.6) at 4°C for 12-16h. Cells were washed three times with the wash buffer (0.02% Triton X-100 in 1x PBS) and incubated with secondary antibodies (Table 2.6) for 1 h. After incubation with secondary antibodies, cells were washed three times with wash buffer and incubated in 1x PBS. Cells were either imaged immediately for Scan 1 or stored at 4°C until imaged. After completing the first scan, cells were stained for F-actin, nucleus and cytoplasm (Table 2.6) for 20-30 min at RT. Cells were washed once, supplemented with 1x PBS and imaged for Scan 2. Transfection efficiency was estimated by siTOX transfection control ("Materials and Methods") in each plate that was used for

imaging, which was always above 95% (Figure S4). For the multiple readout proteins, the antibodies for immunostaining were carefully selected to avoid cross-reactivity (Figure S5a) and bleed-through of fluorophores (Figure S5b).

| | Primary Ab | Catalogue Number | Company | Secondary Ab | Catalogue number | Company |
|---|---|---|---|---|---|---|
| **Scan 1** | α-tubulin | ab89984 | Abcam | DYLight 350 | SA5-10069 | Thermo Scientific |
| | Tensin | NBP1-84129 | Novus Biologicals | Alexa 568 | A11036 | Life Technologies |
| | PINCH | 612710 | BD Biosciences | Alexa 647 | A31571 | Life Technologies |
| **Scan 2** | Atto 740 phalloidin | 07373 | Sigma | | | |
| | HCS cell mask | H32714 | Thermo Fischer Scientific | | | |
| | Hoechst | H21491 | Thermo Fischer Scientific | | | |

**Table 2.6: Reagents used for live and fixed cell imaging**

## 2.8 Automated image acquisition for fixed cells screen

The automated microscope system[149] based on IX81 microscope (Olympus) was used for automatic image acquisition with the following excitation and emission filters: Alexa 350 ex. 350/50, em. 440/40, YFP ex. 510/10, em. 542/27, Alexa 568 ex. 560/40, em. 628/40, Alexa 647 ex. 643/20, em. 692/40 and Alexa 750 ex. 725/40, em. 810/90. Images were acquired using 40× air objective (0.95 NA, Olympus, Japan), as per each well 100 field of views (10×10 matrix) were collected. Screen imaging was conducted as two consecutive scans (named Scan 1 and Scan 2) i.e. Scan 1 readouts are tubulin, paxillin, tensin-1 and PINCH and Scan 2: DNA, HCS cell mask, tensin-1 and F-actin respectively.

# 3. Results

## 3.1 Multi-scale combinatorial RNAi screening approach

To study the effects of co-depletion of FA proteins in regulating the critical cellular processes, a multi-scale combinatorial RNAi screen was conducted (Figure 3.1). The Multi-scale screen include anchorage-dependent clonogenic assay to study the cell survival and proliferation (named as Screen 1), wound healing assay to explore the cell migration (named as Screen 2) and fixed-cells imaging screen to determine the formation of adhesion sites (named as Screen 3) as shown in Figure 3.1. For the screening purpose, a FA reporter cell line – REF52 expressing YFP-Paxillin (gift from Benjamin Geiger, Weizmann Institute of Science, Israel and Joachim Spatz, MPI for Intelligent System, Germany) was used. Based on the selected set of core FA proteins, there were a total of 10 individual and 45 pairwise combinations (Figure S1a).

In Screen 1, REF52 cells transfected with all individual and combinations of siRNA were subjected to anchorage-dependent colony formation assay (Figure 3.1). To determine the ability of the cells to survive and proliferate, two parameters were extracted for each KD condition; (1) colony area (used as a measure of proliferation) (2) number of colonies (used to estimate the survival fraction/cell survival), explained in details in the "Materials and methods" section 2.6.1.

In Screen 2, the wound healing assay was employed to assess the migration ability of the transfected cells (Figure 3.1). Hoechst staining permitted the tracking of more than 200 cells and extraction of multiple parameters. To identify the modes of migration in REF52 fibroblasts, we used a unique combination of multiple migration associated parameters (MAR) namely: (1) median speed, (2) free area fraction (represents wound closure), (3) average angle of direction, (4) distance from origin and (5) track length (Figure 2.2). Based on these parameters, migration profiles were plotted that allowed the evaluation of overall migration behavior upon pairwise depletion of FA proteins. Additional cell-based parameters were manually assessed as mentioned in Table 3.1 and Table 3.3.

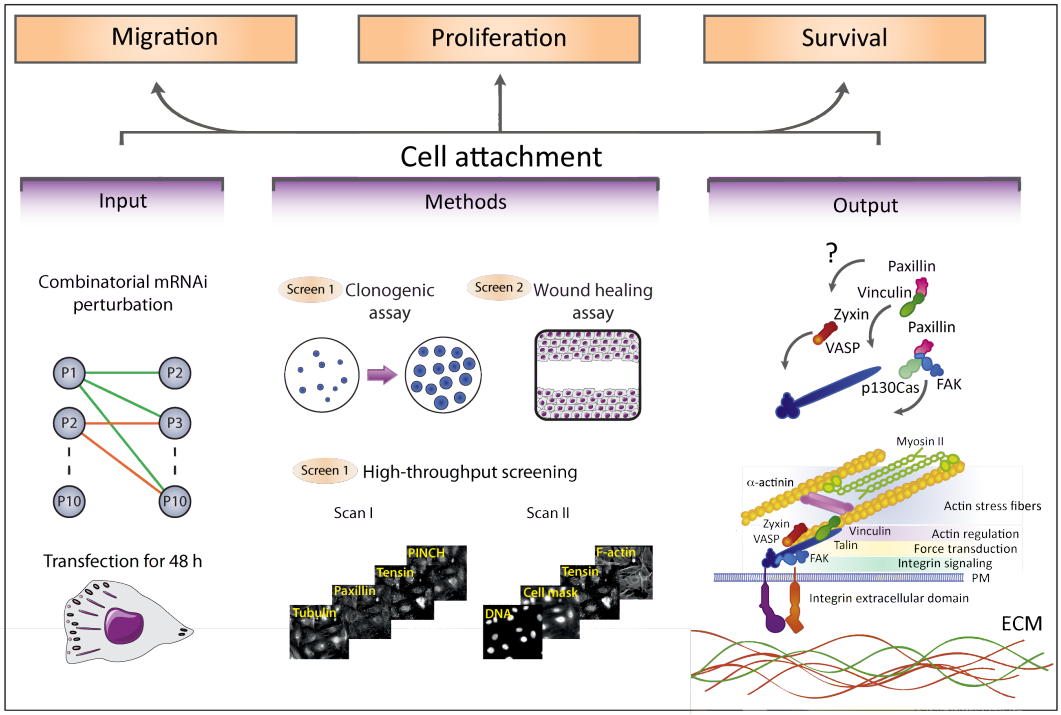


**Figure 3.1 Schematic illustration of multi-scale combinatorial RNAi approach.** In the left panel, the "input" indicates the transfection of cells with individual and combinations of siRNAs. Transfected cells were examined using three different experimental approaches referred as "methods" in the middle panel. The output in the right panel specify the possible interactions, responsible for modulating the cellular functions such as cell survival, proliferation and migration. Part of this figure is adopted from Humphries *et al*., 2015[150].

The term "Semi-collective migration" was used when cells in the leading edge does not display collective migration but follower cells migrate collectively. Free area fraction parameter indicates the conventional outcome of wound healing assay i.e. enhanced, impaired or control-like migration. Migration was considered enhanced in the cases when migrating cells closed the wound earlier than control. Migration was considered impaired when the cells 'failed to close the wound' or 'partially closed the wound' as compared to the control. Image processing and data analysis were performed by Dr. Jana Harizanova (Max Planck Research Institute of Molecular Physiology, Dortmund).

In Screen 3, REF52 cells were transfected, fixed and immunostained for readout proteins (PINCH, tensin-1, tubulin and F-actin and stably expressed YFP-paxillin) followed by automated imaging of all KD conditions. The imaging was conducted in two consecutive scans to acquire the multiple readout proteins (Figure 3.1). Paxillin and PINCH were used as FA reporter proteins whereas tensin-1 was

used as a marker for fibrillar adhesions[151]. Actin and tubulin were selected to visualize the possible defects in actin and tubulin cytoskeleton. Phenotypic descriptors of focal adhesions and fibrillar adhesions were extracted based on paxillin, PINCH and tensin-1, while tubulin, F-actin and DNA were used to extract the parameters to define cellular phenotypes (Not included here. The work is in progress).

Together, the set of readout parameters from multi-scale screen were used to understand how cell attachment via adhesion sites modulates the cellular functions indicated as output (Figure 3.1).

### 3.1.1 Positive and Negative controls

Untransfected cells were used as a negative control. The cell shape, the formation of cellular cytoskeleton, FA and FB in control cells is shown in Figure 3.2a. The downregulation of FAK and kin2 influences on (1) the adhesion sites formation, (2) cell survival and proliferation and (3) migration, were consistent with the published reports therefore selected as positive controls.

(1) siRNA-mediated depletion of FAK is known to affect actin cytoskeleton thereby reducing the number of FA[152]. Likewise, depletion of kin2 reduces the number of FA and cell spreading[153]. These phenotypes were confirmed in this study (Figure 3.2a). (2) We observed a significant reduction in colony area and cell survival upon the individual depletion of kin2 or FAK (Figure 3.2b), the results which is in accordance with the literature[154,155] (3) The wound healing assay exhibited enhanced migration upon downregulation of FAK and impaired migration upon depletion of kin2 (Figure 3.2c), also in line with the published reports[156,157]. These results corroborated the published phenotypes validating the multi-scale screening approach.

As stated above, the individual depletions of FAK and kin2 clearly reduced CA and SF (Figure 3.2b). However, upon concurrent depletion of both proteins, the cells proliferated in a control-like fashion (Figure 3.3a). Similarly, co-depletion of FAK and kin2 resulted in different migration behavior as compared to the respective individual KD conditions (Figure 3.3b), indicating the epistatic interaction. The identification of new protein-relations hints the potential to detect the epistatic interactions involved in regulation of the selected cellular functions.

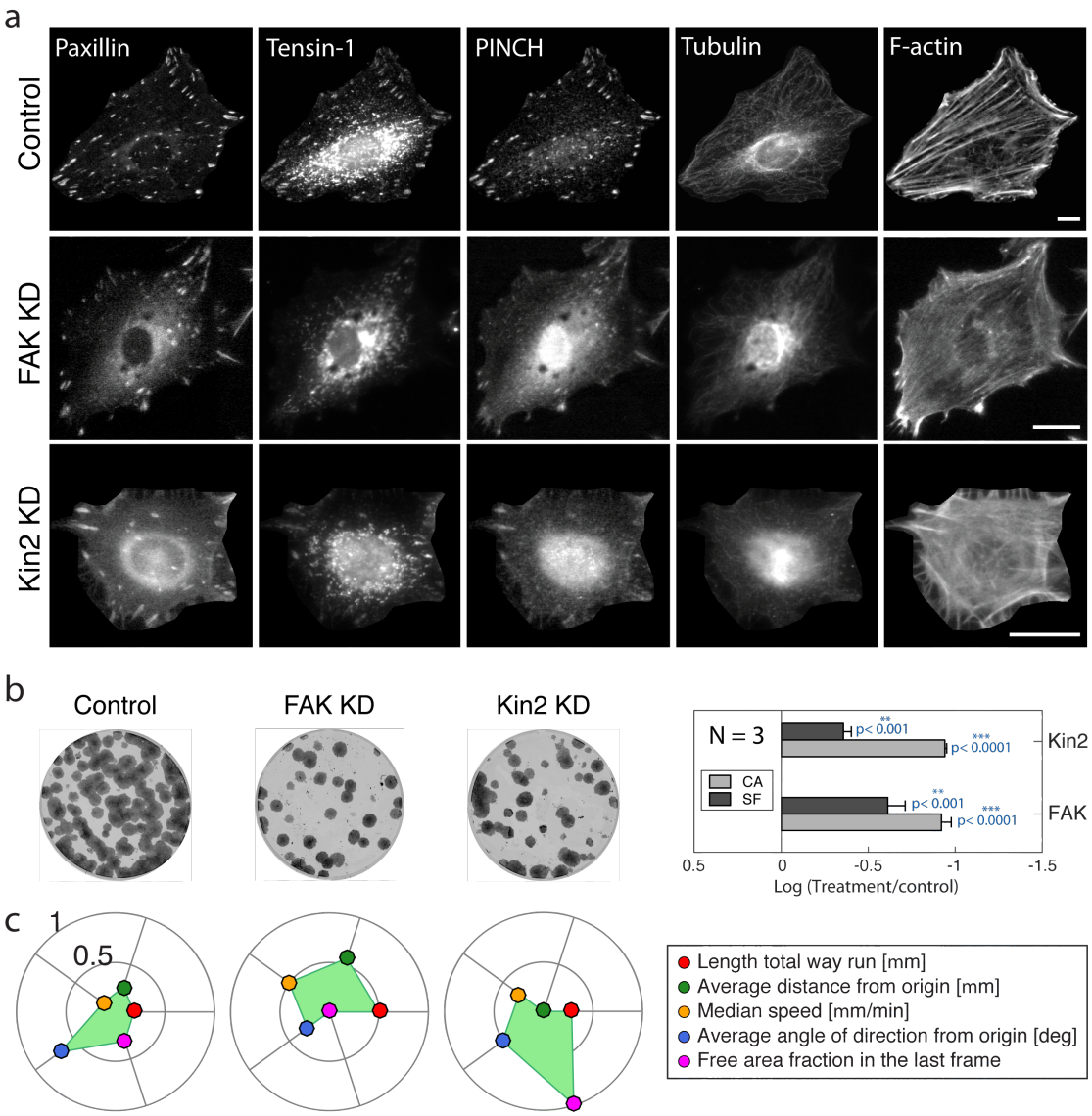


**Figure 3.2 Negative and positive controls for multi-sclae RNAi screen.** (a) Representative images of each indicated condition present the staining of tensin-1 in fibrillar adhesion; paxillin, PINCH and tensin-1 in FA; F-actin, and tubulin in cytoskeleton. (b) Representative images from the anchorage-dependent assay exhibit the clonogenic ability in control as well as in cells depleted with FAK and kin2. All the images are presented under the same brightness and contrast settings. Bar plots showing the comparison of the KD effect on colony area (CA) and survival fraction (SF). p-values are mentioned above each bar. Error bars represent standard error of mean (SEM). (c) Migration profiles of control cells and two single KDs. The free area fraction indicates enhanced migration in FAK-depleted cells (pink dot at 0) and impaired migration in case of kin2-depleted cells (pink dot at 1). Each parameter is plotted in the range of [0 1] and the limits are valid for each profile.

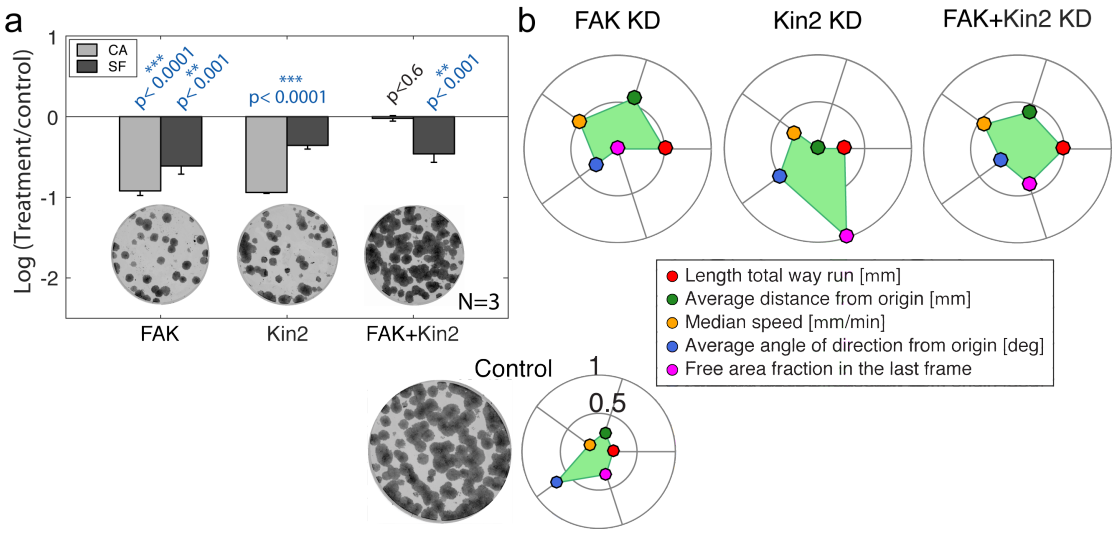


**Figure 3.3 Epistatic interaction between FAK and Kin2 for regulating cell survival, proliferation and migration.** (a) Effect of individual and combined KD of FAK and kin2 on cell survival and proliferation. All the images are shown under the same brightness and contrast settings. p-values are mentioned above each bar. Error bars represent standard error of mean (SEM). (b) Migration profiles of FAK and kin2 plotted for 5 selected parameters as indicated in the legend. Each parameter is plotted in the range of [0 1] and the limits are valid for each profile.

Here, we co-perturbed FA proteins to investigate the protein relations or functional epistasis. Functional epistasis explains the interactions of proteins with one another, that occurs either in the same or different signaling pathways or proteins which form a complex. This description is strictly related to the functions without a direct genetic link[105]. Based on this description, I have explained the existence of proteins in similar or in alternative pathways to regulate cell survival, proliferation and migration. There are two types of functional epistasis: negative and positive. Negative epistasis between two mutations is observed when the combined effect is lower than the individual mutations (drastic reduction). On the other hand positive epistasis between two mutations is observed when the combined effect is higher than the individual mutations (improved fitness)[105] as shown in Figure 3.3.

## 3.2 Role of FA proteins in cell survival and proliferation

To determine the impact of single protein depletions on cell survival and proliferation, two parameters – colony area and survival fraction – were extracted and compared with the control. Decrease in the expression of FA proteins led to the significant reduction in proliferation. The involvement of vin, zyx and α-par in

regulating proliferation is reported for the first time (Table 3.1, Figure S6). Depletion of FAK, tln1, kin2, CAS, ILK, VASP and α-par produced significant reduction in cell survival (Table 3.1, Figure S6). VASP was previously not known to affect cell survival. Four proteins tln1, vin, zyx and α-act1 had no significant effect on cell survival (Table 3.1, Figure S6). The known and validated as well as new effects with the corresponding proteins are summarized in Table 3.1.

| **Proteins** | **Colony area** | **Survival fraction** | **References** |
|---|---|---|---|
| FAK | *** | *** | 158,57,154 |
| Vin | *** | 0 | |
| Tln1 | *** | 0 | 159,160 |
| Kin2 | *** | *** | 155,161,72 |
| CAS | *** | *** | 162,163,163,164 |
| ILK | *** | *** | 165,166 |
| Zyx | *** | 0 | |
| VASP | *** | *** | 167 |
| α-par | *** | *** | 168 |
| α-act1 | *** | 0 | 169 |

**Table 3.1 List of the proteins screened in the clonogenic assay with annotation of the siRNA knockdown effect on cell survival and proliferation.** The column "colony area" depicts the effect of proteins KD on cell proliferation. The "survival fraction" column specifies the effects of protein downregulation on cell survival ( "***" shows significnat reduction, "0" shows no significnat difference from the control, based on t-test). Orange highlighted color expresses the known as well as validated phenotypes in this screen. The pink color indicates newly discovered effects of the siRNA KDs.

To identify the effects of 'combined perturbations' on cell survival and proliferation, the two parameters i.e. CA and SF were similarly extracted for all KD conditions. Thirty-nine out of forty-five combinations displayed significant negative regulation of colony area, ranging from a slight decrease (α-act1+zyx$_{KD}$) to a drastic reduction (tln1+kin2$_{KD}$) (Figure 3.4). Only six pairs were similar to the control. Tln1 and α-act1 were present in 5 and CAS in 3 combinations which displayed a significant

reduction in colony area (Figure 3.4). These findings facilitated the identification of epistatic interactions involved in regulation of the cell proliferation.

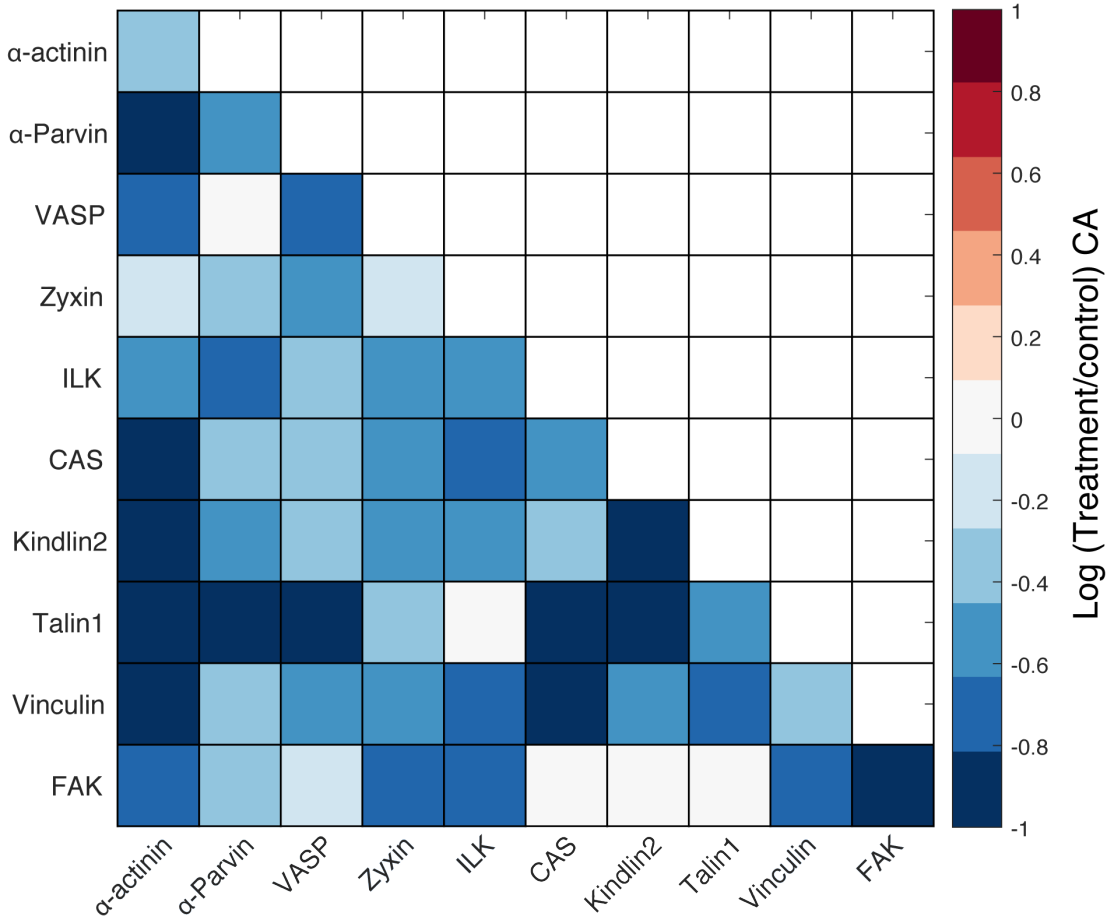


**Figure 3.4 Effects on CA upon individual and pairwise depletion of FA proteins.** (a) The outcomes of single (diagonal of the matrix) and pairwise depletions of FA proteins on colony area is presented in matrix form. The scale bar shows relative change in colony area, normalized to the control in log scale. The quantification is based on three independent biological repeats.

Likewise, survival fraction was significantly reduced in 38 pairs while remain unaffected in 3 pairs. An insignificant increase in survival fraction was observed in α-par+VASP$_{KD}$ (Figure 3.5). In contrast to an insignificant effect of individual depletion, vin in combination with all other nine proteins negatively regulates the cell survival. Only two combinations (α-act1+vin$_{KD}$ and kin2+tln1$_{KD}$) display a pronounced reduction in survival (Figure 3.5). For each combination, a representative image of colony formation is shown in Figure S7. The KD combinations such as kin2 and CAS exhibits control-like survival, suggesting a positive epistasis since the individual depletions of corresponding proteins clearly reduced survival (Figure 3.5).

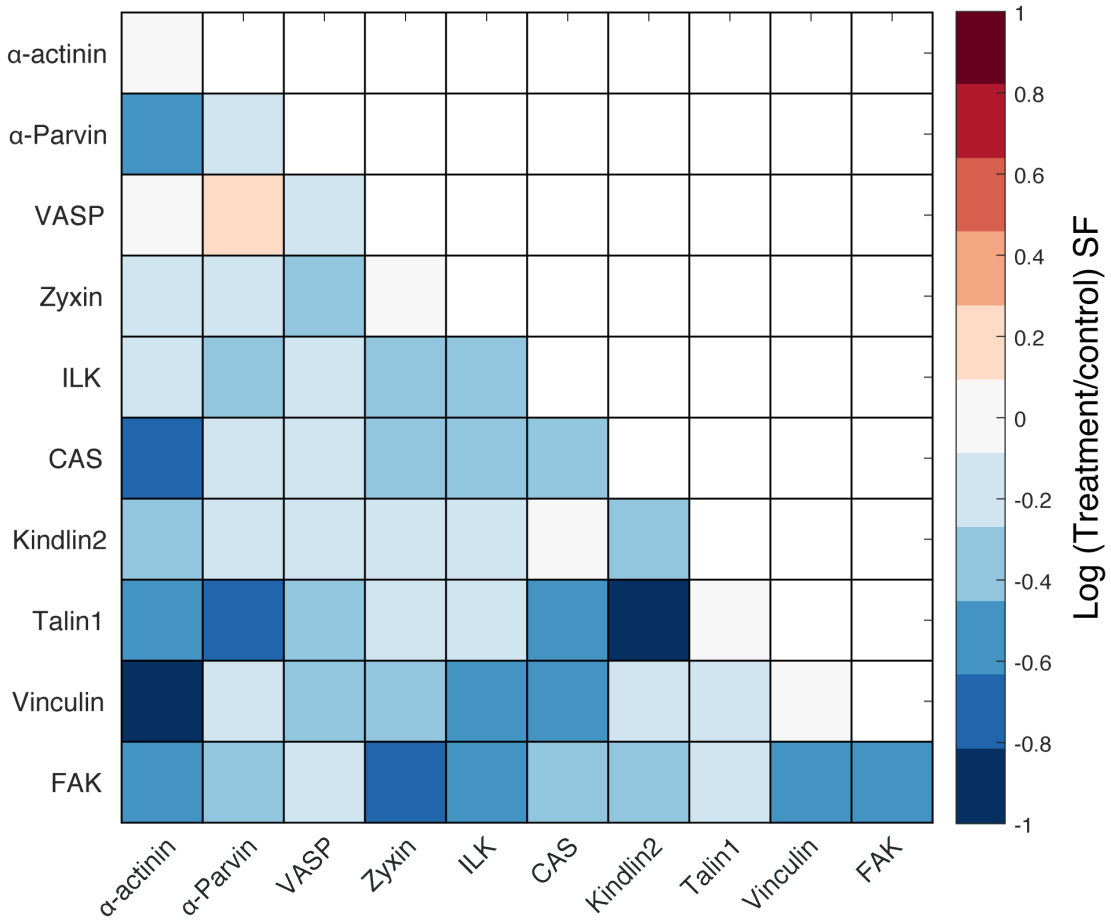


**Figure 3.5 Impacts of depletions of FA proteins on cell survival.** The matrix represents the effects of single (diagonal of the matrix) and double perturbations on survival fraction in the entire set of combinations. The scale bar shows the relative change in SF, normalized to the control in log scale. The quantification is based on three independent biological repeats.

A hierarchical clustering approach was employed to determine the protein pairs which regulate the cell survival and proliferation in similar fashion. Based on the computed z-scores for CA and SF, the data were grouped in six clusters (Figure 3.6). For all pairs, a representative image of colony formation, arranged according to the clusters, is shown in Figure S7. The image processing and data analysis was performed by Dr. Jana Harizanova (Max Planck Research Institute of Molecular Physiology, Dortmund).

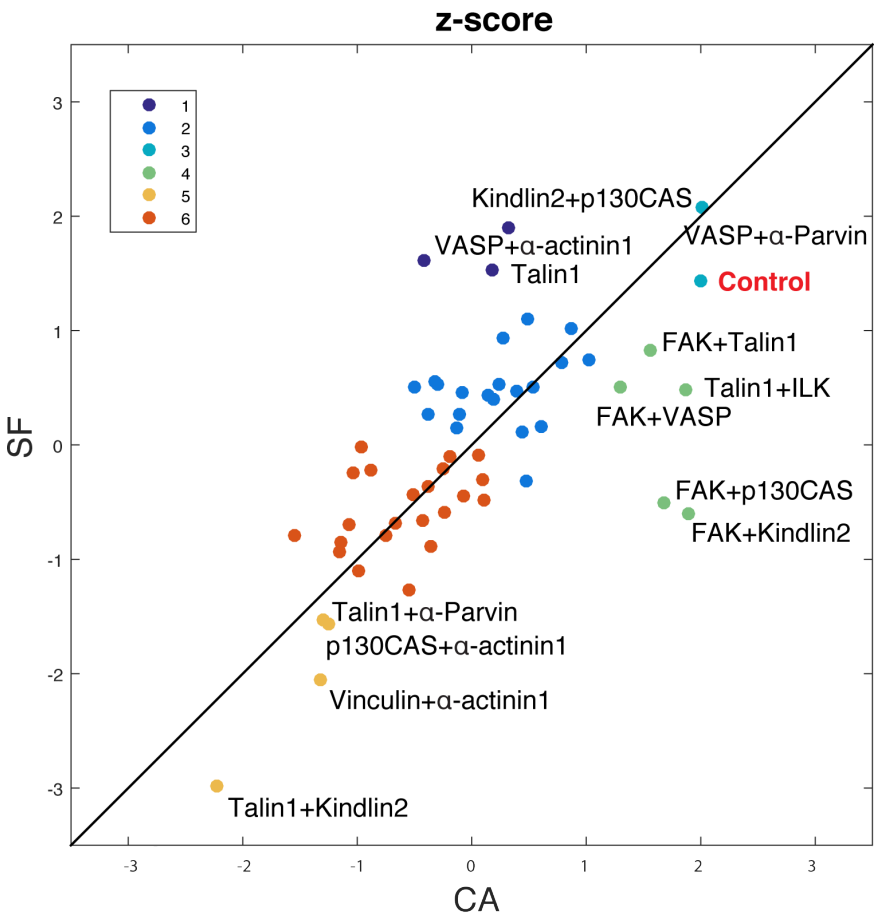


**Figure 3.6 Clustering of KD conditions that regulate the cell survival and proliferation.** Z-score for CA and SF were computed for each condition, including single and double KD. The clustering unified the KD conditions into six groups, symbolized with different colors in the legend on 'left top'. Control is highlighted in red color. The names of the proteins are mentioned for distant clusters (1, 3, 4 and 5) whereas for cluster 2 and 6, names of proteins are mentioned in Figure S8.

### 3.2.1 Specific clusters outline differential regulation of cell survival and proliferation

Knockdown conditions in cluster 1 reduced CA while the survival fraction remain unaffected (Figure 3.6). Kin2+CAS$_{KD}$ slightly modulated CA and SF as compared to the more prominent effect of individual depletions (Figure 3.9a). Improved cell survival upon combined depletion signifies the presence of both proteins in the same pathway or their close association. It also points out their co-depletion had no effect on the compensatory pathway, especially for survival. Possibly unperturbed FAK, which is a signaling hub for controlling survival and proliferation, served as a compensatory route[3]. The effect of VASP-depletion seems to dominate on controlling CA in VASP+α-act1$_{KD,}$ as indicated by relatively smaller

colonies, while the effect of α-act1 KD dominated on SF (Figure 3.9b). These results imply that both the proteins regulate CA and SF independently.

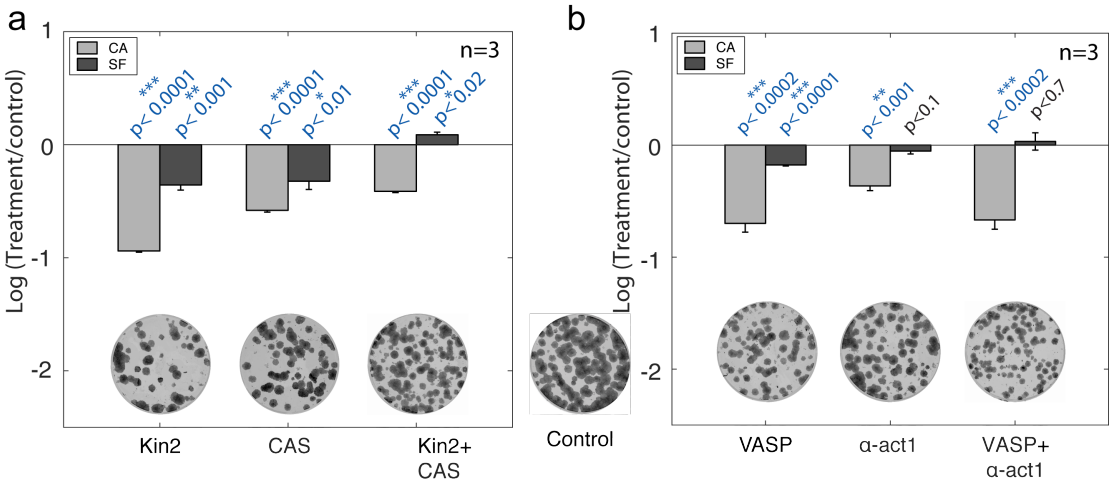


**Figure 3.7 Cluster 1 regulates the colony area.** Bar plots indicate the quantification of CA and SF for single as well combined depletion of (a) kin2 and CAS (b) VASP and α-act1. It is also indicated by the representative colony formation images. All the images were presented under the same brightness and contrast settings. The values were normalized to the control and represented in the log scale. Zero represent control and the values close to zero indicate KD effect similar to the control. p-values are mentioned above each bar. Error bars represent standard error of mean (SEM).

The protein pairs identified in cluster 2 exhibited reduction in cell survival and proliferation. In 10 combinations, the effect of mutually depleted proteins on CA (Figure S8) or SF (Figure S18a) was related to one of the contributing proteins. Most common proteins in this cluster were α-par (in 5 pairs), zyxin (in 4 pairs), vin (in 3 pairs), VASP (in 3 pairs) and α-act1 (in 2 pairs). The individual KD of α-par, zyxin, vin, VASP and α-act1 were also present in this cluster which explain the reason of their dominant effect in combined depletion. A representative example of zyx+α-par$_{KD}$ disclosed decrease in both parameters (Figure 3.10a).

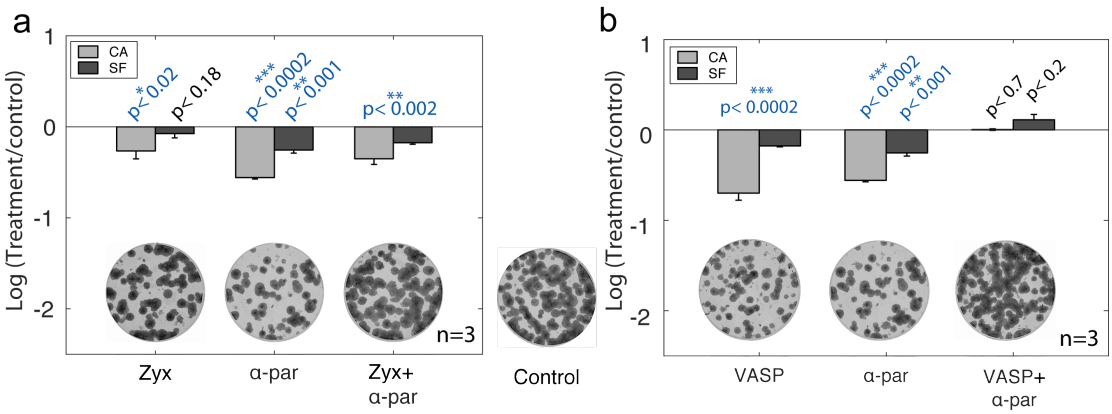


**Figure 3.8 Regulation of proliferation and survival in cluster 2 and 3.** Bar plots denote the quantifcation of CA and SF for (a) zyx+α-parKD from cluster 2 (b) VASP+ α-parKD from cluster 3. Clonogenic assay images for all labelled KD conditions were presented under same brightness and contrast settings. The values were normalized to the control and represented in the log scale. Values close to zero indicate KD effect similar to the control. p-values are mentioned above each bar. Error bars represent standard error of mean (SEM).

Clustering analysis identified cluster 3 with only two members i.e. α-par+VASP$_{KD}$ and control (Figure 3.6). The quantification of CA and SF of α-par+VASP$_{KD}$ revealed no significant difference from control. The co-depletion of α-par and VASP improved the colony forming ability as compared to the individual KDs (Figure 3.10b), indicating positive epistasis and their presence in the common pathway. Simultaneous depletion led to the activation of a compensatory pathway for cell survival.

All members of cluster 4 slightly reduced SF but exert no effect on CA (Figure 3.6). Representative example tln1+ILK$_{KD}$ shows improvement in proliferation as compared to the individual knockdowns (Figure 3.9a), suggesting a positive epistasis and involvement in the same pathway. FAK was present in all the combinations of cluster 4. FAK KD strongly affects cell survival and proliferation[154] which is in accordance with our results (Figure 3.9b). It was expected that the mutual depletion of FAK with other FA proteins would give rise to adverse effects. Surprisingly, the combined depletion of FAK with CAS, tln1, kin2 and VASP led to improved survival and proliferation (Figure 3.9b-e), suggesting their presence in the same pathway. All aforementioned KD conditions regulated cell survival and proliferation in a similar manner as control, most likely due to the function of alternative pathways that maintained these essential cellular processes.

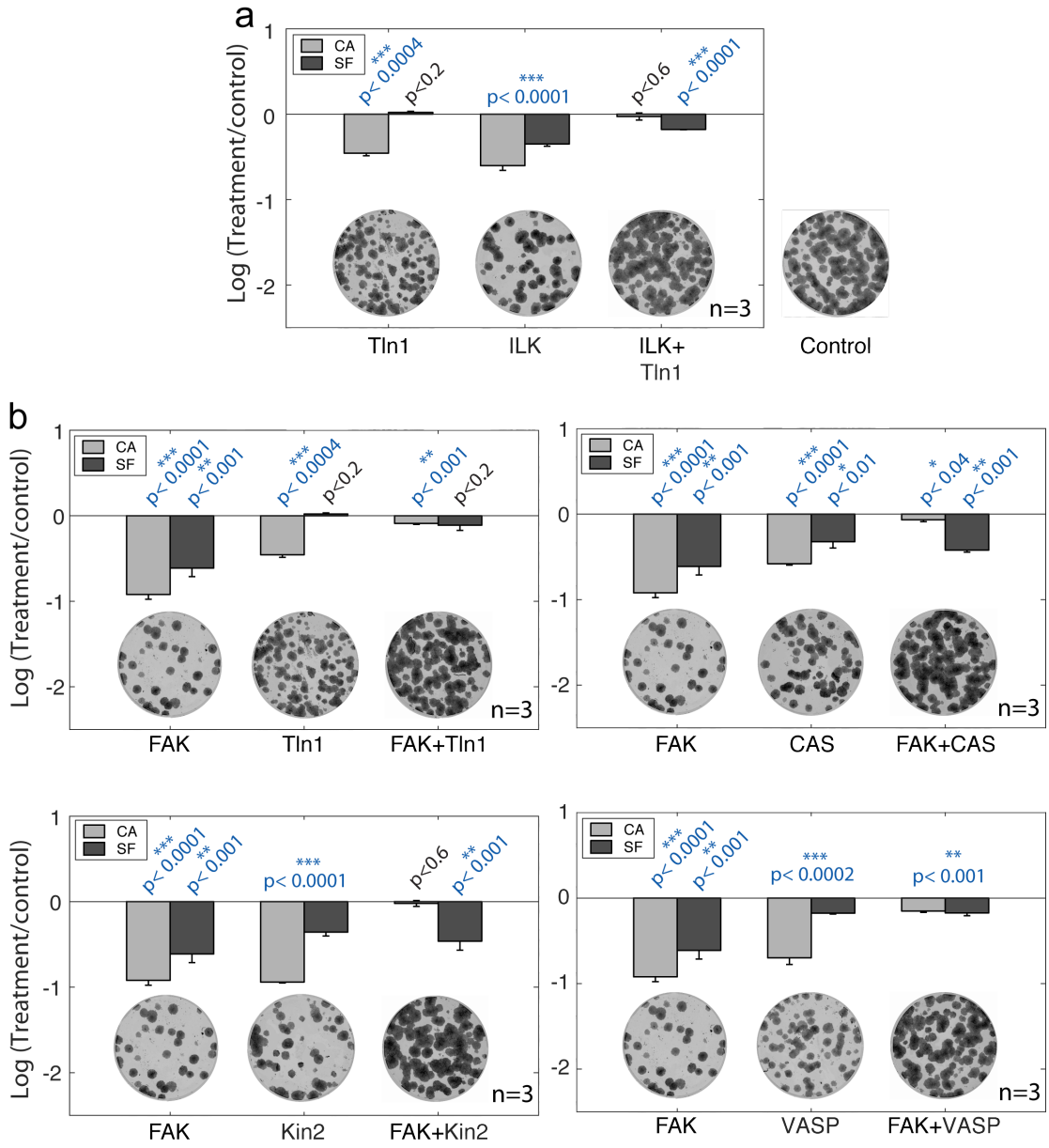


**Figure 3.9 Cluster 4 regulates cell survival and exhibit positive epistasis.** Bar plot of CA and SF quantifcation of (a) Tln1+ILK KD (b) and four combinations of FAK, as specified. The values were normalized to the control and represented in the log scale. Values close to zero indicate KD effect similar to the control. p-values are mentioned above each bar. Error bars represent standard error of mean (SEM). All the images were presented under same brightness and contrast settings.

Combinations in cluster 5 showed significant decrease in both parameters. Individual depletion of vin or α-act1 caused decrease in CA but no significant effect on SF. However, their combined depletion produces severe reduction in both parameters, displaying a clear example of negative epistasis (Figure 3.10a). This suggests the involvement of vin and α-act1 in two parallel pathways, thereby

combined disturbance in both pathways led to the prominent decrease. The depletion of tln1 marginally reduced CA and SF but its co-depletion with α-par resulted in severe effects (Figure 3.6). This result specifies the significance of mutual function of FA proteins from different structural layer to control the cell survival and proliferation. The results obtained from the depletion of tln1 and kin2 are discussed in more detail in section 3.4.1.

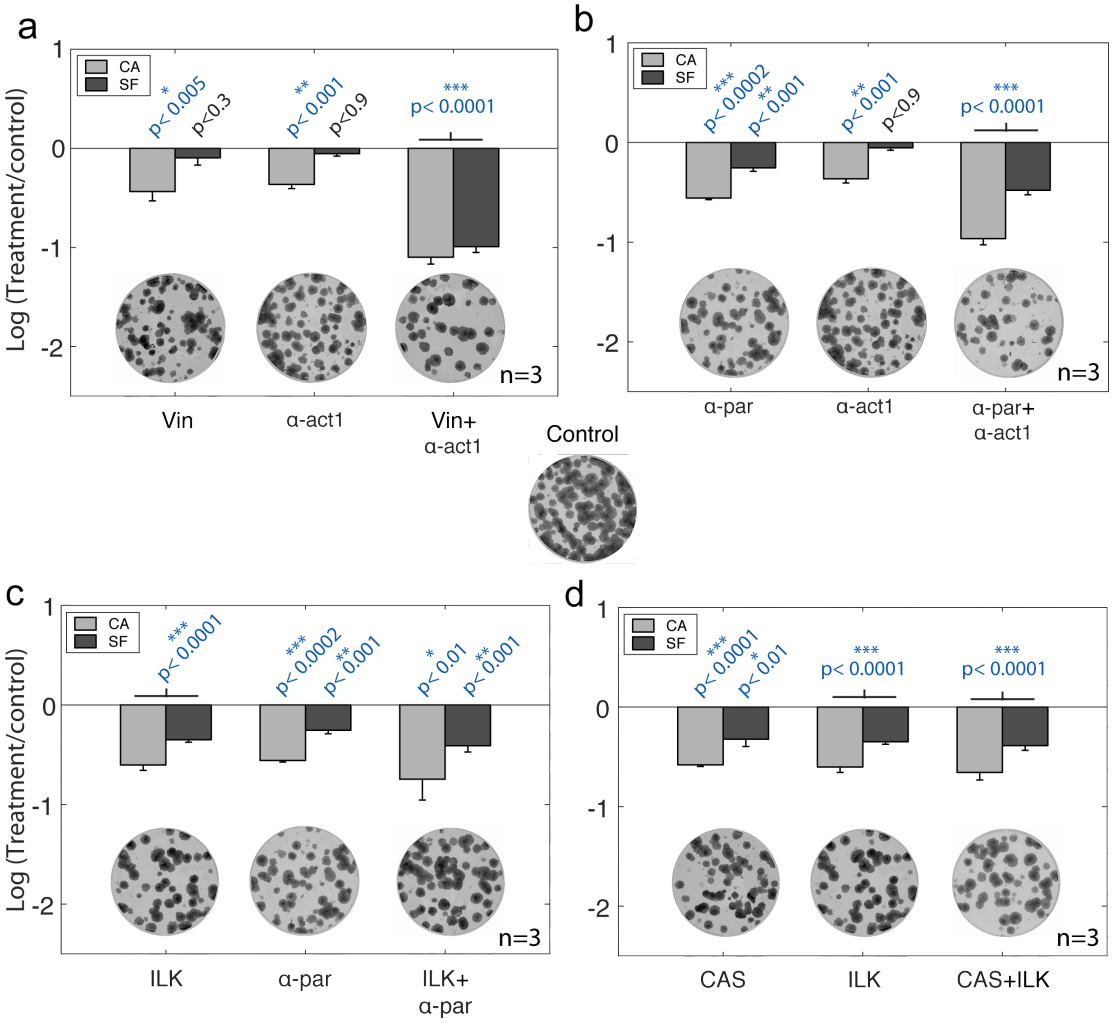


**Figure 3.10 Regulation of CA and SF by cluster 5 and 6.** Bar plots of CA and SF quantifcation for (a) Vin+α-act1KD from cluster 5 and (b-d) from cluster 6 for the lebelled KD conditions. The values were normalized to the control and represented in the log scale. Values close to zero indicate KD effect similar to the control. p-values are mentioned above each bar. Error bars represent standard error of mean (SEM). All the images were presented under same brightness and contrast settings.

Cluster 6 causes prominent reduction in both the parameters. Similar to cluster 2, the effect of one of the individually depleted protein prevailed in case of proliferation (Figure S8) or survival (Figure S10a) in 13 combinations. Knockdown of ILK (in 5 pairs), FAK (in 4 pairs), CAS (in 4 pairs) and kin2 (in 1 pair) were also included in this cluster, which justify the dominance of their effect in mutual depletions. Interestingly, two pairs (α-par+$ILK_{KD}$ and CAS+$ILK_{KD}$) displayed CA and SF, significantly indifferent from their respective single KDs (Figure 3.10c ,d). In these two pairs, ILK and α-par form PINCH – ILK– α-parvin (PIP) trimeric complex[170]. Immunostaining revealed paxillin and tensin-1 positive FA in α-par+$ILK_{KD}$ while CAS+$ILK_{KD}$ cells lack PINCH (Figure S10b). When proteins are in a complex, the effect on the phenotype is often not further increased upon depletion of one of its components[171]. This supports our results that components of PIP complex regulate CA and SF in the similar manner upon individual as well as combined depletion of these proteins (Figure 3.10c), further hints towards the constitution of PINCH– ILK– CAS complex.

The mutual depletion of proteins in six combinations of this cluster affected CA and SF differently as compared to corresponding individual KDs. One example is α-par+α-$act1_{KD}$ where CA and SF were more prominently decreased as compared to individual KDs of both the proteins (Figure 3.10b), indicating negative epistasis and their involvement in parallel pathways. This cluster included 22 KD conditions and the most frequent proteins were modulators of cell survival and proliferation namely: α-par, vin (found in this study), FAK, CAS, ILK and kin2 (known modulators that were confirmed in this study).

Most of the genetic interactions in yeast and human occur within the same pathway/complex produce similar or aggravated effects. Fewer interactions are reported between different pathways which are usually lethal. In this manner, cells perform different functions via alternative pathways to maintain cellular homeostasis and normal functioning[172]. Results of survival and proliferation assay also indicate the similar pattern since most of the epistatic interactions were positive except few negative epistatic interactions.

## 3.3 Identification of the critical adhesion site proteins regulating migration

Multiparameteric profiles were generated to evaluate the effects of individual protein depletions on migration (Figure S11), which in combination with manual assessment of time-lapse imaging resulted in the identification of several modes of migration (Table 3.2). Manual assessment revealed prominent difference in cell shape and size, ability of collective migration and number of FA in different KD conditions (Table 3.2). Depletion of seven proteins (FAK, zyx, vin, α-act1, VASP, ILK and tln1) enhanced the migration. Kin2 impaired the migration while α-par and CAS revealed control-like migration (Table 3.2). A clear relation was observed between enhanced migration and presence of numerous FA in vin, ILK, VASP and α-act1 KDs, while fewer FA were observed in case of tln1, FAK and zyx downregulation (Figure S12). On the other hand, impaired migration in case of kin2 KD was associated with lower number of FA (Table 3.2, Figure S12). These results are in line with the findings of Wong *et al.,* 2007. These authors reported the relation of lower number of focal adhesions and impaired migration[173]. The known and validated effects of individually depleted proteins as well as novel effects are summarized in Table 3.2. These findings provided the basis for comparing the effects, induced by the co-depletion of FA proteins.

*k*-means clustering approach was employed to identify how similarly or dissimilarly the KD conditions (individual and pairwise depletions) regulates the migration. Z-scores were calculated for each parameter to create unique migratory profiles which were further classified into 9 clusters (Figure 3.11) ("Materials and methods" section 2.5.1). Forty-two out of forty-five combinations displayed different migration profiles as compared to the control profile (Figure 3.11). The KD conditions in each cluster are mentioned in Figure S13 and the line profiles in Figure S14. Our analysis discovered most of the pairs with the combined depletion of proteins were involved in the regulation of cell migration, very likely due to the highly interconnected network of adhesion site proteins[20].

| Proteins | Cell shape | Cell size | Collective migration | FA | Mode | Migration | Ref. |
|---|---|---|---|---|---|---|---|
| FAK | Round<br>Elongated | Small | Yes | F | Amoeboid-blebby | Enhanced | 174, 157 |
| Vin | Round<br>Elongated | Medium | Yes | N | Amoeboid-ruffling | Enhanced<br>Impaired | 175,176 |
| Tln1 | Round<br>Multi-protrusive | Medium<br>Small | Semi | F | Lamellipodial-tethering | Enhanced<br>Impaired | 103,177,178 |
| Kin2 | Moon shape<br>Round | Small | Random movement | F | Confined | Impaired | 179,180,72,153,180-182 |
| CAS | Control like | Control like | Yes | N | Control like-Lamellipodial | Control like<br>Impaired | 183 |
| ILK | Elongated<br>Round | Large<br>Small | Semi | N | Lamellipodial-tethering | Enhanced<br>Impaired | 184,185,186 |
| Zyx | Semi-round<br>Polygonal | Large | Yes | F | Amoeboid-blebby | Enhanced<br>Impaired | 187 188 ,189 |
| VASP | Semi-round | Large | Yes | N | Amoeboid-pseudopodal | Enhanced<br>Impaired | 190,191 |
| α-par | Control like | Control like | Yes | N | Control like | Control like<br>Enhanced | 168 |
| α-act1 | Semi-round | Control like | Yes | N | Amoeboid-pseudopodal | Enhanced<br>Impaired | 192 |

**Table 3.2 The effects of core FA proteins depletion on different cellular and migration-associated phenotypes.** The "cell shape" column shows the most prominent cellular morphologies upon proteins downregulation. Next column of "cell size" lists – small, control like and large cell sizes (comparison to control). The "collective migration" column shows three outcomes – ability to migrate collectively – yes, iniability to migrate collectively – no and semi-collective migration – semi. The column "migration" lists three most conventional outcomes of migration assays i.e. enhanced, impaired, no effect (indifferent from control). The column FA (focal adhesions) enlists the formation of numerous (N) and few (F) FA in each KD condistion. The representative images are included in Figure S18. Orange highlighted color shows the known as well as validated phenotypes in this screen. Blue color indicates known phenotypes, but not validated in this screen. The pink color illustrates the newly discovered phenotypes.

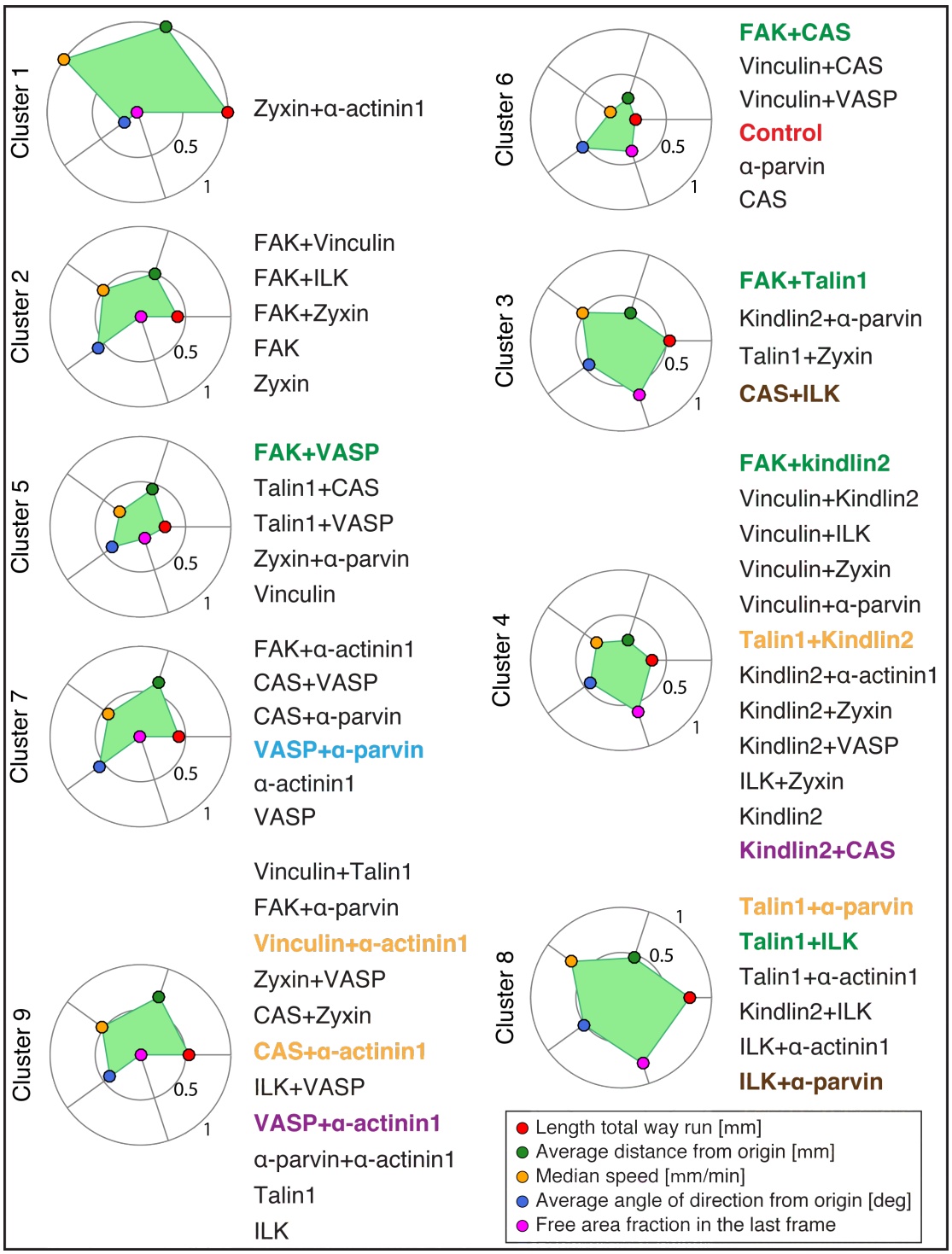


**Figure 3.11 Classification of the KD conditions regulating migration by *k*-means clustering.** The clustering approach identified 9 different clusters. Colored dots in migration profile represent unique parameters mentioned in the legend in bottom right panel. Each parameter is plotted in the range of [0 1]. Highlighted protein pairs belong to the clusters 1,3, 4 and 5 of cell survival and priferation, therefore colored accordingly.

### 3.3.1 Cluster 1: 3D-Lamellipodial mode of migration

Migration cluster 1 (MC1) comprises only one pair zyx+α-act1$_{KD}$ display the speediest migration to close the wound after 6 h of insert removal (Figure S15), specified by the maximum track length and distance from the origin (Figure 3.12a). Cells in this KD condition migrate individually and randomly (Movie 3.1) as compared to collective migration of control cells (Movie 3.2, Figure 3.12d). Time-lapse video microscopy revealed dramatic changes in cell morphology (Figure 3.12b, Movie 3.1). The rapid migration was due to the spontaneous switching between elongated and polarized cell shapes (Movie 3.1). Notably, zyx+α-act1$_{KD}$ migration behavior was entirely different from individual depletion of zyx (MC2) and α-act1 (MC7). The anchorage-dependent assay revealed slight reduction in cell proliferation and survival (Figure 3.12c).

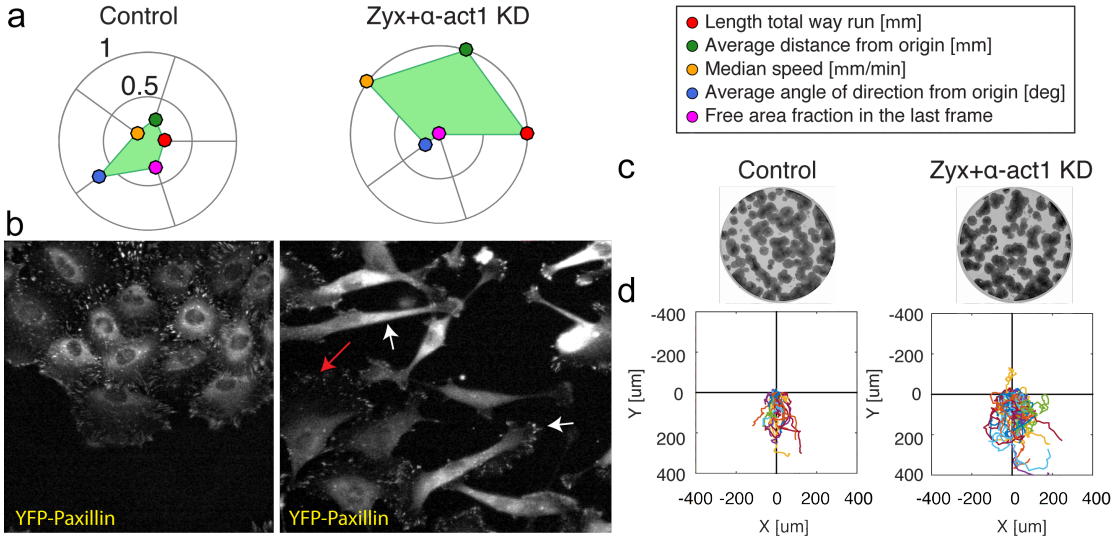


**Figure 3.12 3D-Lamellipodial mode of migration.** (a) The migration profile of zyx+α-act1 KD suggests the fast migration as compared to the control. (b) Representative images of migrating cells after 5 h of live-cell imaging showing zyxin+α-act1KD induce different cellular shapes. Red arrow indicates polarized and white arrows indicate elongated cellular phenotypes (c) Representative images of anchorage-dependent assay showing the survival and proliferation upon zyxin+α-act1KD. (d) Trajectories of randomly selected 30 cells indicate highly random and miss-directed migration upon KD of zyx and α-actinin-1. Each parameter is plotted in the range of [0 1] and the limits are valid for each profile.

Experiments performed with fixed-cells imaging corroborated these cellular morphologies (Figure 3.13). To determine the distribution of actin/tubulin cytoskeleton and adhesion site proteins, fixed cells imaging results were manually

assessed. Elongated cells revealed disorganized and dramatically reduced tubulin-actin cytoskeleton as well as accumulation of actin at the cell borders (Figure 3.13). These cells failed to form adhesion sites as shown by the YFP-paxillin and PINCH staining in case of FAs and tensin-1 staining as marker of FB (Figure 3.13b).

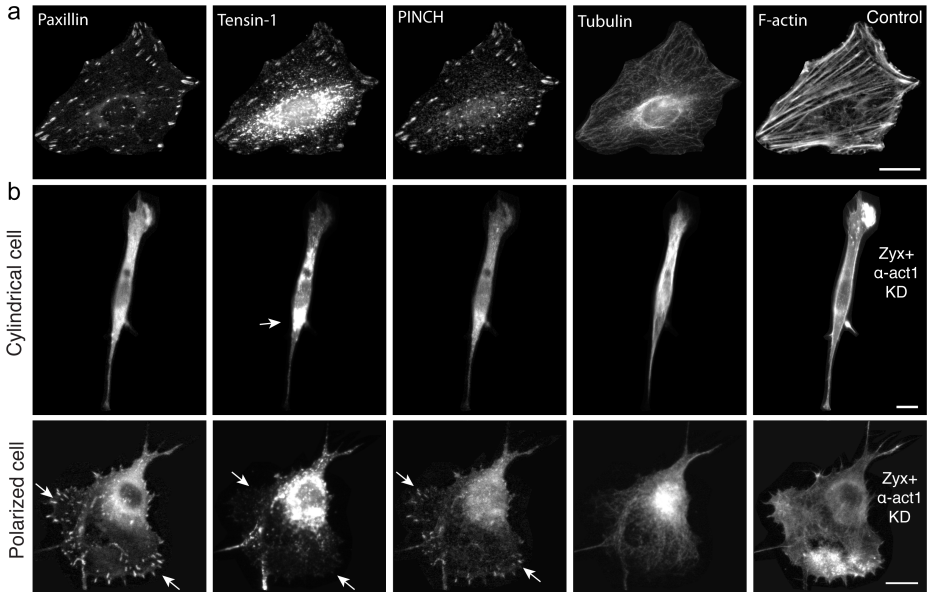


**Figure 3.13 Elongated and polarized cellular phenotypes in α-act1+zyx$_{KD}$.** The top panel indicates control cells with multiple adhesion sites and well-organized cytoskeleton. Control cells were acquired under the same conditions for all migration experiments. The control cells are presented only in this figure and are also valid for further results. (b) Cells transfected with zyx and α-act1 siRNA exhibits elongated (middle panel) and polarized (bottom panel) cellular morphologies. In elongated cell, arrow indicates accumulation of tensin-1 in perinuclear areas. In polarized cells, arrows indicate presence of paxillin and PINCH positive FA without tensin-1. Scale bar is 20 μm.

Elongated cell shape and inability to form stress fibers (low level of actin) is a characteristic feature of 3D-lamellipodial cells[84]. In contrast, polarized cells observed in this KD condition had relatively more FA and spread cytoskeleton. The stress fibers (SF) and microtubules (MT) were disorganized. Polarized cells produced FA but tensin-1 was missing from FA and FB (Figure 3.13b), demonstrating the role of α-act1+zyx in localization of tensin-1 to FA. Collectively, these findings indicate that α-act1+zyx$_{KD}$ display 3D-Lamellipodial mode of migration that is characteristic for cells in 3D matrices[84]. Furthermore, these results suggest that the combined expression of α-act1+zyx is critical for lamellipodia formation, cytoskeletal organization, cell polarization, FA formation and stabilization.

### 3.3.2 Cluster 2: Amoeboid-blebby mode of migration

MC2 KD conditions exhibit ill-defined lamellipodia, lack of cellular protrusions or, if present, shorter ones and majority of round/semi-round cells (Figure 3.14a). These features hint modulations in Rac1 signaling, which a known mediator of lamellipodia formation[83]. Interestingly, the most common protein in MC2 was FAK (Figure 3.14a), suggesting phenotypic dominance of FAK in three pairs. Cells presenting this cluster tend to move collectively except few leader cells with minimum cell-cell contact (Figure 3.14a) as observed in the case of FAK+vin$_{KD}$ (Movie 3.3). Less number of FA, which are particularly arranged along the periphery, (Figure 3.14a) were linked with fast migrating cells (Figure 3.14b). Collectively, these features relate this migration pattern with characteristic amoeboid-blebby mode of migration[84,193], except the difference in number of FA i.e. reported low number of cell-matrix adhesion sites[84] versus several FA in MC2 (Figure 3.14a,c).

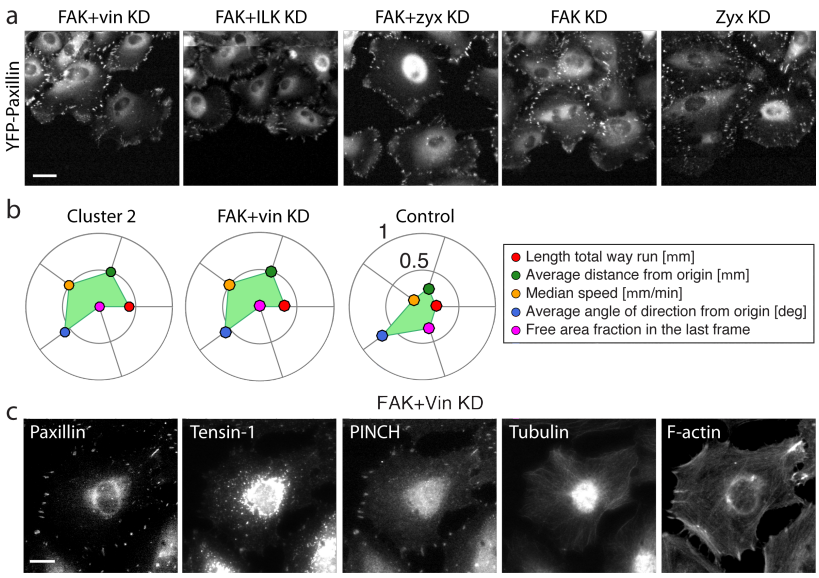


**Figure 3.14 Cluster 2 exhibits amoeboid-blebby mode of migration.** (a) Shown here are the representative images from live-cell video microscopy for indicated KD conditions, representing leader cells at the wound edge (b) Average migration profile of cluster 2, one selective KD condition (FAK+vin) and control are shown. Each parameter is plotted in the range of [0 1] and the limits are valid for each profile. (c) Immunostaining and imaging of FAK+vin KD display the formation of FA (paxillin, PINCH) and inability to formulate FB (tensin-1 staining) as well as distribution of SF and MT (using actin and tubulin). Scale bar is 20 μm.

The migration profile of representative example FAK+vin$_{KD}$ indicates higher speed as compared to control, leading to the coverage of more area to close the wound completely (Figure 3.14b). Immunostaining of cells depleted with FAK and vin confirmed formation of peripheral FA containing paxillin and PINCH. Thinner SF and MT were formed but the organization was clearly disturbed (Figure 3.14c). These results suggest the involvement of MC2 proteins in the following processes; stabilization of FA, formation of characteristic lamellipodia of fibroblasts, cytoskeleton organization and semi-amoeboid mode of migration.

### 3.3.3 Cluster 3: Discontinuous and confined mode of migration

Knockdown conditions categorized in in cluster 3 negatively regulate the cell motility (Figure 3.15a). This unique mode of migration displays two distinct sub-modalities named as confined, represented by immotile cells (Figure 3.15b) and discontinuous, a mode characterized by the cells which are able to move around origin with continuous change in their shape and form short and long cellular protrusions (Figure 3.15c). Cells in confined modality produce several FA as compared to the cells exhibiting discontinuous sub-mode (Figure 3.15b, c). Depletion of FAK+tln1, tln1+zyx, kin2+α-par and CAS+ILK resulted in severe reduction in cell spreading, cell polarization and directional cell migration (Figure 3.15b, c).

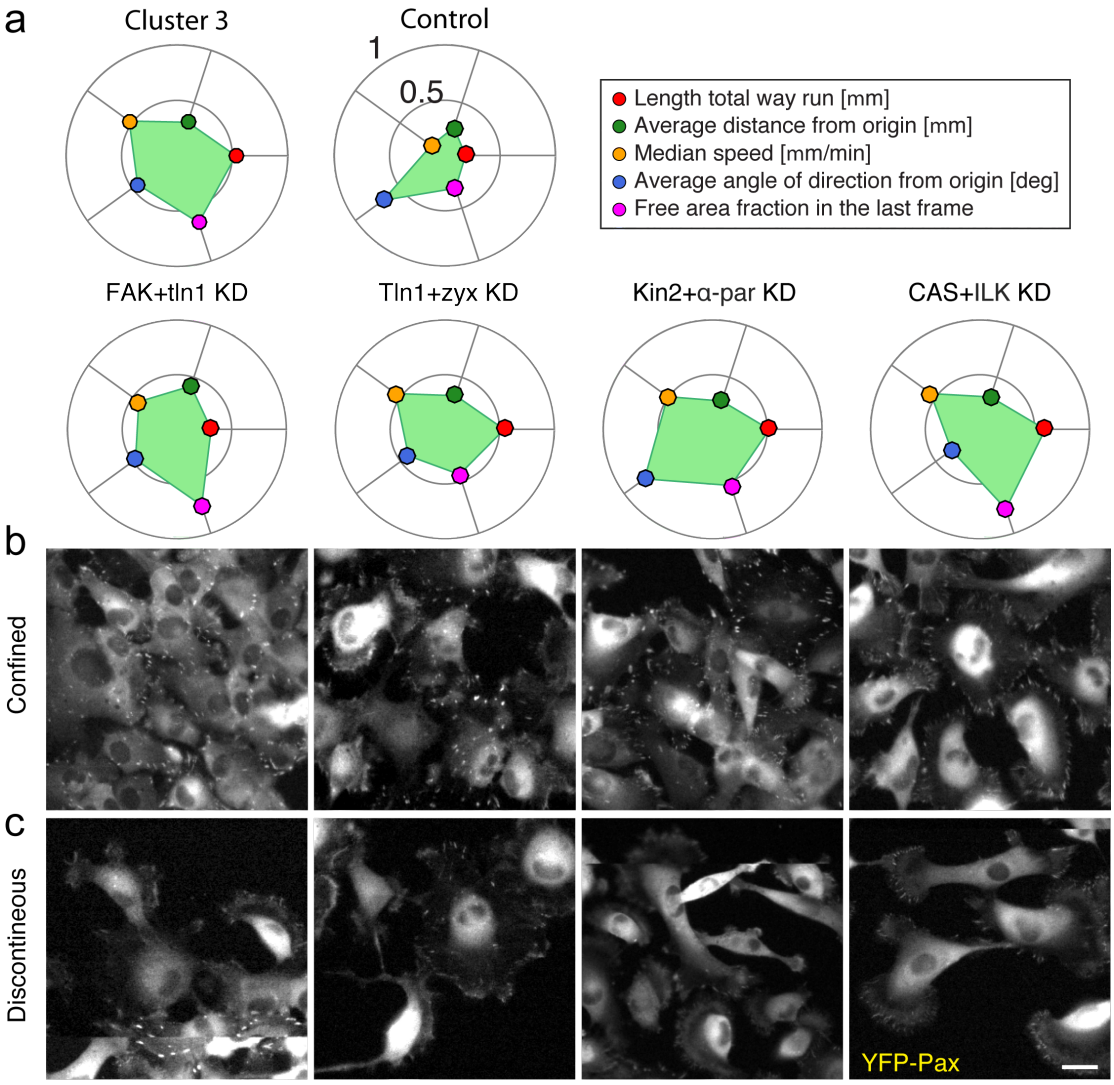


**Figure 3.15 Cluster 3 represents heterogeneous modes of migration.** (a) Average migration profiles of cluster 3, all KD conditions and control is mentioned. Each parameter is plotted in the range of [0 1] and the limits are valid for each profile. (b) Live-cell imaging of REF52 cells, stably expressing YFP-paxillin, migrating during wound healing assay for labelled KD conditions show two different cellular phenotypes (b) confined and (c) discontinuous. Scale bar is 20 µm.

Immunostaining of co-depleted cells of FAK and tln1 indicate presence of several FA in the cells that correspond to confined modality (Figure 3.16, Movie 3.4). Fewer focal adhesions were observed in cells that exhibit protrusive and discontinuous modality (Figure 3.16, Movie 3.5). Interestingly, tensin-1 was present in FA in cells exhibiting confined modality and absent in cells displaying discontinuous modality. In former condition, the cells failed to form FB although tensin-1 was present in FA, suggesting the role of these proteins in segregation of FA into FB due to the essential involvement of tensin-1 in this process[194]. Cytoskeleton

was less affected in confined modality but severely disorganized with almost no stress fibers and very few microtubules in discontinuous modality as indicated by the actin and tubulin staining (Figure 3.16). Time-lapse imaging clearly shows the co-existence of both modalities in FAK+tln1$_{KD}$ (Movie 3.4 and Movie 3.5). In all KD conditions of MC3, either tln1 or kin2 or ILK was present. Confined sub-modality indicates the strong involvement of MC3 protein pairs in cell polarization and the formation of FB to induce cell migration. Presence of discontinuous mode signifies the importance of these proteins in maintaining cell polarity, typical lamellipodia formation and FA stabilization.

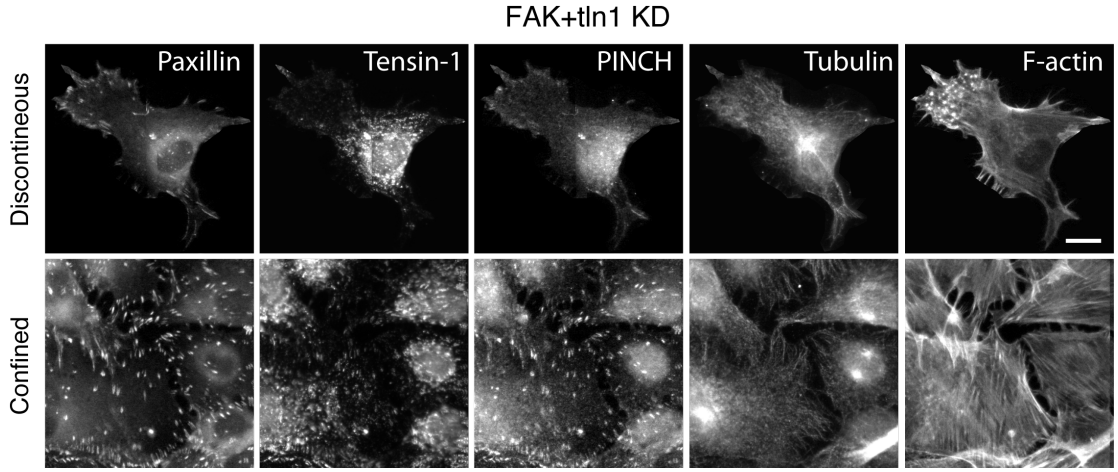


**Figure 3.16 FAK + tln1 KD exhibits heterogeneous cellular phenotypes.** Immunostaining and imaging was conducted for 5 proteins as shown in the figure. Two different cellular shapes, elongated and roundish, corresponding to confined and discontinuous modalities, were present in cells depleted with FAK+tln1. Scale bar is 20 μm.

### 3.3.4 Cluster 4: Confined mode of migration

The KD conditions in cluster 4 led to the restricted and impaired migration which is evident by lower track lengths and distance form origin in the average migration profiles of MC4 (Figure 3.17a). The cells transfected with kin2, the most frequent in MC4, in combination with four other proteins (FAK, vin, tln1, α-act1) showed less and peripheral FA, small and round cells leading to the limited movement (Figure 3.17b). Based on these features, cluster 4 depicts confined mode of migration. Similar to MC3 and MC8, almost all KD conditions of MC4 had one of the three integrin binding proteins; tln1, kin2 and ILK except in two combinations zyx+vin$_{KD}$ and vin+α-par$_{KD}$ (Figure 3.6).

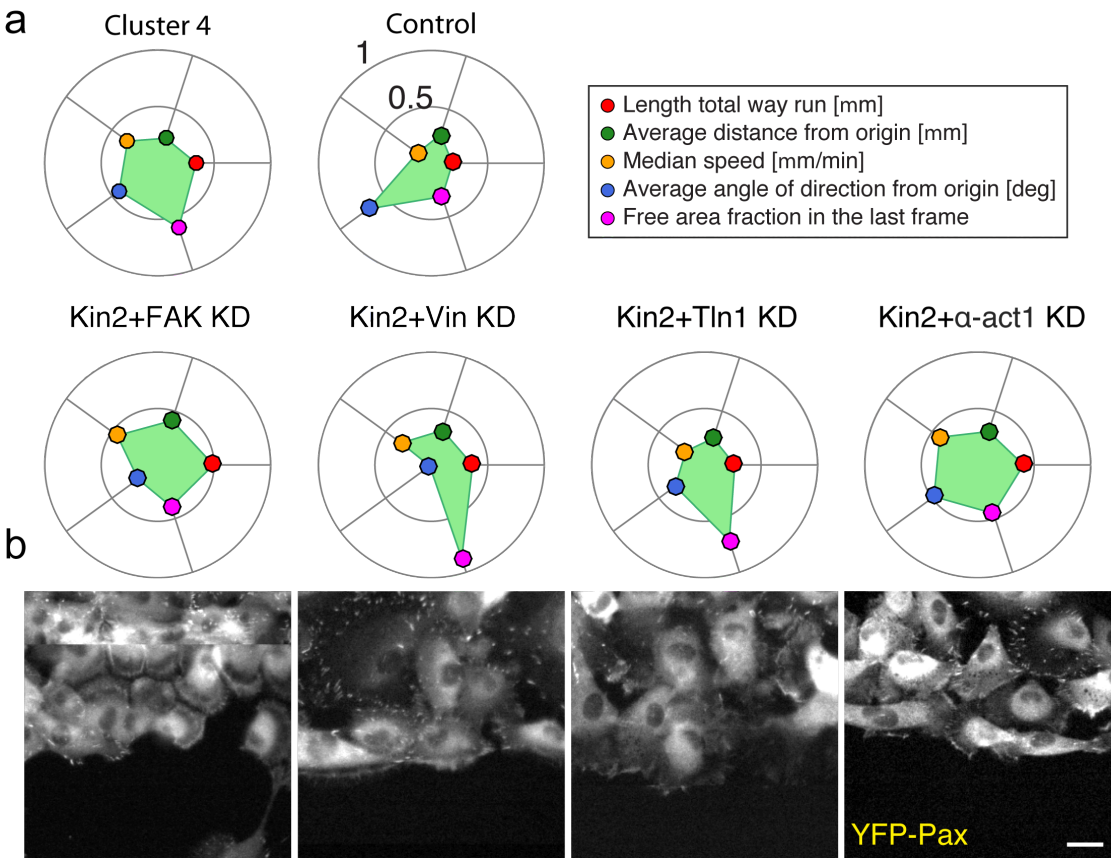


**Figure 3.17 Cluster members of MC 4 display confined mode of migration.** (a) Shown are the migration profiles of MC4 (average profile), control and indicated KD conditions. Each parameter is plotted in the range of [0 1] and the limits are valid for each profile. (b) Images from live cell video microscopy indicate limited number of FA and small, less spread cells in protein depletions mentioned in the figure. Scale bar is 20 µm.

Combined KD of kin2 with CAS or vin completely impaired the migration as compared to control (Figure 3.18a) and more drastically as compared to individual KD of kin2 (Figure 3.17). The inability to migrate was not related with proliferation defects since cells were reasonably proliferative although significantly less than control in both KD conditions (Figure 3.18b). Time-lapse images disclosed that cells in the leading edge failed to develop FA, lamellipodia and changes in cell morphology resulting in incapability to migrate (Figure 3.19). The follower cells (cells behind the leading edge) with several FA (Figure 3.19) move around the original position in kin2+vin$_{KD}$ (Movie 3.6) and kin2+CAS$_{KD}$ (Movie 3.7). Overall, these findings show MC4 is associated with impaired migration, reduced cell spreading, less FA, loss of directionality and cell polarization.

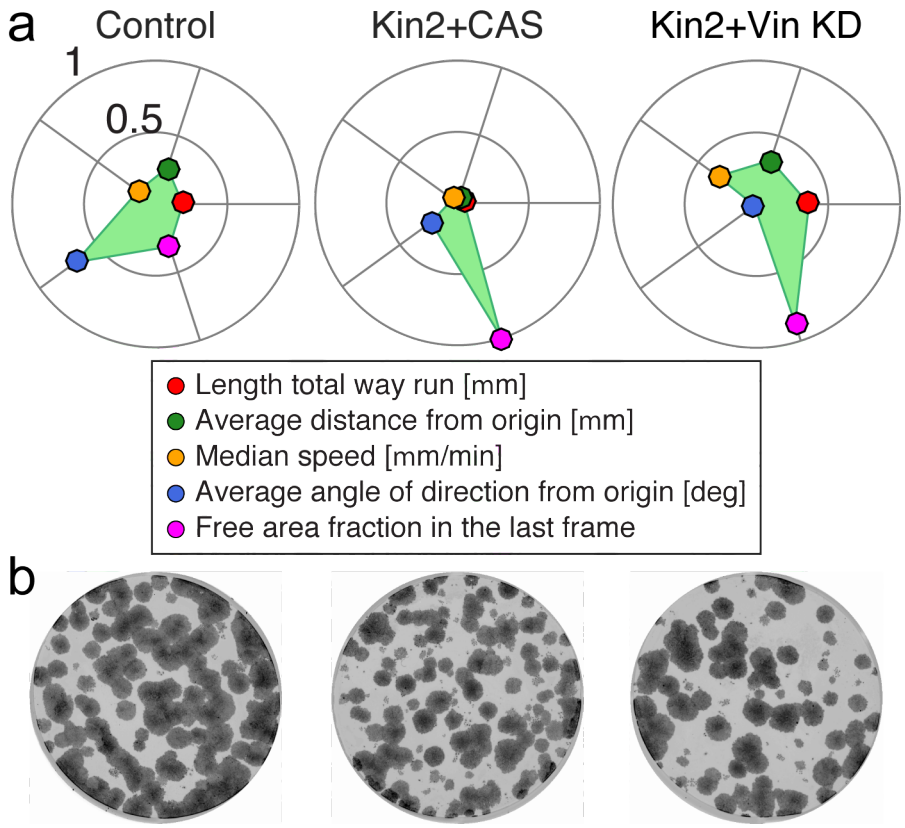


**Figure 3.18 Cell survival, proliferation and migration in kin2+CAS and kin2+vin KD.** (a) The migration profiles indicate the strictly resticted migration of kin2+CAS and Kin2+vin depleted cells as compared to control. Each parameter is plotted in the range of [0 1] and the limits are valid for each profile. (b) Representative images of colony formation assay show marginal reduction in proliferation and survival. All the images were presented under same brightness and contrast settings.

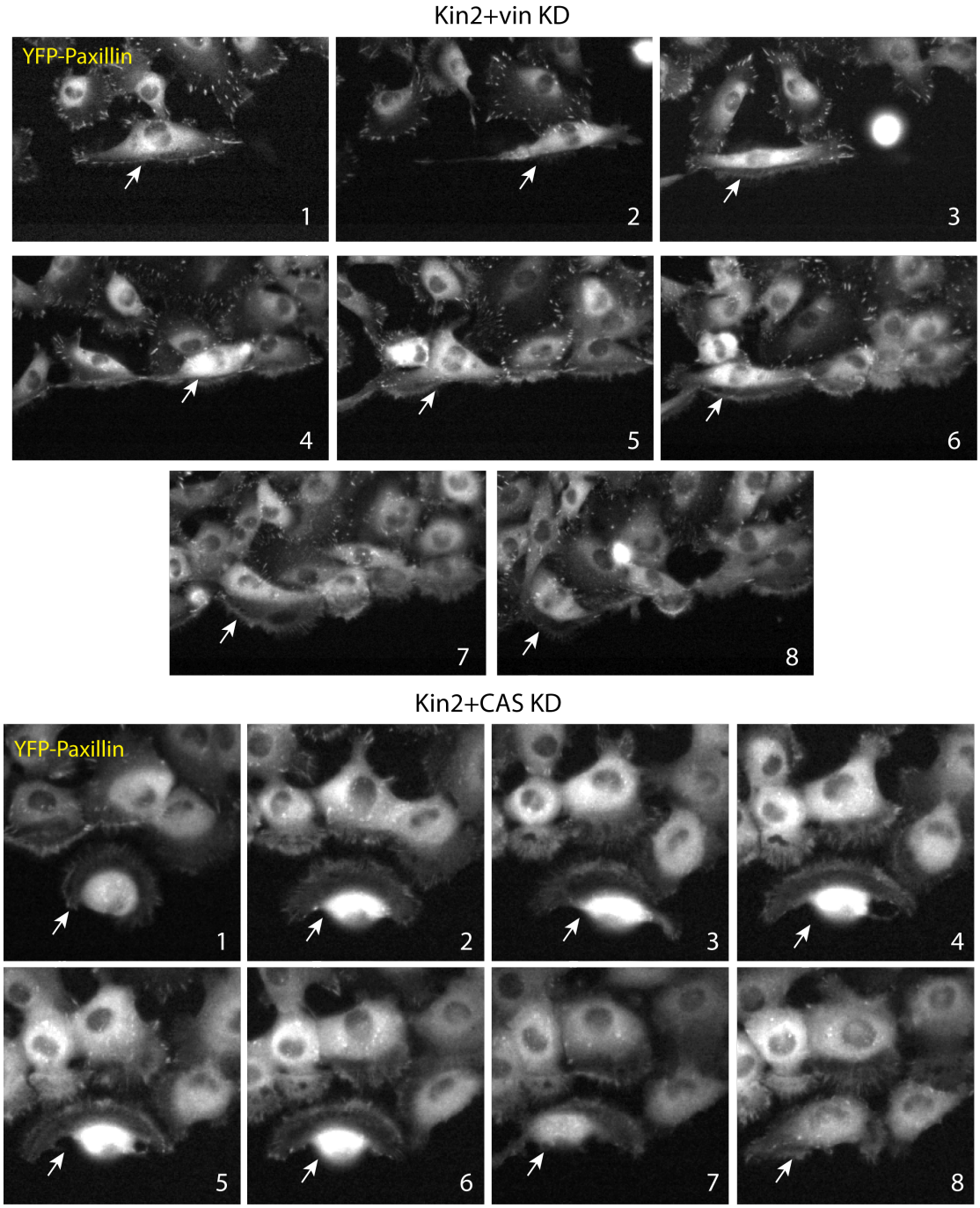


**Figure 3.19 Incapacity of lamellipodia formation and cell morphology change in non-migrating cells in kin2+CAS and kin2+vin KD.** Upper pannel of 8 images specify the kin2+vin KD condition. The cell 'pointed by arrow' exhibit almost no change in shape in 160 min but remained unable to migrate. Each image is taken with the interval of 20 min. Similarly, in case of kin2 and CAS KD, the 'cell pointed by arrow' show same cell size/shape over the period of 160 mins, which failed to migrate. In both KD conditions, there is hardly few FA in cells of the leading edge.

To examine the formation of cytoskeleton and adhesion sites in kin2+$CAS_{KD}$, fixed-cells images were examined. Kin2 and CAS depletion resulted in low spread cells, disorganized actin stress fibers but well-organized tubulin network (Figure 3.20). Tensin-1 was present in FA but fibrillar adhesions were not formed in kin2+$CAS_{KD}$ (Figure 3.20) and kin2+$vin_{KD}$ (data not shown), which suggest these proteins are involved in translocation of tensin-1 to form FB. Notably, tensin-1 was accumulated in focal adhesions only when depletion of FA proteins impaired the migration.

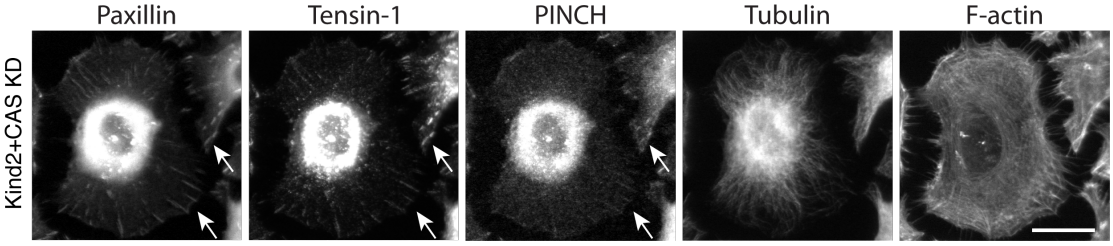


**Figure 3.20 Confirmation of the round cell shape in cells depleted with kin2 and CAS.** Immunostaining of fixed cells depleted with kin2+CAS indiacted few FA containing paxillin and tensin-1, but no PINCH. Actin and tubulin network was re-organized. Scale bar is 20 µm.

### 3.3.5 Cluster 5: Amoeboid-ruffling mode of migration

Cells in MC5 migrate slowly but eventually closed the wound (Figure 3.21a). This migration behavior is featured by the failure to form the lamellipodia. Instead leader cells show membrane ruffling with relatively little number and tiny FA which are distributed at the cell periphery. All the KD conditions in this cluster showe semi-collective cell migration (Figure 3.21b). Although the migration behavior was closely related to MC2, the major difference includes the lower speed of and membrane ruffles in migrating cells in MC5 (Figure 3.11). Based on these features, this migration behavior was named as amoeboid-ruffling mode of migration. The representative example of FAK+$VASP_{KD}$ (Movie 3.8) is included in the supplementary material. Cells depleted with FAK+VASP had relatively organized cytoskeleton, several FA and dislocation of tensin-1 in perinuclear areas (Figure 3.21c).

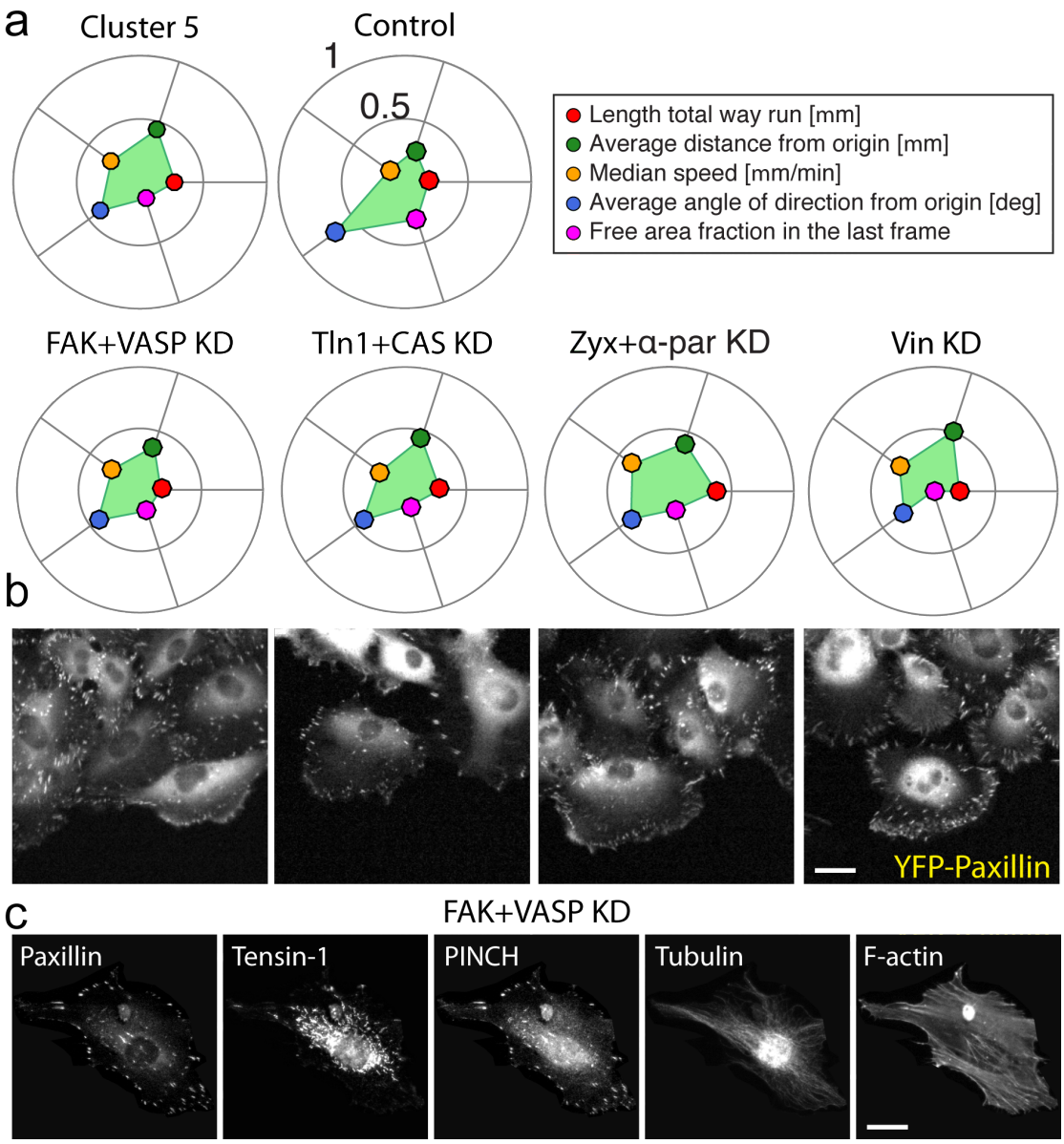


**Figure 3.21 Cluster 5: amoeboid-ruffling mode of migration. (a)** Average migration profile of MC5, profiles of four KD conditions and control**.** Each parameter is plotted in the range of [0 1] and the limits are valid for each profile. (b) Images reveal the improper formation of lamellipodia in leading edge of the cells. Images acquired from live cell imaging using 20x objective. Imaging of YFP-paxillin indicate few and small YFP-paxillin positive FA in the selected KD conditions. (c) Cells co-depleted with FAK and VASP were immunostained and imaged with 40x objective for specified proteins. Scale bar is 20 µm.

### 3.3.6 Cluster 6: Lamellipodial mode of migration

The control cells, α-par-depleted and CAS-depleted cells in addition to three combinations showed relatively similar migration behavior as control (Figure 3.22). These conditions exhibited similar cell size, shape, formation of numerous FA and collective migration as a monolayer. These cells produce lamellipodia in the front

edge to facilitate the directed migration. Relatively thin and long FA was observed in vin+$CAS_{KD}$ and vin+$VASP_{KD}$ (Figure 3.22). Representative example of vin+$CAS_{KD}$ (Movie 3.9) is included in supplementary material. The KD conditions in MC6 define the characteristic mode of migration for fibroblasts.

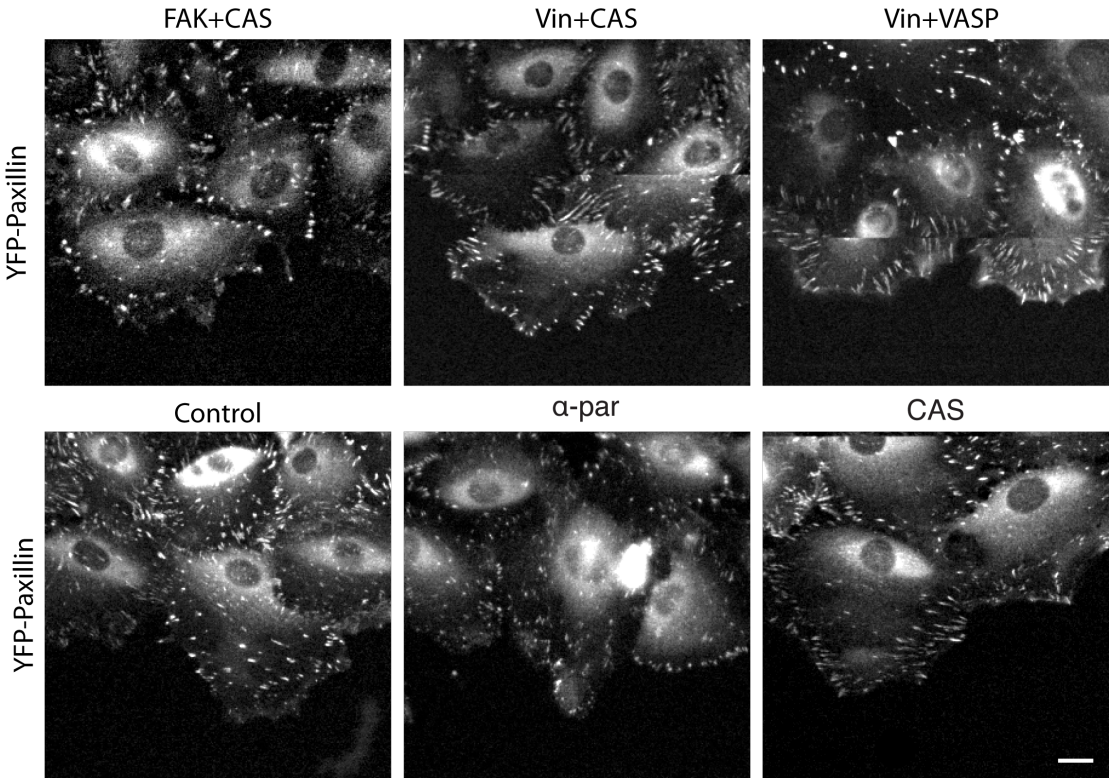


**Figure 3.22 Cluster 6 represent lamellipodial mode of migration.** Shown are the representative images from time-lapse video microscopy of cells either transfected with FAK+CAS, vin+CAS, vin+VASP, CAS, α-par or control. Scale bar is 10 μm.

### 3.3.7 Cluster 7: Semi amoeboid-pseudopodal mode of migration

Migration profile of cluster 7 exhibits higher speed as compared to the control and relatively directed migration as indicated by compass plots resulting in wound closure (Figure 3.23a,c). Cells in these KD conditions were semi-round, make a large protrusion (lacking FA) due to the less defined front and rear of the cell (Figure 3.23b). The members of this cluster display semi-collective type of migration (Figure 3.23b). The representative time-lapse video of VASP+$CAS_{KD}$ (Movie 3.10) is included in supplementary information. Based on these features, I referred this mode as semi amoeboid-pseudopodal, however, presence of many FA (Figure 3.23b), was not in line with the less adhesive feature of amoeboid-pseudopodal mode[193].

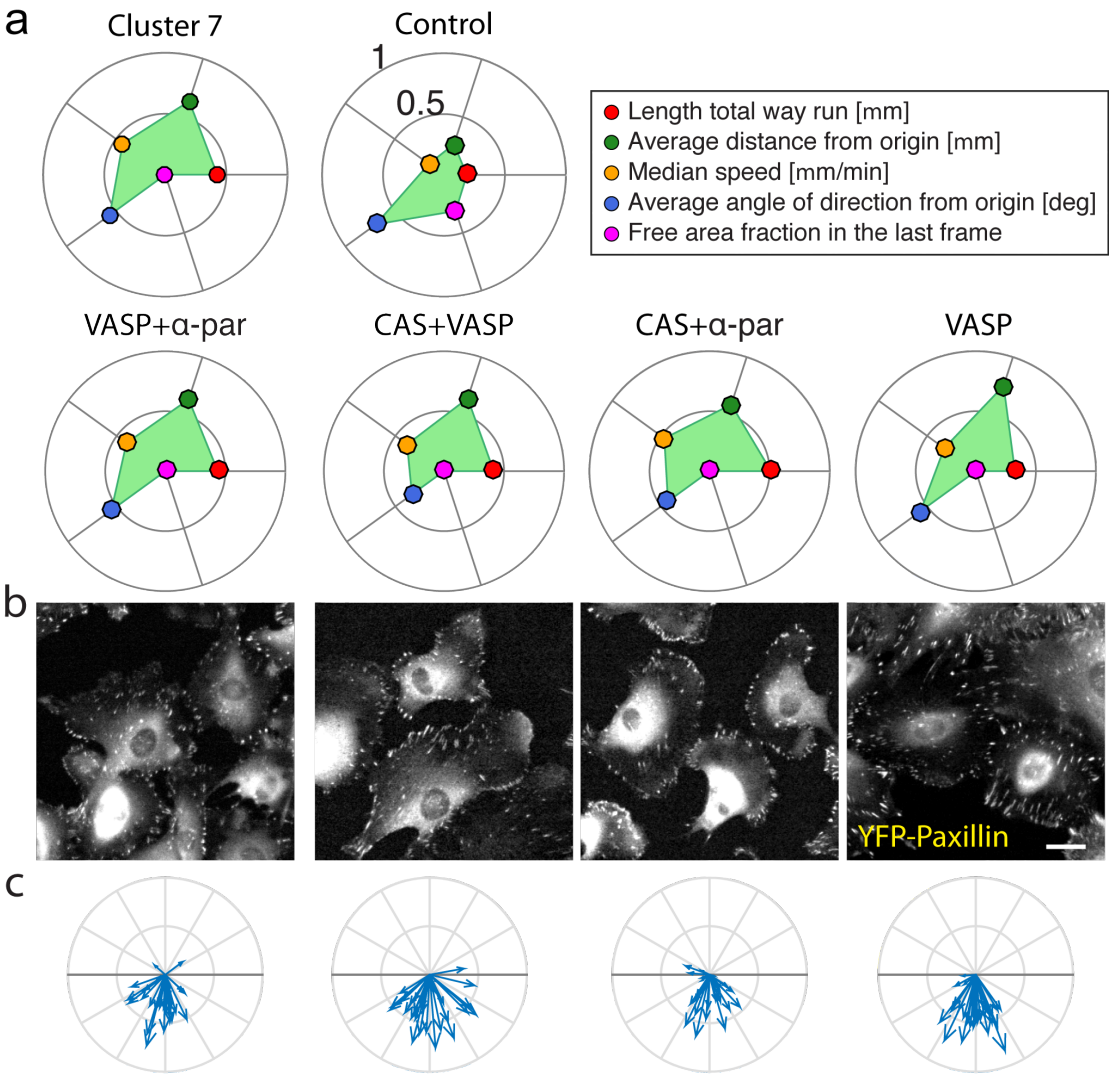


**Figure 3.23 Semi amoeboid-pseudopodal mode of migration exhibited by KD conditions of MC7.** (a) Shown here are the migration profiles of cluster 7 (average profile), control and four KD conditions. Each parameter is plotted in the range of [0 1] and the limits are valid for each profile. (b) Images from time-lapse video microscopy for labeled KD conditions signifying the cell morphology and FA. Cells were imaged for YFP-paxillin. Scale bar is 20 µm. (c) Compass plots indicate the angle of each cell. In total, the data from 30 randomly selected cells is presented.

Fixed cell imaging confirmed the peripheral arrangement of FA and semi-round cell morphology in case of VASP+CAS$_{KD}$ and VASP+α-par$_{KD}$ (Figure 3.24). Tensin-1 was mislocalized to perinuclear areas in both of the KD conditions. Notably, mislocalization of tensin-1 was observed in those KD conditions which positively regulate the migration. Cytoskeleton observed in these cells was well spread and organized except marginally disturbed SF at the cell periphery (Figure 3.24). Overall

MC7 is involved in the regulation of FA, FB and lamellipodia formation as well as stabilization of FA to control the speed of migration.

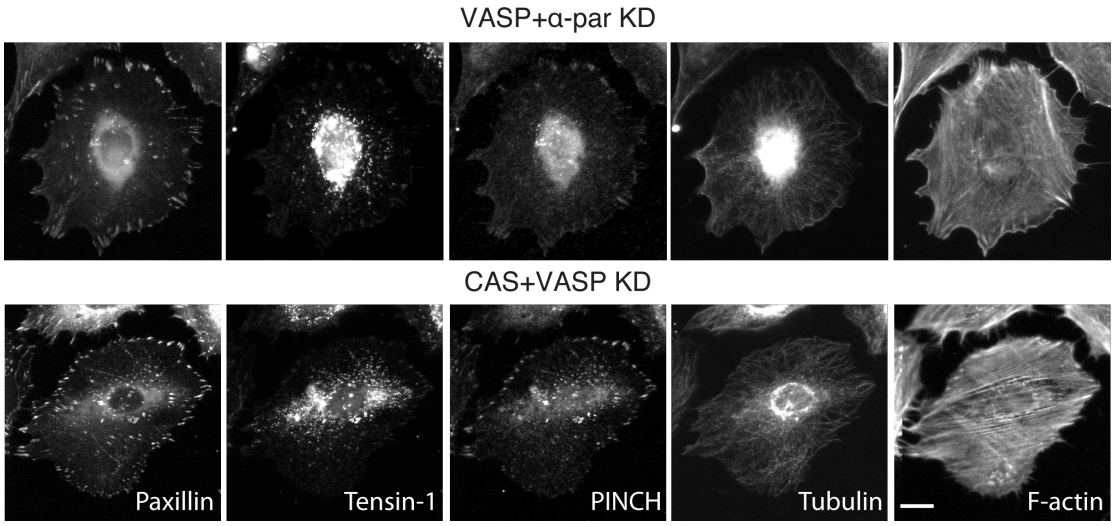


**Figure 3.24 Cytoskeleton organization and adhesion site formation in KD conditions of MC7.** Two pairs VASP+CAS KD and VASP+α-par KD were immunostained for the proteins labeled in the figure and imaged by using 40x objective. Scale bar is 20 μm.

### 3.3.8 Cluster 8: Confined and sporadic mode of migration

The KD conditions in MC8 negatively regulate cell migration (Figure 3.25a). which is associated with less spread cells, fewer peripheral FA and improper lamellipodia formation as indicated by ILK KD combinations; ILK+tln1, ILK+kin2, ILK+α-act1, ILK+α-par (Figure 3.25b). Furthermore, these protein-pairs resulted in the defective polarization of the cells, either introducing protrusions on opposite ends (bipolar-phenotype) or in all directions (Figure 3.25b, c). Based on the defects observed, it is evident that these proteins are responsible for the formation of focal adhesion and lamellipodia as well as controlling the directed cell migration. It is noteworthy, in all KD conditions of MC8, one component was integrin-binding protein (tln1, kin2, ILK) and the other was actin regulatory protein (α-par, α-act1), indicating their combined depletion necessarily impaired the migration. In case of individual knockdowns, only kin2 negatively regulates the migration contrary to the positive regulation of cell migration upon depletions of tln1 or ILK (Figure 3.11).

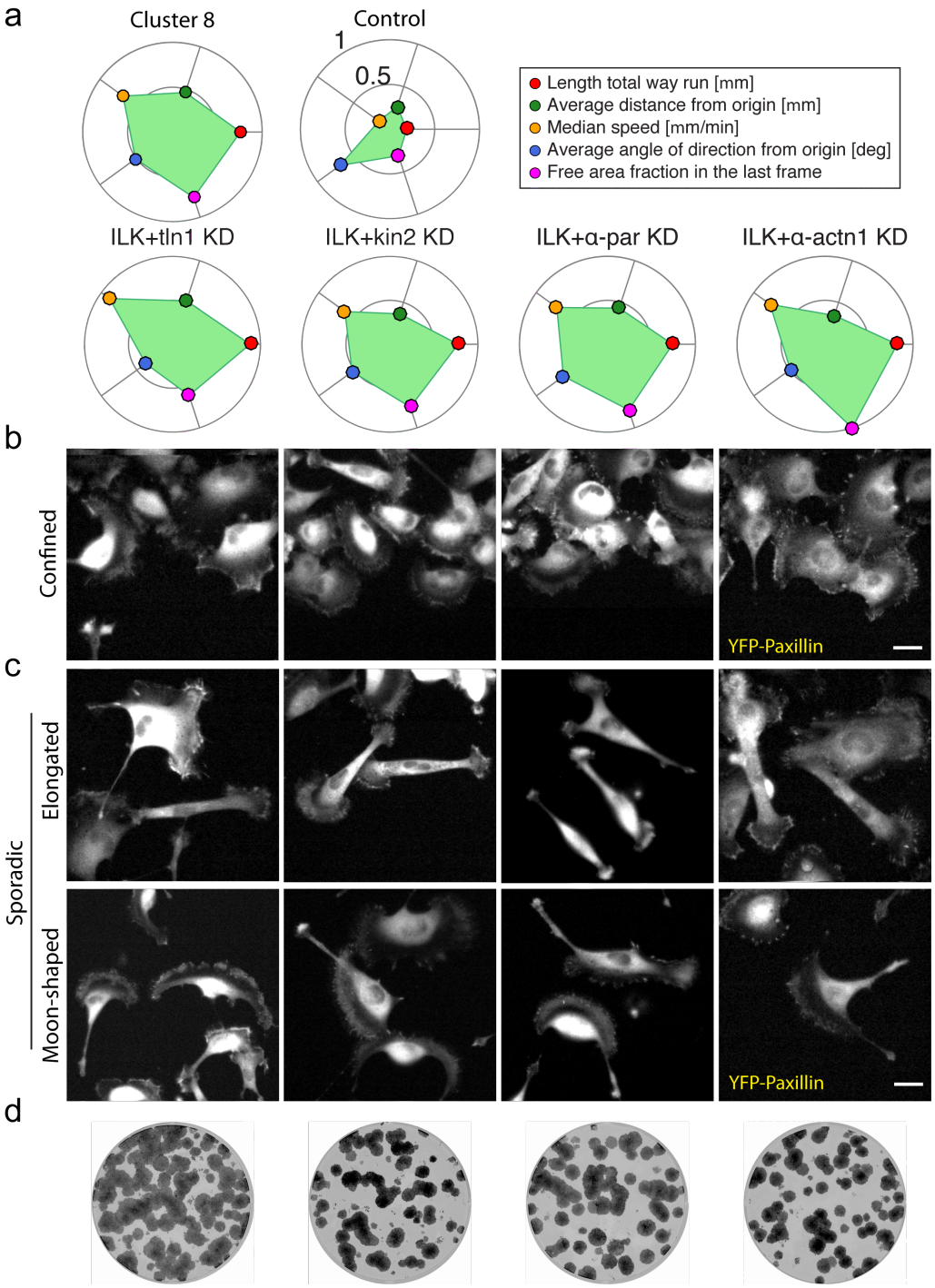


**Figure 3.25 Heterogeneous modes of migration in cluster 8.** (a) Average migration profile of cluster 8, control and four KD conditions. Each parameter is plotted in the range of [0 1] and the limits are valid for each profile. (b) Live cell video microscopy of specified KD conditions during wound healing assay indicate the cell morphology associated with the confined modality (c) Indicated KD conditions gave rise to sporadic modality with two distinct cell morphologies; cylindrical cells and moon shaped cells. Scale bar is 20 µm. (d) Representative images of each KD condition for colony formation. All the images were presented under the same brightness and contrast settings.

The most significant observation was the concurrent presence of two distinct migration sub-modalities showing the unrelated behavior. One of the sub-modality resembled to the well-defined confined mode of migration (as seen in MC4) in which cells failed to migrate. Representative example of ILK+tln1$_{KD}$ display the confined modality is shown in Movie 3.11. Alternatively, cells display fast migration in random manner and switch rapidly between different cellular shapes referred as sporadic modality. The representative example of sporadic modality (ILK+tln1$_{KD}$) is shown in Movie 3.12. In sporadic sub-modality, the knockdown combinations of ILK disclose heterogeneous cellular phenotypes including long, thin and moon-shape cells (termed in this study) as shown in Figure 3.25c. In both sub-modalities, cells have few FA and they have lost the cell-cell contact during migration (Figure 3.25b, c). The depletion of ILK along with kin2, α-act1 and α-par negatively regulates the cell survival and proliferation in similar manner except ILK+tln1$_{KD}$ where colony forming ability matches to the control (Figure 3.25c).

Time-lapse images revealed the presence of both above-mentioned migration sub-modalities in ILK combinations (1) confined migration ILK+tln1$_{KD}$ (Movie 3.11), ILK+kin2$_{KD}$ (Movie 3.13), ILK+α-act1$_{KD}$ (Movie 3.15) and ILK+α-par$_{KD}$ (Movie 3.17), (2) sporadic migration ILK+tln1$_{KD}$ (Movie 3.12), ILK+kin2$_{KD}$ (Movie 3.14), ILK+α-act1$_{KD}$ (Movie 3.16) and ILK+α-par$_{KD}$ (Movie 3.18).

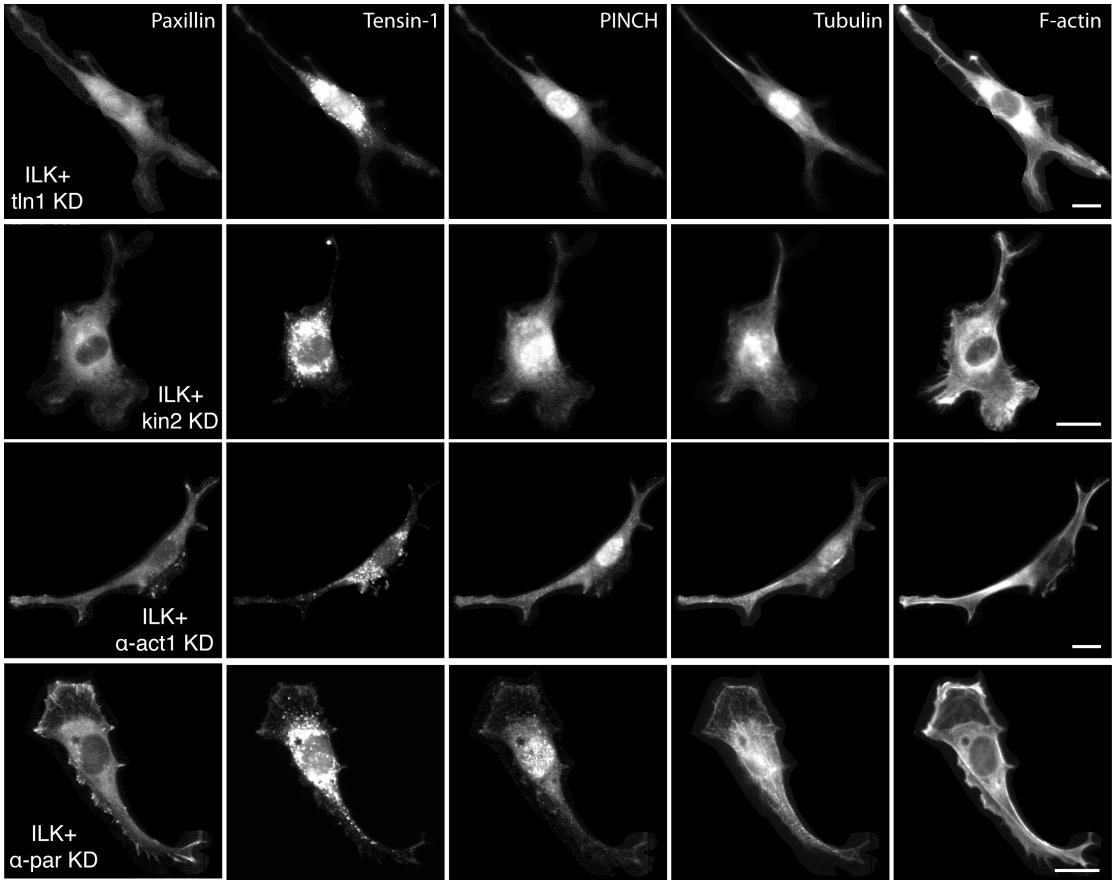


**Figure 3.26 Cellular phenotypes associated with sporadic sub-modality in ILK KD combinations from cluster 8.** REF52 cells were transfected with siRNA of specified proteins for 48 h. Then cells were fixed and immunosted for the stated proteins. Scale bar is 20 μm.

Fixed cells imaging in above-mentioned ILK combinations aided the visualization of cytoskeletal organization and adhesion sites formation. Imaging confirmed the presence of distinct cellular phenotypes in these KD conditions related in sub-modalities observed in wound healing assay. Long and thin cells had few FA which contains paxillin while PINCH was absent. Cells failed to form fibrillar adhesion (shown by the staining of tensin-1) while the cytoskeleton was condensed and severely disorganized (Figure 3.27).

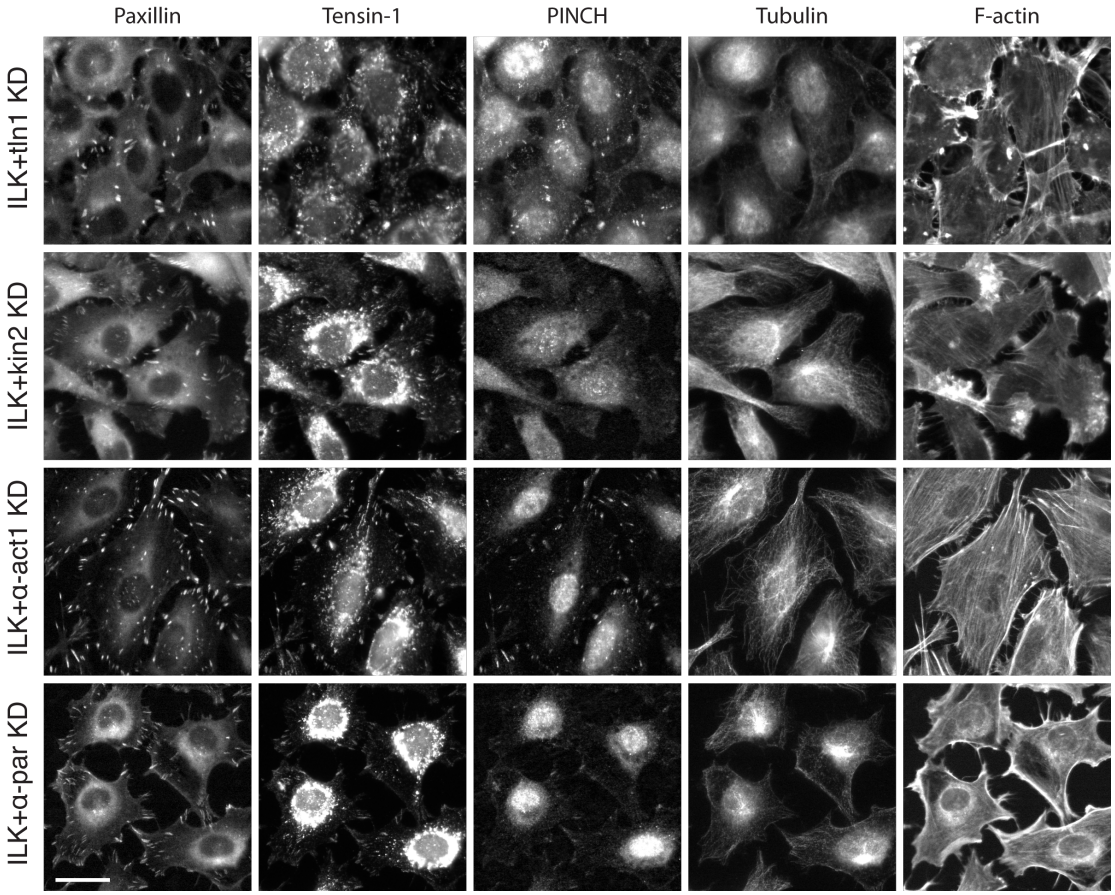


**Figure 3.27 Spread cells associated with the confined sub-modality in ILK KD combinations from cluster 8.** Immunostaining and imaging of ILK KD combinations revealed the formation of several FA in ILK+tln1, ILK+kin2, ILK+α-act1 and ILK+α-par. Tensin-1 was present in FA in all combinations as well as marginally accumalated around the nuclues. PINCH was absent in all combinations except low expression in case of ILK and α-act1 KD. Actin and tubulin cytoskeleton was disorganized and actin was accumalated in the cell edges and boarders. Scale bar is 20 μm.

Cells in confined mode produce relatively more FA with the characteristic presence of paxillin (Figure 3.27). The absence of PINCH in these cells is consistent with the findings of Gagne *et al.,* 2010. These authors reported the lower levels of PINCH and α-parvin in cells depleted with ILK, due to the disruption of PIP complex[185]. Tensin-1 was present in FA but the cells failed to form mature FB. In addition, cytoskeleton was disorganized and concentrated in the cell edges or borders (Figure 3.27). These findings suggest that proteins in MC8 induce cell migration, adhesion site formation (FA and FB), cytoskeletal organization, protrusions, cell polarization, directed and collective cell migration.

### 3.3.9 Cluster 9: Lamellipodial-tethering mode of migration

The 11 KD conditions of MC9 are comprised of cytoskeletal and force modulating proteins such as α-act1, α-par, VASP, tln1 and vin. The larger track lengths indicate that longer distance covered by the fast migrating cells (Figure 3.28a). Time-lapse images from wound healing assay show heterogeneous cell sizes and shapes with numerous focal adhesions (Figure 3.28b). The distinguishing feature was the formation of single to multiple tethers in the leading cells in addition to the multiple small lamellipodia (Figure 3.28b). Live-cell imaging showed random and fast movement of cells as well as the formation of tethers as shown in tln1+vin KD (Movie 3.19). Based on these features, the migration behavior was termed as lamellipodial-tethering mode of migration. MC9 KD conditions up-regulated migration that suggests their role in FA stabilization, lamellipodia formation and control of directionality.

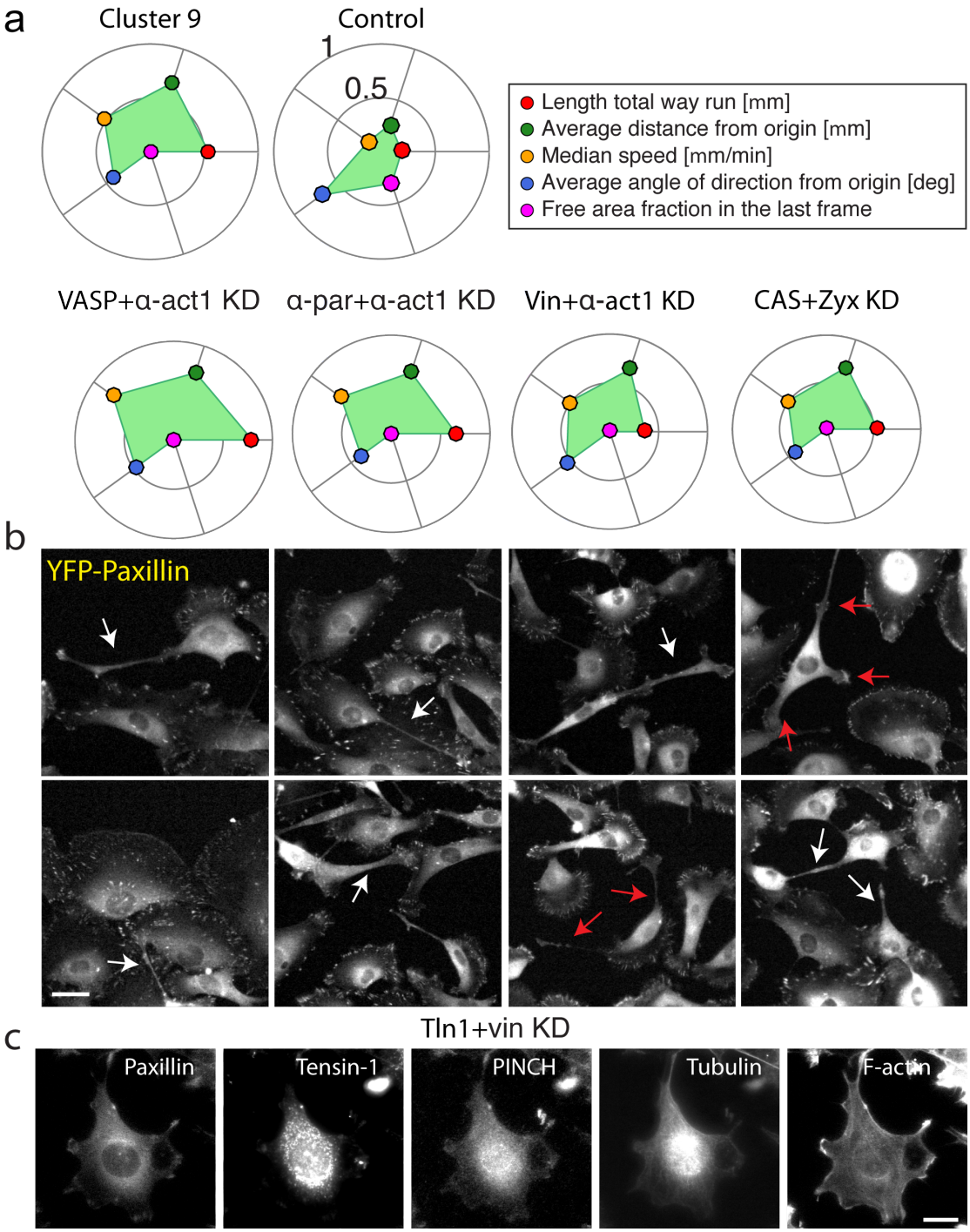


**Figure 3.28 MC9 exhibit lamellipodia-tethering mode of migration.** (a) Avergae migration profiles of cluster 9, control and four representative KD conditions of MC9 are presented. Each parameter is plotted in the range of [0 1] and the limits are valid for each profile. (b) REF52 cells transfected with indicated KD conditions were imaged during wound healing assay. The leading cells form single (white arrows) or multiple tethers (red arrows). Scale bar is 30 µm. (c) Representative images of immunostaining of the cells depleted with tln1 and vin. Cells were stained for indicated proteins. Scale bar is 20 µm.

Immunostaining confirmed the presence of relatively large cells and the formation of tethers. Disorganized actin-tubulin cytoskeleton was observed in tln1+vin KD. However, tensin-1 was absent from FA and no fibrillar adhesions were formed (Figure 3.28c). The mislocalization of tensin-1 suggests strong involvement of MC9 proteins in controlling tensin-1 localization.

For each cluster manually assessed cellular phenotypes to define modes of migration are mention in Table 3.3.

| **Mode of Migration** | **Cell shape** | **Protru-sions** | **FA** | **FB** | **Stress fibers** | **Micro-tubules** | **Migration form** |
|---|---|---|---|---|---|---|---|
| **MC1** *3D Lamellipodial* | Elongated | Yes | Low/No | No | No | No | Individual |
| **MC2** *Amoeboid-blebby* | Roundish | No | High (P) | No | Thin | Yes | Semi |
| **MC3** | Multiple | | | No | | | Random movement |
| *Confined* | | No | Medium | | Thick | Yes | |
| *Discontinuous* | | Yes | Low | | No | No | |
| **MC4** *Confined* | Round | No | Medium | No | Thick | Yes | Random movement |
| **MC5** *Amoeboid ruffling* | Roundish | No | High (P) | No | Thin | Yes | Collective |
| **MC6** *2D Lamellipodial* | Spindle shape | Yes | High | Yes | Like-control | Yes | Collective |
| **MC7** *Amoeboid pseudopodal* | Roundish | No | High (P) | No | Thin | Yes | Semi |
| **MC8** | Multiple | | | | | | Random movement |
| *Confined* | | No | Medium | | Thick | Yes | |
| *Sporadic* | | No | Low | | No | No | |
| **MC9** *Lamellipodial tethering* | Multiple | Yes | High or No | No | No | No | Tethers |

**Table 3.3 Summary of selected determinants of modes of migration.** Table include cellular phenotypes, manually assessed from wound healing assay data and immunostaining of FA and FB proteins. (P) - pheripheral arrangeent of FA.

## 3.4 FA proteins regulate tensin-1 localization and adhesion sites segregation

Immunostaining of cells depleted with act1+zyx showed failure to assemble the adhesion sites. The same KD condition were associated with fast migration (Figure 3.13). In contrast, FAK+tln1 depleted cells formed tensin-1 positive FA and the same KD condition reduced migration (Figure 3.16). To find out the defects of tensin-1 localization and its association with cell migration, KD conditions were divided into two groups based on the free area fraction.

First group comprised of KD conditions from MC3, 4, and 8 in which all KD pairs impaired the cell migration. Fixed-cells imaging screen revealed the presence of tensin-1 in FAs as well as slight accumulation of tensin-1 around the nucleus in all the KD conditions which have reduced the migration. Out of 22 KD conditions a total of 13 combinations and 1 single KD (kin2) display markedly decreased migration (Figure S16). The representative images of these combinations with paxillin and tensin-1 staining are shown in Figure 3.29. Most of these pairs produced plenty of FA (Figure 3.29a) while other have less FA (Figure 3.29b), observed with the presence of paxillin and tensin-1. These cells failed to form fibrillar adhesions (Figure 3.29), suggesting the failure of segregation of tensin-1 to develop into FB. The selection of tensin-1 facilitated to determine its localization in both adhesions sites in comparison to its other isoform tensin-2 which is predominantly present in FA and tensin-3 which is exclusively present in FB. Furthermore, tensin-1 is considered a marker of mature FB[151,195]. In the control cells, the proper localization of tensin-1 in FA and FB ensures the segregation of FA into FB (Figure 3.30).

The second group included KD conditions in MC1, 2, 5, 7 and 9 that led to the enhanced migration. In all the combinations displaying fast migration, tensin-1 mislocalizes from FA to the perinuclear areas (Figure 3.32). Out of 28 KD conditions, 16 combinations prominently enhanced the cell migration (Figure S17) in which tensin-1 expression was checked by fixed-cell imaging screen. Notably cells in some combinations formed plenty of paxillin-positive FA even though tensin-1 was not present (Figure 3.32a). Results show the strong association of these KD pairs in regulating the localization of tensin-1.

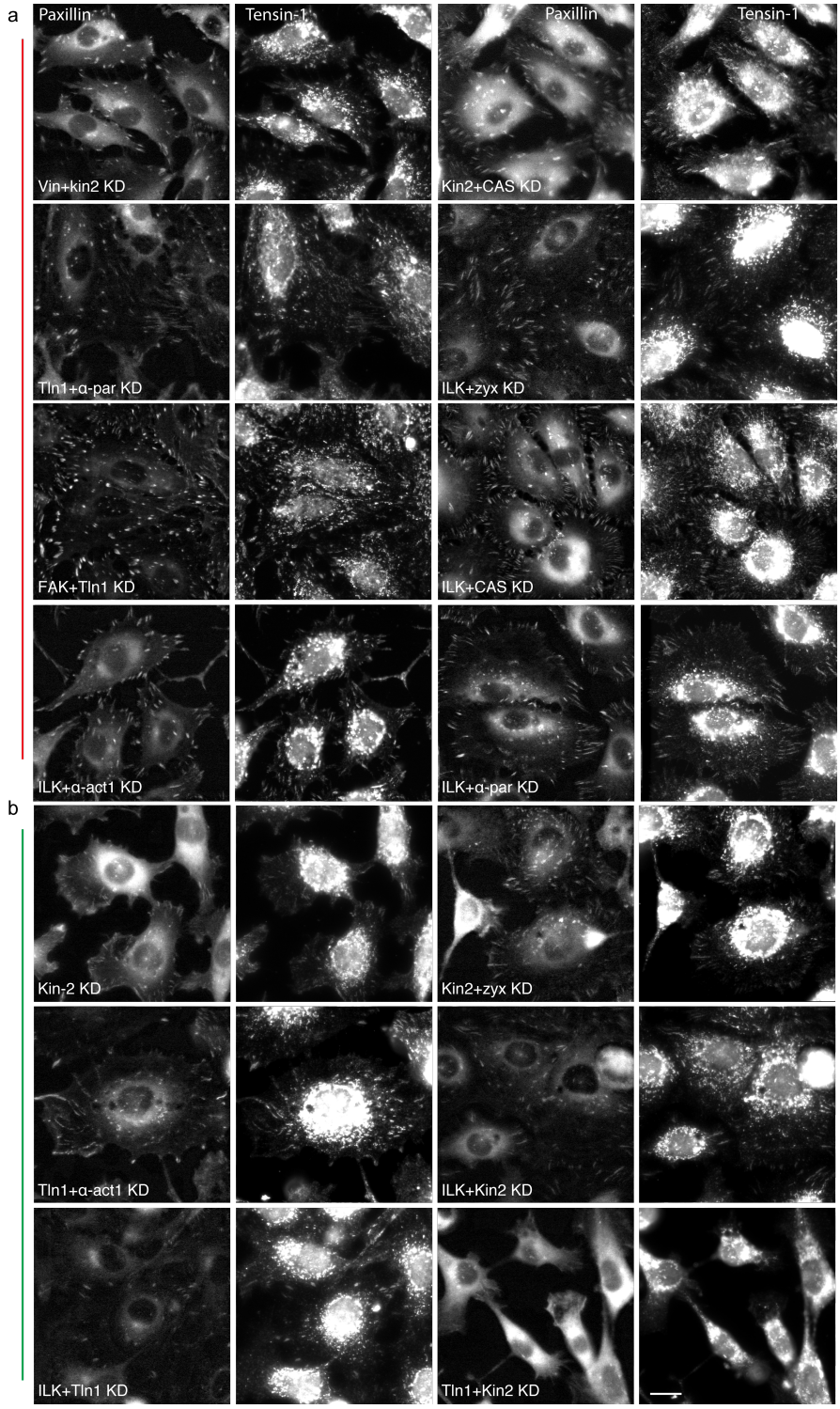


**Figure 3.29 Tensin-1 localization in FA in KD conditions associated with impaired migration.** Imaging of tensin-1 and paxillin in the indicated KD conditions show the failure of tensin-1 dependant FB formation. Scale bar is 20 μm.

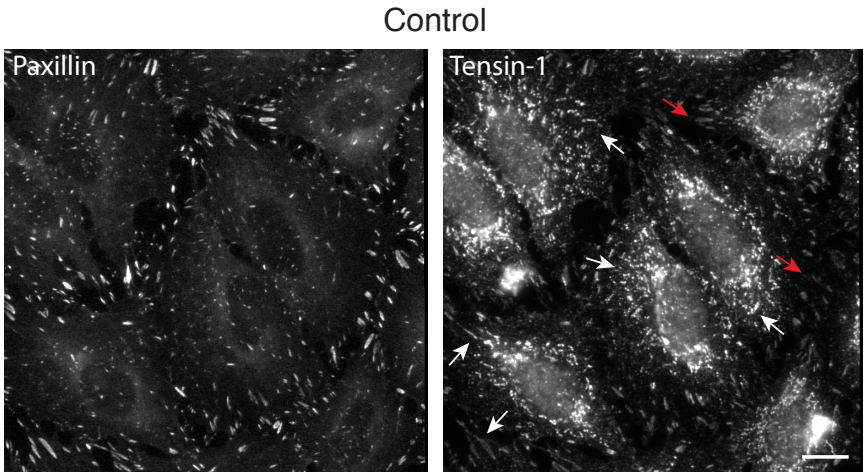


**Figure 3.30 Tensin-1 localizes in focal adhesions and fibrillar adhesion in control cells.** Imaging of tensin-1 and paxillin in control cells. White arrows in tensin-1 image indicate beaded and thread like FB whereas red arrows indicate its presence in FA. Scale bar is 20 µm.

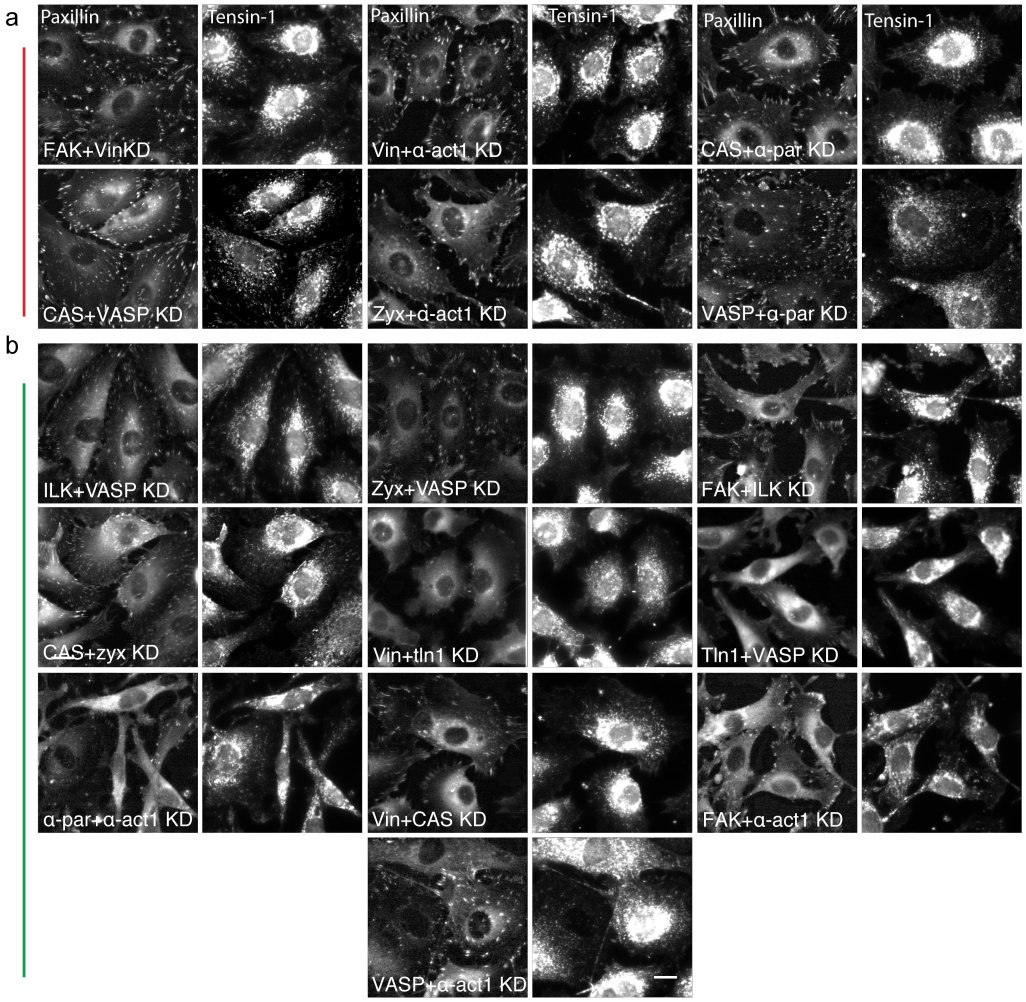


**Figure 3.31 Set of KD conditions induce the mislocalization of tensin-1.** Imaging of tensin-1 and paxillin in the indicated KD conditions. Scale bar is 20 µm.

### 3.4.1 Kindlin-2 and talin-1 mutually regulate cell survival, proliferation and migration

Cells depleted with tln1 showed cell survival similar to the control whereas the proliferation is reduced marginally. In contrast, kin2 KD clearly and significantly reduced CA and SF (Figure 3.32a), indicating its strong involvement in the regulation of cell survival and proliferation as compared to tln1 KD. Interestingly, the combined depletion of tln1 and kin2 (survival and proliferation cluster 5) drastically and significantly reduced the colony area and survival fraction as compared to the corresponding individual KDs (Figure 3.32a). This finding suggests the involvement of tln1 and kin2 in different signaling cascades. Furthermore, it suggests the strong negative epistatic interaction between tln1 and kin2 that critically regulates cell survival and proliferation.

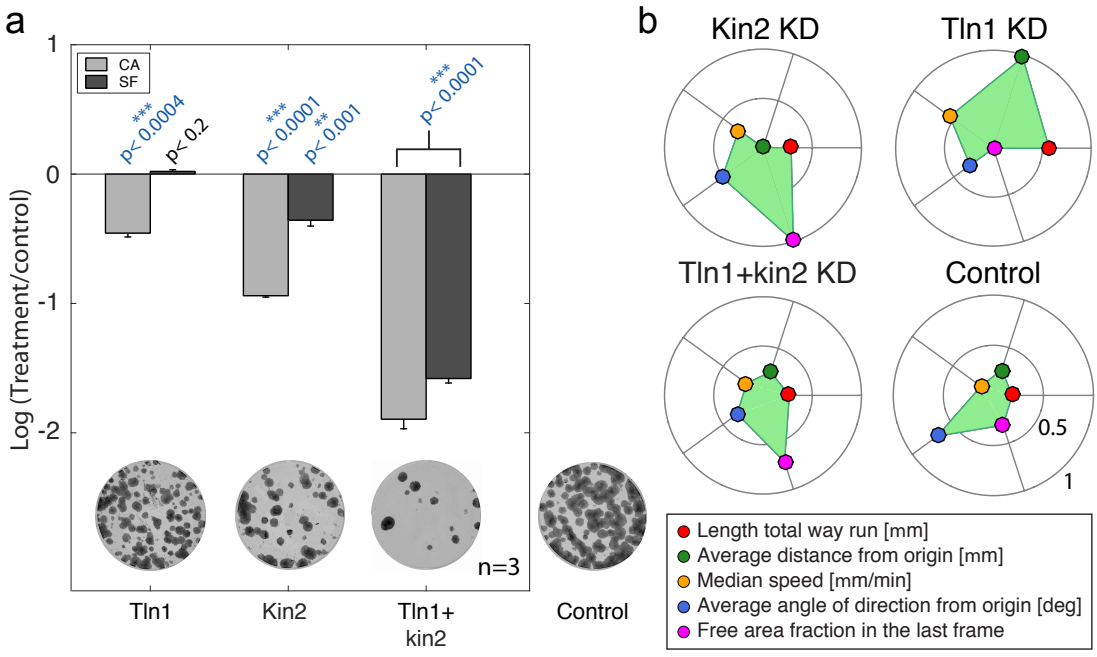


**Figure 3.32 Kin2 and tln1 critically regulate cell survival, prolifetration and migration.** (a) The individual and mutual effects of tln1 and kin2 on colony area and survival fraction is indicated by bar plots and representative colony image. The values were normalized to the control and represented in log scale. Values close to zero indicate effect similar to the control. p-values are mentioned above each bar. Error bars represent standard error of mean (SEM). All the images were presented under the same brightness and contrast settings. (b) Migration profiles of the specified double and single KD conditions to compare the motility behavior. Each parameter is plotted in the range of [0 1] and the limits are valid for each profile.

I hypothesized whether kin2 have a different role in cell migration as compared to tln1. We found tln1 KD was associated with randomly moving fast cells due to the changes in cellular morphologies and fewer FA (Movie 3.20) led to the enhanced migration (Figure 3.32) indicated by wound closure (Figure S18). Tln1-depleted cells manifested multi-lamellipodial mode of migration (described in section 3.3.9). In contrast, kin2 exhibited confined mode of migration (Figure 3.32b) with cells having few adhesion sites (Movie 3.21) (described in section 3.3.4). These results show the prominent role of tln1 and kin2 in the regulation of migration but in a distinct manner. Cells co-depleted with Tln1 and kin2 showed adverse effect on migration and exhibited confined mode of migration (Figure 3.32b) as compared to lamellipodial mode of migration in control cells (Movie 3.2). Lamellipodial mode of migration is described in section 3.3.6. Time-lapse video microscopy revealed tln1+kin2$_{KD}$ cells failed to form YFP-paxillin positive FA (Movie 3.22). These results clearly show different role of tln1 and kin2 in cell motility.

To investigate the significance of concerted activity of kin2 and tln1 in the formation of adhesion sites, results of fixed-cell imaging screen were compared with individual and combined depletion of proteins. Tln1$_{KD}$ (Figure 3.33a) and kin2$_{KD}$ (Figure 3.33b) led to the reduction in the number of FA and disorganization of cytoskeleton. Reduction in the number of FA was consistent with the published reports of tln1[103,177] and kin2[196]. Kin2 depleted cells displayed severe reduction in cell spreading as compared to the control (Figure 3.33d). Tensin-1 was present in FA in kin2-depleted cells but these cells failed to form FB and there was no dectable tensin-1 positive adhesion sites in tln1-depleted cells (Figure 3.33b, c). The co-depletion of tln1 and kin2 showed failure to from focal adhesions and fibrillar adhesions as indicated by paxillin, PINCH and tensin-1 staining (Figure 3.33d). The massive disorganization of actin cytoskeleton and microtubules network was coupled with severe effects on cell morphology (Figure 3.33d) as compared to the control (Figure 3.33c) and individual protein depletions (Figure 3.33a, b). These results indicate the combined function of tln1 and kin2 is essential for the formation of adhesion sites.

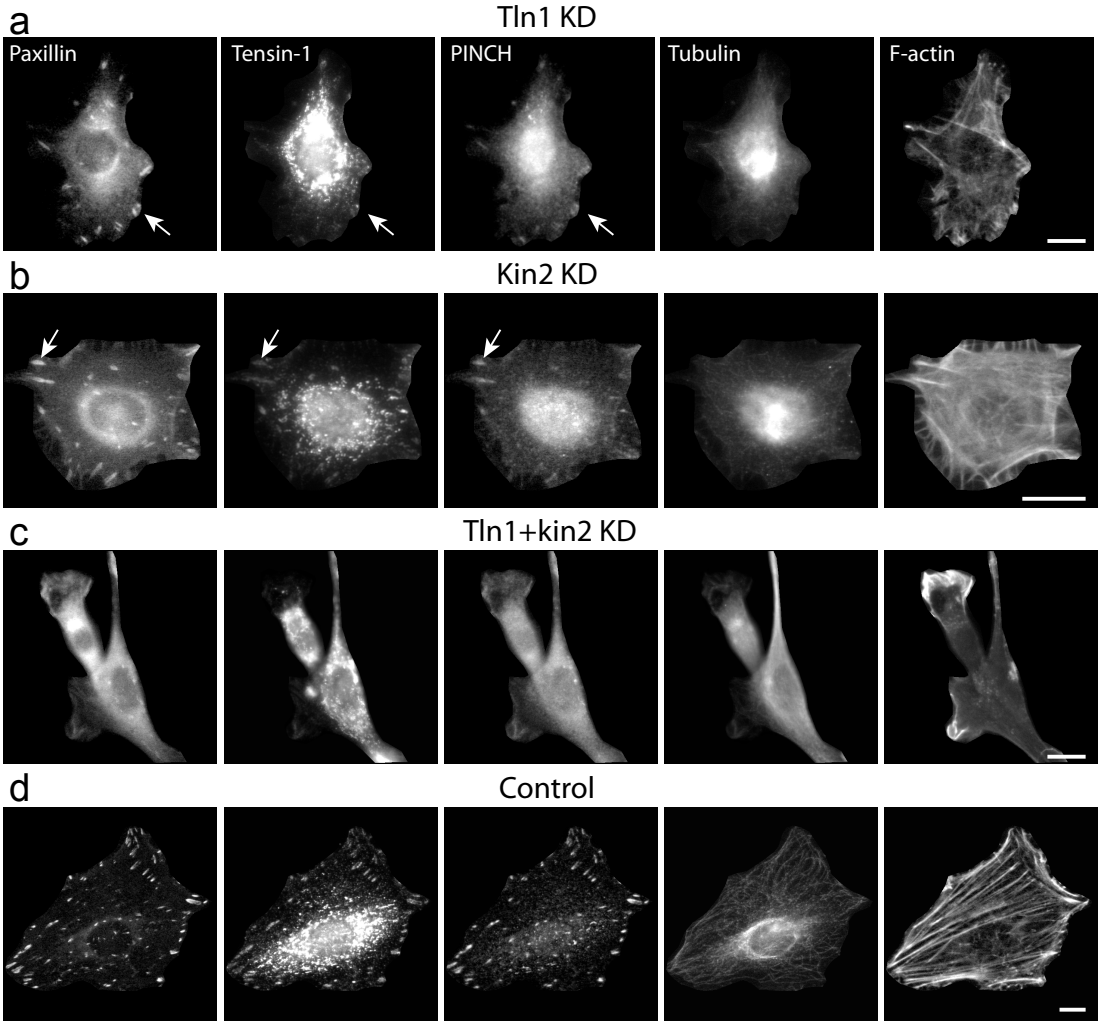


**Figure 3.33 Immunostaining revealed failure of adhesion sites formation in tln1+kin2 KD.** REF52 cells were transfected with (a) tln1 (b) kin2 (c) tln1 and kin2 (d) control, fixed and immunostained for adhesion sites and cytoskeletal proteins. Scale bar is 10 μm.

# 4. Discussion

## 4.1 Functional modules of focal adhesion proteins

Cell-matrix adhesion sites; a complex network of proteins are fundamental for sensing extra cellular environment to perform cellular processes such as adhesion and migration. In order to achieve these multitude functionalities, FA proteins are organized in a certain fashion to perform the diverse tasks in a systematic manner. In this study, we have shown that FA proteins are arranged into functional modules, and that each of these modules are responsible to regulate distinct aspects of the adhesion segregation process and cell locomotion.

We functionally characterized core FA proteins in distinct modules for regulating tensin-1-dependent adhesion segregation process (Figure 4.1a). Talin-1[24], kindlin-2[197] and ILK[198] are integrin-binding structural proteins are classified as 'adhesion-segregation module'. Co-depletion of talin-1 and kindlin-2 revealed the concurrent requirement of these proteins for adhesion-based cellular processes (Figure 4.2), defining the 'adhesion-building sub-module' (Figure 4.1a). FA proteins involved in adhesion-based signaling such as FAK[34] and CAS[123,125] are related to a 'signaling module'. Actin cytoskeleton regulatory proteins such as α-actinin-1[40], zyxin[132], and VASP[130] give rise to the 'actin-regulatory module' (Figure 4.1a).

Upon phosphorylation, signaling proteins (FAK, CAS) interact with tensin-1[199]. Depletion of signaling-module proteins revealed their significance in localization of tensin-1. Binding of tensin-1 with actin and its FA localization are independent events[200,201]. Besides signaling module, actin-regulatory module mislocalizes tensin-1 to perinuclear areas, signifying their role in tensin-1 localization. Adhesion-segregation module (ILK, talin-1 and kindlin-2) arrests tensin-1 in FA, delineating their function in the formation of FB. Overall, three newly identified modules are involved in tensin-1-dependent formation of FB and FB translocation from FA (Figure 4.3).

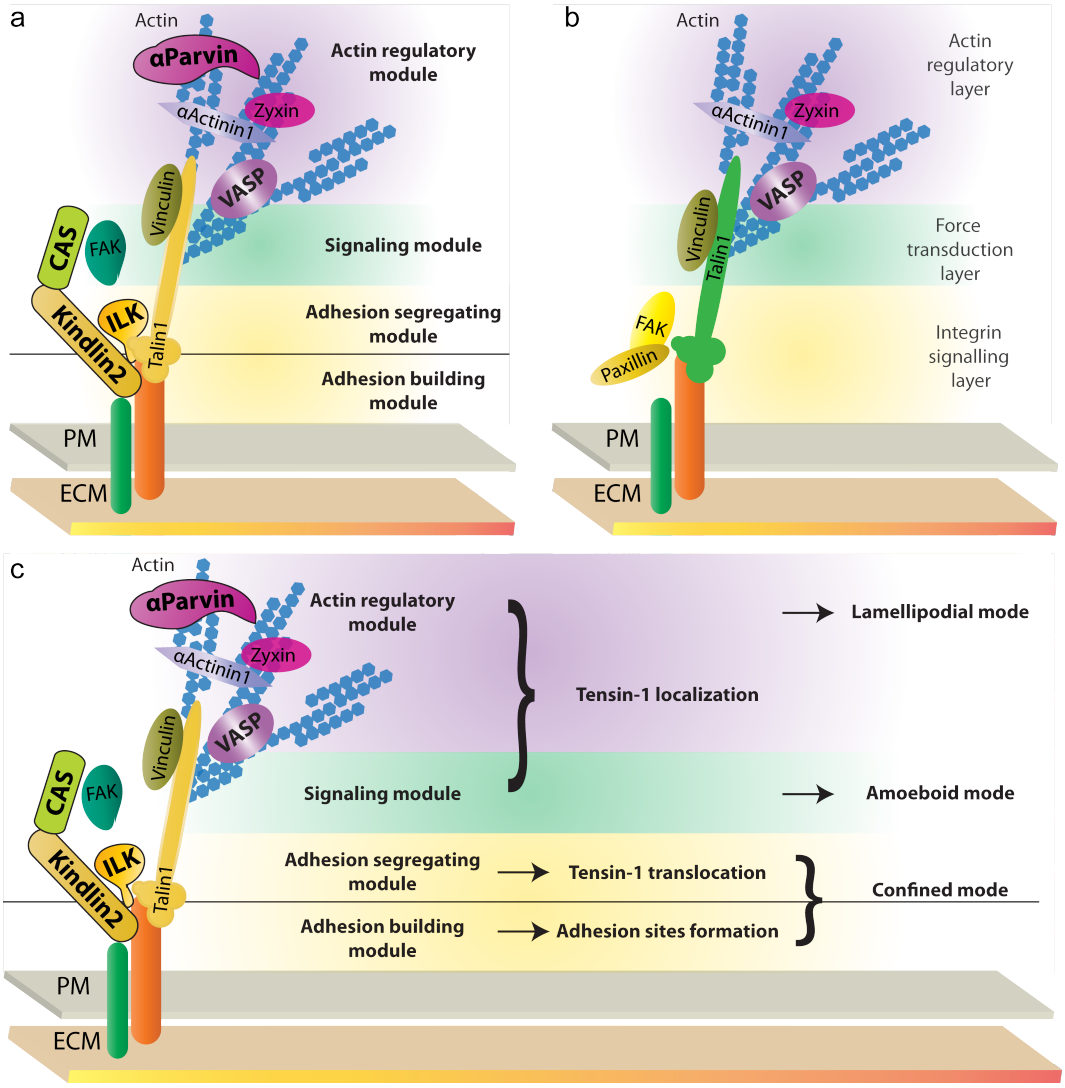


**Figure 4.1 Schematic presentation of FA proteins in distinct functional modules.** (a) Proteins in the adhesion-segregation module including talin-1, kindlin-2, and ILK specify the addition of two new components kindlin-2 and ILK. Signaling-module enlists FAK along with new component CAS. The actin-regulatory module contains α-actinin-1, zyxin, VASP in addition to new component, α-parvin. Vinculin has still overlapping position in signaling and actin-regulatory module, a situation which is very similar to the model proposed by Kanchanawong *et al.,* 2010 (b) Schematic presentation of FA proteins described by Kanchanawong *et al*., 2010 in three signaling layers[24]. (c) Identical modules are associated with distinct modes of the cell migration. See text for detailed discussion.

Interestingly, the same modules regulate the specific stage of classical migration cycle to shape distinct modes of cell migration. The usual process of cell migration starts with polarizing signals via Rac1 that directs actin polymerization to initiate the cellular protrusion followed by their stabilization via integrins-mediated nascent adhesion. Next, newly formed adhesion matures into FA by Rho-mediated actomyosin contractility. Finally, myosin-II disassembles the mature FA to facilitate

migration[73,74,83]. Trailing the same sequence, how distinct modules regulate different stages of migration is explained as follows: (1) Signaling module (FAK, CAS) is involved in the initial stage of migration by strongly modulating the lamellipodia formation evident from 'amoeboid mode' where cells failed to proper lamellipodia. (2) Adhesion building/segregating module (ILK, talin-1, kindlin-2) is involved in "rather middle stage" of migration during which integrin adhesions are formed in cooperation with actin cytoskeleton to promote migration learned from 'confined mode'. (3) Finally, actin-regulatory module is implicated in the last stage of migration where cytoskeleton organization results in maturation of FA and cell polarization to establish front-back cell polarity, understood from 'lamellipodial mode' (Figure 4.4). Taken together, we characterized FA components belonging to structural layers as well as new components in functional modules (Figure 4.1b).

Functional modules were identified based on the combined depletion of proteins. The proteins were selected based on their frequent appearance and their functional relevance e.g. adhesion-segregating module is represented by the structural proteins (talin-1, kidnlin-2 and ILK). Each KD condition associated with respective module is mentioned in Figure S19.

## 4.2 Kindlin-2 cooperates with talin-1 as adhesion-building module

REF52 cells depleted with integrin-binding proteins such as ILK+talin-1 and ILK+kindlin-2 assembled several FA (data not shown). Conversely, cells co-depleted with talin-1+kindlin-2 were unable to form FA and FB, revealed via immunostaining of paxillin, PINCH and tensin-1 (Figure 3.33). Cells individually depleted with talin-1 or kindlin-2 formed few FA (Figure 3.33) which is in line with the previous reports demonstrating the effect of talin-1 and kindlin-2 KD on FA[103,153]. Debatably, cells co-depleted with talin-1 and kindlin-2 were able to spread, perhaps due to the compensation by un-perturbed kindlins or talin-2. The severe defects in actin-tubulin cytoskeleton which is an integral part of adhesion assembly, indicate low chances of adhesion formation in talin-1 and kindlin-2 KD.

The combined KD of talin-1 and kindlin-2 drastically reduced cell survival, proliferation and migration as compared to the individual KD of these proteins (Figure 3.32). We report here talin-1 and kindlin-2 are indispensible for adhesion

sites-assembly and adhesion-mediated cellular processes, therefore considered as adhesion-building module. Taking these findings into account and the role of kindlin-2, for controlling cell spreading in talin independent-manner[2], we postulated that talin-1 and kindlin-2 proteins initiate different pathways to control cell survival/proliferation and migration (discussed below).

### 4.2.1 Kindlin-2 via CAS assembles an essential signaling node

Anchorage-dependent assay screen was employed to find a mechanistic explanation for the involvement of talin-1 and kindlin-2 in alternative signaling pathways. In line with previous report[72], depletion of kindlin-2 reduced the cell survival. Whereas control-like survival was observed in cells depleted with talin-1 which is opposite to the reported reduced survival of metastatic prostrate cancer cells[71]. Our results suggest talin-1 and kindlin-2 exist in compensatory pathways, which is in connection with the binding of talin-1 and kindlin-2 to different motifs of β-integrins[202]. Quite unlikely is the compensation provided by un-perturbed talin-2 for its isoform (talin-1 KD) to rescue the cell survival, which otherwise must have been compensated in combined depletion of talin-1 and kindlin-2 (which is not observed). Our results identified kindlin-2 as a positive/alternative regulator, necessary for mediating downstream signaling for cell survival.

Three FA proteins FAK, CAS and ILK are known modulators of survival and proliferation signaling[3,203] (Figure 4.2). The mechanistic details of these proteins are explained in the box. Their depletion in combination with talin-1 or kindlin-2 suggests the presence of two complementary pathways (Figure 3.7 and Figure 3.9). For example, cells depleted with FAK+kindlin-2 and FAK+talin-1 survived in the similar manner (Figure 3.9), indicating a central position of FAK in both parallel acting proteins. Interestingly, downregulation of kindlin-2 only with CAS (Figure 3.7) and FAK (Figure 3.9) displayed improved survival/proliferation as compared to the individual depletions, which indicate presence of these proteins in the same pathway. Association of Kindlin-2 with FAK is expected due to direct interaction of both proteins with paxillin[2,204]. Particular is new association of kindlin-2 with CAS. These results indicate kindlin-2, in association with CAS, give rise to the compensatory pathway for survival. In case of co-depletion of kindlin-2 and CAS, possibly talin-1 mediated pathway governs cell survival/proliferation (Figure 4.2).

**Box1** Common pathways involving FAK, CAS and ILK describing the survival signaling mediated by talin-1 or kindlin-2- are given in Figure 4.2. 'Kidnlin-2' directly bind with paxillin that in turn recruit FAK to focal adhesions[1,2]. FAK is the major hub of signaling for critical cellular processes such as cell survival, proliferation and migration[3]. Paxillin/FAK complex, in association with EGFR signaling, initiate the activation of Erk and Akt to promote the cell survival[3,4]. In an alternate process/way, FAK via Src, mediates CAS downstream signaling to regulate these cellular processes. 'Talin-1' perform its functions in cell survival signaling by promoting the binding of its intracellular effector ILK with $\beta_3$-integrin, which in turn phosphorylate Akt[5]. The other route of talin-1 for mediating survival signaling is FAK and Src followed by downstream activation of Akt[3].

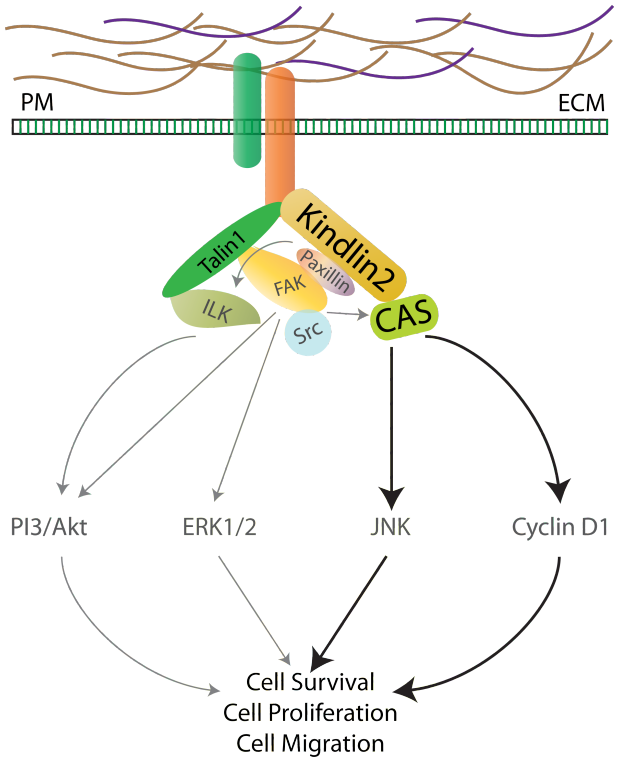


**Figure 4.2 Schematic illustration of alternative pathways generated by kindlin-2 and talin-1 for cell survival, proliferation and migration signaling.** Talin-1 and kindlin-2 signals in downstream cascades, which are mediated by FAK and ILK. Scheme highlights the association of kindlin-2 with CAS as a putative 'direct link' in comparison with the indirect involvement of talin-1 and CAS in the same pathway. The dim arrows, text and proteins indicate the presence but less-context specific importance. The literature used to draw this scheme was adopted from these reports[1-3,67,71,117,161,179] and concise description is included in Box1. Abbreviations; PM, plasma membrane and ECM, extra-cellular matrix. See text for detailed discussion.

Interestingly, the wound healing assay revealed impaired migration upon KD of kindlin-2 while talin-1 depletion enhanced the migration. This further strengthens our postulation of independent regulatory pathways of both critical structural proteins. Remarkably, among the ten proteins studied during this work, the individual as well combined depletions of kindlin-2 resulted in reduced migration (Figure 3.11). Only mutual depletion of kindlin-2 with CAS stringently impaired the migration, hinting towards their strong functional association (Figure 4.2, Movie 3.7). Kindlin-2 seems to be a fundamental 'positive/upstream regulator' of cell motility. Contrariwise, the individual and combined depletion of talin-1 along with CAS, VASP, vinculin led to the increased cell motility while its downregulation in combinations with FAK, zyxin, kindlin-2, ILK, α-parvin, α-actinin-1 slowed the cell migration. In this way, talin-1 generates two distinct signaling cascades, different from kindlin-2, to regulate the cell motility, strictly depending on functional association with other core FA proteins. Taken together, talin-1 and kindlin-2 function as adhesion-building module due to their critical role in the formation of adhesion sites and adhesion-associated cellular processes.

## 4.3 FA protein functional modules regulate adhesion sites formation and segregation

It is well established that focal adhesions assemble at the cell periphery, further move towards the cell center and transform into fibrillar adhesions[26,205]. Time-lapse video microscopy demonstrated that cells expressing GFP-tensin displayed a continuous centripetal flow of tensin from FAs to FB, indicating that FB are derived from FAs[26]. The relationship between formation of FB and tensin-1 translocation is well-established[206]. The expression and localization of tensin-1 upon KD of core FA proteins determined new functional associations.

FA proteins organized in functional modules (Figure 4.1) are canonical components of cell adhesion machinery. The current study emphasized that these functional modules participate in three distinct stages of tensin-1-mediated adhesion segregation process: (1) regulating tensin-1 localization to FA via signaling proteins (2) recruitment of tensin-1 to FA via actin-regulatory proteins (3) translocation of FB. In the following commentary, the role of functional modules in regulating different stages of adhesion segregation process is discussed.

### 4.3.1 Involvement of signalling module in localization of tensin-1 to FA

Here, we show that in the absence of signaling-module proteins, FB does not form. As a consequence, tensin-1, the hallmark of FB, is accumulated in the perinuclear areas. Not surprisingly, tensin-1 interacts with tyrosine-phosphorylated proteins such as FAK, CAS and PI3-kinase[200]. How this interaction implicates tensin-1 localization to FA is not known? Our result not only enlists new tyrosine-phosphorylated proteins such as α-actinin-1[207] and VASP[208], as potential interactors of SH2-domain of tensin-1 but also identified their un-reported function in localization of tensin-1 to FA. It has been proposed that phosphorylation of tensin-1 is required for FA turnover, resulting in the development of FB[194]. But phosphorylation-dependent localization of tensin-1 is not known. Considering the function of signaling proteins in modulating phosphorylation, we propose the necessary role of FAK in tensin-1 phosphorylation, important for its recruitment to FA. It is plausible as PTB domain of tensin-1 is essential but not sufficient for FA localization[200]. However, future studies need to address this question.

### 4.3.2 Actin-regulatory module regulate tensin-1 localization in FA

Actin-regulatory proteins (VASP, a-actinin-1, zyxin) mislocalizes tensin-1 in perinuclear areas. Interestingly, actin and tubulin cytoskeleton was prominently affected in KD conditions of actin-regulatory module (Figure 3.13 and Figure 3.28). We suggested the ABD (actin binding domain)-dependent binding of tensin-1 with actin[201] was curtailed, most likely due to disorganized actin-meshwork. For example, α-actinin-1 and zyxin KD resulted in severely disorganized actin-tubulin network (Figure 3.13). Direct interaction between α-actinin-1 and zyxin, in addition to their critical role in regulating the assembly of actin stress fibers[209], explain the reason of adverse effects on cytoskeleton that resulted in dislocation of tensin-1. Based on extensive literature review, it is difficult to find the role of ABD-I domain in tensin-1 localization. Our results demonstrated the correct localization of tensin-1 depends on its interaction with actin filaments and facilitated by actin-regulatory proteins (Figure 3.33).

So far, we have demonstrated particular functional modules of FA proteins that drive the localization of tensin-1, most likely by curtailing its interactions with tyrosine-phosphorylated proteins (signaling module) and actin (actin-regulatory

module). These modules might exhibit selective or competitive interactions with tensin-1 domains (Figure S19), which need further validation.

### 4.3.3 Adhesion segregating module regulate translocation of tensin-1

In contrast to, previously explained modules, here tensin-1 was successfully recruited in FA. However, the cells failed to form FB (Figure 3.29). In control cells, tensin-1 effectively segregated from FA and translocated to fibrillar adhesions (Figure 3.30). ILK, talin-1, kindlin-2 as well as tensin-1 are β-integrin binding proteins. Talin-1 and tensin-1 interacts with NPxY motifs via PTB domain, kindlin-2 with NxxY motif and ILK in an unknown manner[202,210]. Moreover, recently talin1&2 and kindlin-2 have been shown to activate $\alpha_5\beta_1$ integrin[2], and it is well known that $\alpha_5\beta_1$ integrins translocate tensin-1 towards cell center[206]. In the light of these reports, lower expression of integrins is expected, which in turn arrests tensin-1 in FA, possibly due to the strong/context-dependent binding of tensin-1 with available integrins (most likely with $\alpha_v\beta_3$ and $\alpha_5\beta_1$).

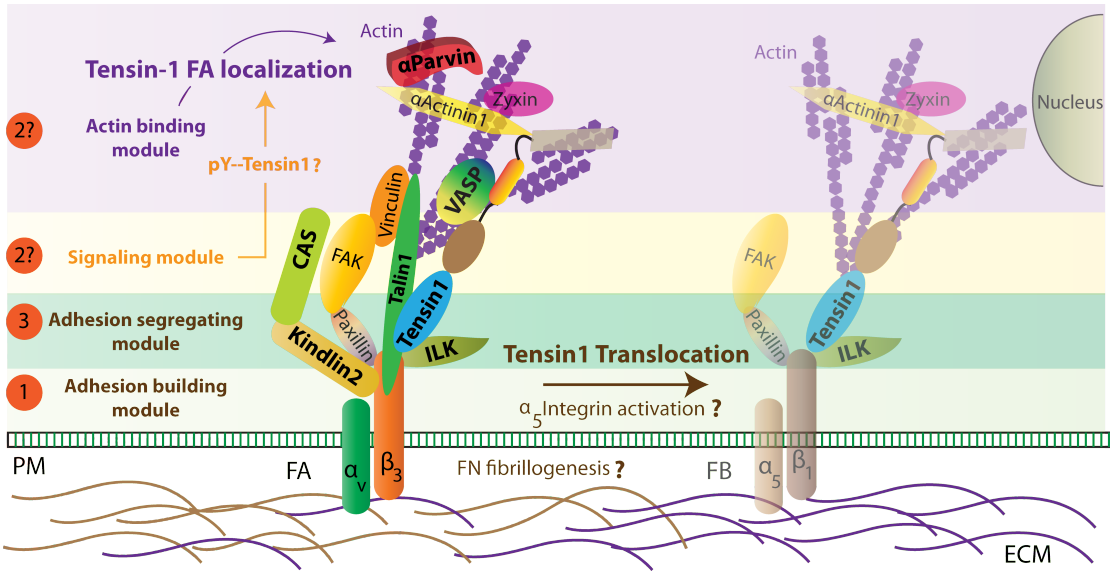


**Figure 4.3 Model of fibrillar adhesion formation by the FA proteins functional modules.** **(1)** Formation of Focal adhesion is dependent on 'adhesion-building module' (talin-1, kindlin-2). Tensin-1 is localized to FA either due to the tensin-1 interactions with **(2?)** tyrosine-phosphorylated proteins such as CAS, FAK in 'signaling-module' or by interactions with **(2?)** actin-cytoskeleton due to 'actin-regulatory module' (VASP, α-actinin-1, zyxin). **(3)** FA segregation process is driven by 'adhesion-segregation module' comprising of structural proteins such as talin-1, kindlin-2 and ILK. See text for detailed discussion.

Tensin-1 KD has no apparent effect in FN fibrillogenesis or FB formation[211]. But other than integrins, ILK is involved in fibronectin (FN) fibrillogenesis and FB formation[211]. Thus adhesion-segregation module proteins are more likely candidates to regulate the FN fibrillogenesis required for FB translocation. It has been proposed that tensin-1 phosphorylated by Src and FAK might be the switch for segregating FB from FA[194]. In addition to phosphorylation switch, the results of this study show the role of structural proteins in tensin-1 segregation to form FB, very likely by regulating integrins and fibrillogenesis that, in turn, faciliate assembly of fibrillar adhesions.

## 4.4 FA protein functional modules control different aspects of cell migration

Cell migration is a dynamic process, mediated by the interactions of cell-matrix adhesion sites with ECM and intracellular cytoskeleton. Our findings provide a preview of functional architecture of FA proteins in regulating the overall cell motility behavior, controlled by functional modules of core FA proteins. We show that mutual downregulation of FA proteins, in addition to reducing/increasing migration, modulates speed, directionality, polarization, alteration in adhesion sites, protrusions and cytoskeleton formation. In addition to the typical 2D lamellipodia migration, based on the varying degree of the listed features, we classified three main modes of migration comprised of 2-3 sub-modes (Figure 4.1). Typically, migration types are observed in 3D matrices and has been previously reported in keratocyte[212], fibroblasts[14,213] and mesenchymal cells[87]. Various studies unravel the relations among cell-matrix adhesion sites, cellular phenotypes/protrusions, and RhoA, ROCK, myosin-II activity[83-85,193,214]. Our results provided the molecular insight in the form of FA protein modules, for regulating known modes of fibroblasts migration. Most importantly four new modes of migration are defined. Of note, these modes were identified based on the quantified as well as manually assessed features.

### 4.4.1 Signalling module defines amoeboid mode of migration

Amoeboid sub-modalities (Figure 4.4) in which cells failed to form lamellipodia (Figure 3.14 and Figure 3.24) is a Rac1-mediated event[84]. Rac1 activity is lower in 3D-amoeboid mode as compared to 3D-lamellipodial[84]. It is plausible that Rac1 activity was decreased in the FAK and CAS (signaling module), illuminating

the possible reason for ill-defined cellular protrusions. These results support the putative link of FAK in regulating the Rac1-mediated cellular protrusions[215] and propose a same role of CAS. Rac and Rho are tightly regulated[84]. If Rac activity is lower, speculated to be the case in amoeboid-modes, Rho activity is elevated which is supported by the organized cytoskeleton (Figure 3.14). Altogether, we have shown a module, enlisting critical FA proteins that are expected to be involved in lamellipodia formation. These proteins can be the potential target for understanding amoeboid mode of migration, commonly observed in cancerous cells[84].

### 4.4.2 Adhesion building and segregating module defines confined mode of migration

After lamellipodia formation, adhesion sites are formed by structural proteins such as ILK, talin-1 and kindlin-2 in association with actin cytoskeleton. We found adhesion segregation module was involved in confined mode of migration (Figure 4.4). Migration-associated features such as loss of cell polarity, defects in biogenesis of lamellipodia, reduced cell spreading and less FA collectively explain the wide spread effects of these proteins. In MC3 and MC8, confined as well as fast randomly migrating cells featured the second sub-modality in which ILK/talin-1 was depleted with α-parvin/α-actinin-1/zyxin and represent a functional crosstalk between two modules (Figure 4.4 and Figure 3.11). Heterogeneity is underrepresented aspect of cell migration. We found the parallel emergence of two heterogeneous sub-modalities (Figure 3.26) based on speed (quantified) and protrusions, in addition to set of quantified features such as angle of direction, total distance from origin, ability to close the wound as well as manually assessed features like actin and tubulin cytoskeleton, FA (paxillin, PINCH) and FB (tensin-1) features. This set of parameters provides a new quality of information. A unique cell shape (moon-shape) was commonly observed in these sub-modalities, which enabled cells to quickly cover large distance but with random movement. The knockdown efficiency was more than 70% in cells showing heterogeneous migration behavior (Figure S1e), alleviating the possibility of heterogeneity due to ineffective KD.

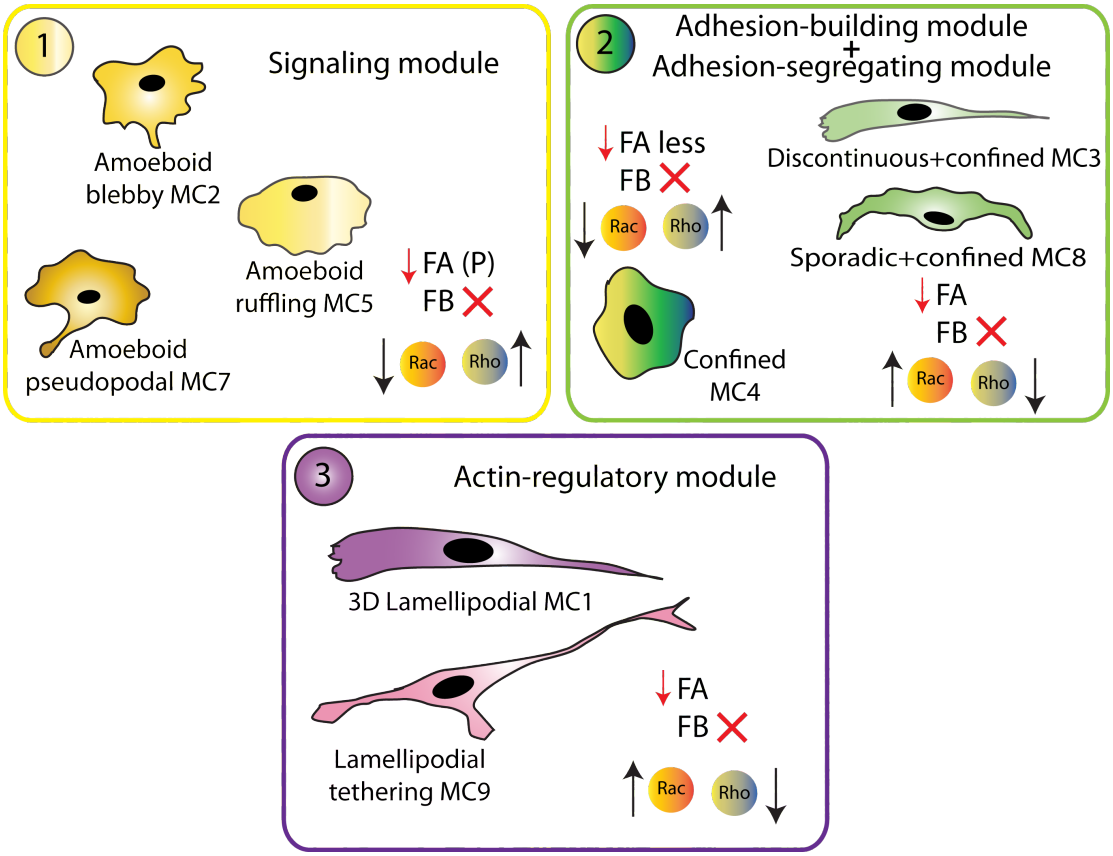


**Figure 4.4 Distinct modules regulate specific aspects of cell migration behavior.** Signalling-module (FAK, CAS) was linked with amoeboid-modalities in which several peripherally arranged FA were observed although cells lacked FB. Confined and two heterogeneous modalities (discontinuous and sporadic) were related with adhesion building and segregation module. Actin regulatory module (α-actinin-1, zyxin, VASP) were involved in regulating lamellipodia-based modes, in which few FA assembled and cells failed to develop FB (represented with red cross). Less and more FA are mentioned based on the comparison (without quantification) between different modes because number of FA was lower as compared to control. The 'upward arrow' designates 'possibly elevated activity' and 'downward arrow' specifies expected 'decrease in activity' in Rac and Rho signaling. See text for detailed discussion.

These findings symbolize an important advancement that may boost the future investigations of the fibroblast migration archetype in 2D. Particularly, facilitating the improved understanding of natural and experimental variability by accounting for different cellular phenotypes and modes of migration instead of unintentionally combining cells and taking an average[87]. Recognition of these modes as well as associated differences may facilitate a more accurate understanding of the heterogeneity and regulation of fibroblasts migration as a whole.

### 4.4.3 Actin-regulatory module outlines lamellipodial mode of migration

In the last stage of migration, organized cytoskeleton ensures the maturation of FA, stabilizes the migration speed and ensure front-back cell plorization. We found actin regulatory module regulate this stage by forming remarkably long and thin cells (Figure 4.4). We found drastically reduced cytoskeleton upon co-depletion of α-actinin-1 and zyxin due to elongated cells with bi-polar lamellipodia (Figure 3.13). α-actinin-1, is a regulator of microtubules and stress fibers, potentially contributed to the drastic reduction in actin and tubulin cytoskeleton[80,216]. Live-cell video microscopy exposed transient cell-cell adhesions and rapid switching of cellular phenotypes via long protrusions (Movie 3.1), suggesting the role of these proteins in stabilizing the adhesion and migration. The mode-switching behavior is often dictated by the level of RhoA, ROCK and myosin-II[84]. These proteins are not assessed in this study, however disturbed cytoskeleton proposes high Rac level (due to rapid lamellipodia formation) and low rho activity (due to reduced cytoskeleton). These results provide experimental evidence that α-actinin1–zyxin is an important axis of cell-matrix adhesion sites and may serve as promising therapeutics to potentiate the fast migration and proliferation for wound healing

It is conceivable that systematic perturbation of integrin adhesome by gene modulation or different environmental cues, combined with functional assays such as wound healing assay and clonogenic assay presented here, will become a mainstream approach to characterize the functional molecular architecture of adhesion sites.

# 5. References


1 Bouchard, V. *et al.* Fak/Src signaling in human intestinal epithelial cell survival and anoikis: differentiation state-specific uncoupling with the PI3-K/Akt-1 and MEK/Erk pathways. *J Cell Physiol* **212**, 717-728, doi:10.1002/jcp.21096 (2007).

2 Theodosiou, M. *et al.* Kindlin-2 cooperates with talin to activate integrins and induces cell spreading by directly binding paxillin. *Elife* **5**, e10130, doi:10.7554/eLife.10130 (2016).

3 Sulzmaier, F. J., Jean, C. & Schlaepfer, D. D. FAK in cancer: mechanistic findings and clinical applications. *Nat Rev Cancer* **14**, 598-610, doi:10.1038/nrc3792 (2014).

4 Deakin, N. O., Pignatelli, J. & Turner, C. E. Diverse roles for the paxillin family of proteins in cancer. *Genes Cancer* **3**, 362-370, doi:10.1177/1947601912458582 (2012).

5 Lynch, D. K., Ellis, C. A., Edwards, P. A. & Hiles, I. D. Integrin-linked kinase regulates phosphorylation of serine 473 of protein kinase B by an indirect mechanism. *Oncogene* **18**, 8024-8032, doi:10.1038/sj.onc.1203258 (1999).

6 Jarvelainen, H., Sainio, A., Koulu, M., Wight, T. N. & Penttinen, R. Extracellular matrix molecules: potential targets in pharmacotherapy. *Pharmacol Rev* **61**, 198-223, doi:10.1124/pr.109.001289 (2009).

7 Wozniak, M. A., Modzelewska, K., Kwong, L. & Keely, P. J. Focal adhesion regulation of cell behavior. *Biochim Biophys Acta* **1692**, 103-119, doi:10.1016/j.bbamcr.2004.04.007 (2004).

8 Gumbiner, B. M. Cell adhesion: the molecular basis of tissue architecture and morphogenesis. *Cell* **84**, 345-357 (1996).

9 Berrier, A. L. & Yamada, K. M. Cell-matrix adhesion. *J Cell Physiol* **213**, 565-573, doi:10.1002/jcp.21237 (2007).

10 Hynes, R. O. Integrins: bidirectional, allosteric signaling machines. *Cell* **110**, 673-687 (2002).

11 Liddington, R. C. & Ginsberg, M. H. Integrin activation takes shape. *J Cell Biol* **158**, 833-839, doi:10.1083/jcb.200206011 (2002).

12 Miranti, C. K. & Brugge, J. S. Sensing the environment: a historical perspective on integrin signal transduction. *Nat Cell Biol* **4**, E83-90, doi:10.1038/ncb0402-e83 (2002).

13 Luo, B. H., Carman, C. V. & Springer, T. A. Structural basis of integrin regulation and signaling. *Annu Rev Immunol* **25**, 619-647, doi:10.1146/annurev.immunol.25.022106.141618 (2007).

14 Abercrombie, M., Heaysman, J. E. & Pegrum, S. M. The locomotion of fibroblasts in culture. IV. Electron microscopy of the leading lamella. *Exp Cell Res* **67**, 359-367 (1971).

15 Fuchs, E., Dowling, J., Segre, J., Lo, S. H. & Yu, Q. C. Integrators of epidermal growth and differentiation: distinct functions for beta 1 and beta 4 integrins. *Curr Opin Genet Dev* **7**, 672-682 (1997).

16 Burridge, K., Fath, K., Kelly, T., Nuckolls, G. & Turner, C. Focal adhesions: transmembrane junctions between the extracellular matrix and the cytoskeleton. *Annu Rev Cell Biol* **4**, 487-525, doi:10.1146/annurev.cb.04.110188.002415 (1988).

17 Schaller, M. D. *et al.* pp125FAK a structurally distinctive protein-tyrosine kinase associated with focal adhesions. *Proc Natl Acad Sci U S A* **89**, 5192-5196 (1992).

18 Burridge, K. & Chrzanowska-Wodnicka, M. Focal adhesions, contractility, and signaling. *Annu Rev Cell Dev Biol* **12**, 463-518, doi:10.1146/annurev.cellbio.12.1.463 (1996).

19 Zamir, E. & Geiger, B. Molecular complexity and dynamics of cell-matrix adhesions. *J Cell Sci* **114**, 3583-3590 (2001).

20 Zaidel-Bar, R., Itzkovitz, S., Ma'ayan, A., Iyengar, R. & Geiger, B. Functional atlas of the integrin adhesome. *Nat Cell Biol* **9**, 858-867, doi:10.1038/ncb0807-858 (2007).

21 Horton, E. R. *et al.* Definition of a consensus integrin adhesome and its dynamics during adhesion complex assembly and disassembly. *Nat Cell Biol* **17**, 1577-1587, doi:10.1038/ncb3257 (2015).

22 Geiger, B., Bershadsky, A., Pankov, R. & Yamada, K. M. Transmembrane crosstalk between the extracellular matrix--cytoskeleton crosstalk. *Nat Rev Mol Cell Biol* **2**, 793-805, doi:10.1038/35099066 (2001).

23 Izzard, C. S. & Lochner, L. R. Cell-to-substrate contacts in living fibroblasts: an interference reflexion study with an evaluation of the technique. *J Cell Sci* **21**, 129-159 (1976).

24 Kanchanawong, P. *et al.* Nanoscale architecture of integrin-based cell adhesions. *Nature* **468**, 580-584, doi:10.1038/nature09621 (2010).

25 Wolfenson, H., Bershadsky, A., Henis, Y. I. & Geiger, B. Actomyosin-generated tension controls the molecular kinetics of focal adhesions. *J Cell Sci* **124**, 1425-1432, doi:10.1242/jcs.077388 (2011).

26 Zamir, E. *et al.* Dynamics and segregation of cell-matrix adhesions in cultured fibroblasts. *Nat Cell Biol* **2**, 191-196, doi:10.1038/35008607 (2000).

27 Theriot, J. A. & Mitchison, T. J. Comparison of actin and cell surface dynamics in motile fibroblasts. *J Cell Biol* **119**, 367-377 (1992).

28 Kaverina, I., Krylyshkina, O. & Small, J. V. Regulation of substrate adhesion dynamics during cell motility. *Int J Biochem Cell Biol* **34**, 746-761 (2002).

29 Beningo, K. A., Dembo, M., Kaverina, I., Small, J. V. & Wang, Y. L. Nascent focal adhesions are responsible for the generation of strong propulsive forces in migrating fibroblasts. *J Cell Biol* **153**, 881-888 (2001).

30 Galbraith, C. G., Yamada, K. M. & Galbraith, J. A. Polymerizing actin fibers position integrins primed to probe for adhesion sites. *Science* **315**, 992-995, doi:10.1126/science.1137904 (2007).

31 Pollard, T. D. & Borisy, G. G. Cellular motility driven by assembly and disassembly of actin filaments. *Cell* **112**, 453-465 (2003).

32 Case, L. B. *et al.* Molecular mechanism of vinculin activation and nanoscale spatial organization in focal adhesions. *Nat Cell Biol* **17**, 880-892, doi:10.1038/ncb3180 (2015).

33 Nobes, C. D. & Hall, A. Rho, rac, and cdc42 GTPases regulate the assembly of multimolecular focal complexes associated with actin stress fibers, lamellipodia, and filopodia. *Cell* **81**, 53-62 (1995).

34 Mitra, S. K., Hanson, D. A. & Schlaepfer, D. D. Focal adhesion kinase: in command and control of cell motility. *Nat Rev Mol Cell Biol* **6**, 56-68, doi:10.1038/nrm1549 (2005).

35 del Rio, A. *et al.* Stretching single talin rod molecules activates vinculin binding. *Science* **323**, 638-641, doi:10.1126/science.1162912 (2009).

36 Chrzanowska-Wodnicka, M. & Burridge, K. Rho-stimulated contractility drives the formation of stress fibers and focal adhesions. *J Cell Biol* **133**, 1403-1415 (1996).

37 Hu, K., Ji, L., Applegate, K. T., Danuser, G. & Waterman-Storer, C. M. Differential transmission of actin motion within focal adhesions. *Science* **315**, 111-115, doi:10.1126/science.1135085 (2007).

38 Riveline, D. *et al.* Focal contacts as mechanosensors: externally applied local mechanical force induces growth of focal contacts by an mDia1-dependent and ROCK-independent mechanism. *J Cell Biol* **153**, 1175-1186 (2001).

39 Yoshigi, M., Hoffman, L. M., Jensen, C. C., Yost, H. J. & Beckerle, M. C. Mechanical force mobilizes zyxin from focal adhesions to actin filaments and regulates cytoskeletal reinforcement. *J Cell Biol* **171**, 209-215, doi:10.1083/jcb.200505018 (2005).

40 Otey, C. A. & Carpen, O. Alpha-actinin revisited: a fresh look at an old player. *Cell Motil Cytoskeleton* **58**, 104-111, doi:10.1002/cm.20007 (2004).

41 Crowley, E. & Horwitz, A. F. Tyrosine phosphorylation and cytoskeletal tension regulate the release of fibroblast adhesions. *J Cell Biol* **131**, 525-537 (1995).

42 Broussard, J. A., Webb, D. J. & Kaverina, I. Asymmetric focal adhesion disassembly in motile cells. *Curr Opin Cell Biol* **20**, 85-90, doi:10.1016/j.ceb.2007.10.009 (2008).

43 Parsons, J. T., Horwitz, A. R. & Schwartz, M. A. Cell adhesion: integrating cytoskeletal dynamics and cellular tension. *Nat Rev Mol Cell Biol* **11**, 633-643, doi:10.1038/nrm2957 (2010).

44 Austin, J. H. & Carsen, G. M. Letter: Acute raumatic hematoma of aorta. *J Thorac Cardiovasc Surg* **71**, 321 (1976).

45 Franco, S. J. & Huttenlocher, A. Regulating cell migration: calpains make the cut. *J Cell Sci* **118**, 3829-3838, doi:10.1242/jcs.02562 (2005).

46 Burridge, K. Foot in mouth: do focal adhesions disassemble by endocytosis? *Nat Cell Biol* **7**, 545-547, doi:10.1038/ncb0505-545 (2005).

47 Small, J. V., Geiger, B., Kaverina, I. & Bershadsky, A. How do microtubules guide migrating cells? *Nat Rev Mol Cell Biol* **3**, 957-964, doi:10.1038/nrm971 (2002).

48 Kaverina, I., Krylyshkina, O. & Small, J. V. Microtubule targeting of substrate contacts promotes their relaxation and dissociation. *J Cell Biol* **146**, 1033-1044 (1999).

49 Ezratty, E. J., Partridge, M. A. & Gundersen, G. G. Microtubule-induced focal adhesion disassembly is mediated by dynamin and focal adhesion kinase. *Nat Cell Biol* **7**, 581-590, doi:10.1038/ncb1262 (2005).

50 Carragher, N. O. & Frame, M. C. Focal adhesion and actin dynamics: a place where kinases and proteases meet to promote invasion. *Trends Cell Biol* **14**, 241-249, doi:10.1016/j.tcb.2004.03.011 (2004).

51 Flevaris, P. *et al.* A molecular switch that controls cell spreading and retraction. *J Cell Biol* **179**, 553-565, doi:10.1083/jcb.200703185 (2007).

52 Chan, K. T., Bennin, D. A. & Huttenlocher, A. Regulation of adhesion dynamics by calpain-mediated proteolysis of focal adhesion kinase (FAK). *J Biol Chem* **285**, 11418-11426, doi:10.1074/jbc.M109.090746 (2010).

53 Franco, S., Perrin, B. & Huttenlocher, A. Isoform specific function of calpain 2 in regulating membrane protrusion. *Exp Cell Res* **299**, 179-187, doi:10.1016/j.yexcr.2004.05.021 (2004).

54 Chiu, C. L. & Gratton, E. Axial super resolution topography of focal adhesion by confocal microscopy. *Microsc Res Tech* **76**, 1070-1078, doi:10.1002/jemt.22267 (2013).

55 Frisch, S. M. & Francis, H. Disruption of epithelial cell-matrix interactions induces apoptosis. *J Cell Biol* **124**, 619-626 (1994).

56 Meredith, J. E., Jr., Fazeli, B. & Schwartz, M. A. The extracellular matrix as a cell survival factor. *Mol Biol Cell* **4**, 953-961 (1993).

57 Frisch, S. M., Vuori, K., Ruoslahti, E. & Chan-Hui, P. Y. Control of adhesion-dependent cell survival by focal adhesion kinase. *J Cell Biol* **134**, 793-799 (1996).

58 Ozaki, I., Hamajima, H., Matsuhashi, S. & Mizuta, T. Regulation of TGF-beta1-Induced Pro-Apoptotic Signaling by Growth Factor Receptors and

Extracellular Matrix Receptor Integrins in the Liver. *Front Physiol* **2**, 78, doi:10.3389/fphys.2011.00078 (2011).

59 Eliceiri, B. P. Integrin and growth factor receptor crosstalk. *Circ Res* **89**, 1104-1110 (2001).

60 Falcioni, R. *et al.* Alpha 6 beta 4 and alpha 6 beta 1 integrins associate with ErbB-2 in human carcinoma cell lines. *Exp Cell Res* **236**, 76-85 (1997).

61 Miyamoto, S., Teramoto, H., Gutkind, J. S. & Yamada, K. M. Integrins can collaborate with growth factors for phosphorylation of receptor tyrosine kinases and MAP kinase activation: roles of integrin aggregation and occupancy of receptors. *J Cell Biol* **135**, 1633-1642 (1996).

62 Frisch, S. M. & Screaton, R. A. Anoikis mechanisms. *Curr Opin Cell Biol* **13**, 555-562 (2001).

63 Khwaja, A., Rodriguez-Viciana, P., Wennstrom, S., Warne, P. H. & Downward, J. Matrix adhesion and Ras transformation both activate a phosphoinositide 3-OH kinase and protein kinase B/Akt cellular survival pathway. *EMBO J* **16**, 2783-2793, doi:10.1093/emboj/16.10.2783 (1997).

64 Hehlgans, S., Haase, M. & Cordes, N. Signalling via integrins: implications for cell survival and anticancer strategies. *Biochim Biophys Acta* **1775**, 163-180, doi:10.1016/j.bbcan.2006.09.001 (2007).

65 Schwartz, M. A. & Assoian, R. K. Integrins and cell proliferation: regulation of cyclin-dependent kinases via cytoplasmic signaling pathways. *J Cell Sci* **114**, 2553-2560 (2001).

66 Giancotti, F. G. & Ruoslahti, E. Integrin signaling. *Science* **285**, 1028-1032 (1999).

67 Stupack, D. G. & Cheresh, D. A. Get a ligand, get a life: integrins, signaling and cell survival. *J Cell Sci* **115**, 3729-3738 (2002).

68 Wei, L., Yang, Y., Zhang, X. & Yu, Q. Cleavage of p130Cas in anoikis. *J Cell Biochem* **91**, 325-335, doi:10.1002/jcb.10760 (2004).

69 Wei, L., Yang, Y., Zhang, X. & Yu, Q. Anchorage-independent phosphorylation of p130(Cas) protects lung adenocarcinoma cells from anoikis. *J Cell Biochem* **87**, 439-449, doi:10.1002/jcb.10322 (2002).

70 Subauste, M. C. *et al.* Vinculin modulation of paxillin-FAK interactions regulates ERK to control survival and motility. *J Cell Biol* **165**, 371-381, doi:10.1083/jcb.200308011 (2004).

71 Sakamoto, S., McCann, R. O., Dhir, R. & Kyprianou, N. Talin1 promotes tumor invasion and metastasis via focal adhesion signaling and anoikis resistance. *Cancer Res* **70**, 1885-1895, doi:10.1158/0008-5472.CAN-09-2833 (2010).

72 Moslem, M. *et al.* Kindlin-2 Modulates the Survival, Differentiation, and Migration of Induced Pluripotent Cell-Derived Mesenchymal Stromal Cells. *Stem Cells Int* **2017**, 7316354, doi:10.1155/2017/7316354 (2017).

73 Horwitz, R. & Webb, D. Cell migration. *Curr Biol* **13**, R756-759 (2003).

74 Ridley, A. J. *et al.* Cell migration: integrating signals from front to back. *Science* **302**, 1704-1709, doi:10.1126/science.1092053 (2003).

75 Hannigan, G., Troussard, A. A. & Dedhar, S. Integrin-linked kinase: a cancer therapeutic target unique among its ILK. *Nat Rev Cancer* **5**, 51-63, doi:10.1038/nrc1524 (2005).

76 Geiger, B. & Yamada, K. M. Molecular architecture and function of matrix adhesions. *Cold Spring Harb Perspect Biol* **3**, doi:10.1101/cshperspect.a005033 (2011).

77 Johnson, G. L. & Lapadat, R. Mitogen-activated protein kinase pathways mediated by ERK, JNK, and p38 protein kinases. *Science* **298**, 1911-1912, doi:10.1126/science.1072682 (2002).

78 Xue, G. & Hemmings, B. A. PKB/Akt-dependent regulation of cell motility. *J Natl Cancer Inst* **105**, 393-404, doi:10.1093/jnci/djs648 (2013).

79 Webb, D. J., Parsons, J. T. & Horwitz, A. F. Adhesion assembly, disassembly and turnover in migrating cells -- over and over and over again. *Nat Cell Biol* **4**, E97-100, doi:10.1038/ncb0402-e97 (2002).

80 Akhmanova, A., Stehbens, S. J. & Yap, A. S. Touch, grasp, deliver and control: functional cross-talk between microtubules and cell adhesions. *Traffic* **10**, 268-274, doi:10.1111/j.1600-0854.2008.00869.x (2009).

81 Palazzo, A. F. & Gundersen, G. G. Microtubule-actin cross-talk at focal adhesions. *Sci STKE* **2002**, pe31, doi:10.1126/stke.2002.139.pe31 (2002).

82 Huttenlocher, A. & Horwitz, A. R. Integrins in cell migration. *Cold Spring Harb Perspect Biol* **3**, a005074, doi:10.1101/cshperspect.a005074 (2011).

83 Petrie, R. J. & Yamada, K. M. Fibroblasts Lead the Way: A Unified View of 3D Cell Motility. *Trends Cell Biol* **25**, 666-674, doi:10.1016/j.tcb.2015.07.013 (2015).

84 Petrie, R. J. & Yamada, K. M. At the leading edge of three-dimensional cell migration. *Journal of Cell Science* **125**, 5917-5926, doi:10.1242/jcs.093732 (2012).

85 Petrie, R. J., Gavara, N., Chadwick, R. S. & Yamada, K. M. Nonpolarized signaling reveals two distinct modes of 3D cell migration. *J Cell Biol* **197**, 439-455, doi:10.1083/jcb.201201124 (2012).

86 Wolf, K. *et al.* Compensation mechanism in tumor cell migration: mesenchymal-amoeboid transition after blocking of pericellular proteolysis. *J Cell Biol* **160**, 267-277, doi:10.1083/jcb.200209006 (2003).

87 Shafqat-Abbasi, H. *et al.* An analysis toolbox to explore mesenchymal migration heterogeneity reveals adaptive switching between distinct modes. *eLife* **5**, e11384, doi:10.7554/eLife.11384 (2016).

88 Fire, A. *et al.* Potent and specific genetic interference by double-stranded RNA in Caenorhabditis elegans. *Nature* **391**, 806-811, doi:10.1038/35888 (1998).

89 Boutros, M. & Ahringer, J. The art and design of genetic screens: RNA interference. *Nat Rev Genet* **9**, 554-566, doi:10.1038/nrg2364 (2008).

90 Dorsett, Y. & Tuschl, T. siRNAs: applications in functional genomics and potential as therapeutics. *Nat Rev Drug Discov* **3**, 318-329, doi:10.1038/nrd1345 (2004).

91 Boutros, M. *et al.* Genome-wide RNAi analysis of growth and viability in Drosophila cells. *Science* **303**, 832-835, doi:10.1126/science.1091266 (2004).

92 Elena, S. F. & Lenski, R. E. Test of synergistic interactions among deleterious mutations in bacteria. *Nature* **390**, 395-398, doi:10.1038/37108 (1997).

93 Segre, D., Deluna, A., Church, G. M. & Kishony, R. Modular epistasis in yeast metabolism. *Nat Genet* **37**, 77-83, doi:10.1038/ng1489 (2005).

94 Bakal, C., Aach, J., Church, G. & Perrimon, N. Quantitative morphological signatures define local signaling networks regulating cell morphology. *Science* **316**, 1753-1756, doi:10.1126/science.1140324 (2007).

95 Fuchs, F. *et al.* Clustering phenotype populations by genome-wide RNAi and multiparametric imaging. *Mol Syst Biol* **6**, 370, doi:10.1038/msb.2010.25 (2010).

96 Jones, T. R. *et al.* Scoring diverse cellular morphologies in image-based screens with iterative feedback and machine learning. *Proc Natl Acad Sci U S A* **106**, 1826-1831, doi:10.1073/pnas.0808843106 (2009).

97 Neumann, B. *et al.* High-throughput RNAi screening by time-lapse imaging of live human cells. *Nat Methods* **3**, 385-390, doi:10.1038/nmeth876 (2006).

98 Billmann, M. *et al.* A genetic interaction map of cell cycle regulators. *Mol Biol Cell* **27**, 1397-1407, doi:10.1091/mbc.E15-07-0467 (2016).

99 Laufer, C., Fischer, B., Huber, W. & Boutros, M. Measuring genetic interactions in human cells by RNAi and imaging. *Nat Protoc* **9**, 2341-2353, doi:10.1038/nprot.2014.160 (2014).

100 Wang, X., Fu, A. Q., McNerney, M. E. & White, K. P. Widespread genetic epistasis among cancer genes. *Nat Commun* **5**, 4828, doi:10.1038/ncomms5828 (2014).

101 Zaidel-Bar, R. & Geiger, B. The switchable integrin adhesome. *J Cell Sci* **123**, 1385-1388, doi:10.1242/jcs.066183 (2010).

102 Simpson, K. J. *et al.* Identification of genes that regulate epithelial cell migration using an siRNA screening approach. *Nat Cell Biol* **10**, 1027-1038, doi:10.1038/ncb1762 (2008).

103 Winograd-Katz, S. E., Itzkovitz, S., Kam, Z. & Geiger, B. Multiparametric analysis of focal adhesion formation by RNAi-mediated gene knockdown. *J Cell Biol* **186**, 423-436, doi:10.1083/jcb.200901105 (2009).

104 Fokkelman, M. *et al.* Cellular adhesome screen identifies critical modulators of focal adhesion dynamics, cellular traction forces and cell migration behaviour. *Sci Rep* **6**, 31707, doi:10.1038/srep31707 (2016).

105 Phillips, P. C. Epistasis--the essential role of gene interactions in the structure and evolution of genetic systems. *Nat Rev Genet* **9**, 855-867, doi:10.1038/nrg2452 (2008).

106 Mani, R., St Onge, R. P., Hartman, J. L. t., Giaever, G. & Roth, F. P. Defining genetic interaction. *Proc Natl Acad Sci U S A* **105**, 3461-3466, doi:10.1073/pnas.0712255105 (2008).

107 Guarente, L. Synthetic enhancement in gene interaction: a genetic tool come of age. *Trends Genet* **9**, 362-366 (1993).

108 Avery, L. & Wasserman, S. Ordering gene function: the interpretation of epistasis in regulatory hierarchies. *Trends in Genetics* **8**, 312-316, doi:http://dx.doi.org/10.1016/0168-9525(92)90263-4 (1992).

109 Mani, R., St.Onge, R. P., Hartman, J. L., Giaever, G. & Roth, F. P. Defining genetic interaction. *Proceedings of the National Academy of Sciences* **105**, 3461-3466, doi:10.1073/pnas.0712255105 (2008).

110 Lo, S. H. Focal adhesions: what's new inside. *Dev Biol* **294**, 280-291, doi:10.1016/j.ydbio.2006.03.029 (2006).

111 Calderwood, D. A. *et al.* The Talin head domain binds to integrin beta subunit cytoplasmic tails and regulates integrin activation. *J Biol Chem* **274**, 28071-28074 (1999).

112 Ziegler, W. H., Gingras, A. R., Critchley, D. R. & Emsley, J. Integrin connections to the cytoskeleton through talin and vinculin. *Biochem Soc Trans* **36**, 235-239, doi:10.1042/BST0360235 (2008).

113 Montanez, E. *et al.* Kindlin-2 controls bidirectional signaling of integrins. *Genes Dev* **22**, 1325-1330, doi:10.1101/gad.469408 (2008).

114 Rogalski, T. M., Mullen, G. P., Gilbert, M. M., Williams, B. D. & Moerman, D. G. The UNC-112 gene in Caenorhabditis elegans encodes a novel component of cell-matrix adhesion structures required for integrin localization in the muscle cell membrane. *J Cell Biol* **150**, 253-264 (2000).

115 Hayashi, I., Vuori, K. & Liddington, R. C. The focal adhesion targeting (FAT) region of focal adhesion kinase is a four-helix bundle that binds paxillin. *Nat Struct Biol* **9**, 101-106, doi:10.1038/nsb755 (2002).

116 Zhai, J. *et al.* Direct interaction of focal adhesion kinase with p190RhoGEF. *J Biol Chem* **278**, 24865-24873, doi:10.1074/jbc.M302381200 (2003).

117 Schlaepfer, D. D., Jones, K. C. & Hunter, T. Multiple Grb2-mediated integrin-stimulated signaling pathways to ERK2/mitogen-activated protein kinase: summation of both c-Src- and focal adhesion kinase-initiated tyrosine phosphorylation events. *Mol Cell Biol* **18**, 2571-2585 (1998).

118 Schlaepfer, D. D., Hanks, S. K., Hunter, T. & van der Geer, P. Integrin-mediated signal transduction linked to Ras pathway by GRB2 binding to focal adhesion kinase. *Nature* **372**, 786-791 (1994).

119 Legate, K. R., Montanez, E., Kudlacek, O. & Fassler, R. ILK, PINCH and parvin: the tIPP of integrin signalling. *Nat Rev Mol Cell Biol* **7**, 20-31, doi:10.1038/nrm1789 (2006).

120 Mackinnon, A. C., Qadota, H., Norman, K. R., Moerman, D. G. & Williams, B. D. C. elegans PAT-4/ILK functions as an adaptor protein within integrin adhesion complexes. *Curr Biol* **12**, 787-797 (2002).

121 Tucker, K. L. *et al.* A dual role for integrin-linked kinase in platelets: regulating integrin function and alpha-granule secretion. *Blood* **112**, 4523-4531, doi:10.1182/blood-2008-03-148502 (2008).

122 Brakebusch, C. & Fassler, R. The integrin-actin connection, an eternal love affair. *EMBO J* **22**, 2324-2333, doi:10.1093/emboj/cdg245 (2003).

123 Sakai, R. *et al.* A novel signaling molecule, p130, forms stable complexes in vivo with v-Crk and v-Src in a tyrosine phosphorylation-dependent manner. *EMBO J* **13**, 3748-3756 (1994).

124 Harte, M. T., Macklem, M., Weidow, C. L., Parsons, J. T. & Bouton, A. H. Identification of two focal adhesion targeting sequences in the adapter molecule p130(Cas). *Biochim Biophys Acta* **1499**, 34-48 (2000).

125 Barrett, A., Pellet-Many, C., Zachary, I. C., Evans, I. M. & Frankel, P. p130Cas: a key signalling node in health and disease. *Cell Signal* **25**, 766-777, doi:10.1016/j.cellsig.2012.12.019 (2013).

126 Beraud, C. *et al.* Targeting FAK scaffold functions inhibits human renal cell carcinoma growth. *Int J Cancer* **137**, 1549-1559, doi:10.1002/ijc.29522 (2015).

127 Dagnino, L. Integrin-linked kinase: a Scaffold protein unique among its ilk. *J Cell Commun Signal* **5**, 81-83, doi:10.1007/s12079-011-0124-4 (2011).

128 Winkler, U. *et al.* Deletion of the cell adhesion adaptor protein vinculin disturbs the localization of GFAP in Bergmann glial cells. *Glia* **61**, 1067-1083, doi:10.1002/glia.22495 (2013).

129 Goldmann, W. H. Role of vinculin in cellular mechanotransduction. *Cell Biol Int* **40**, 241-256, doi:10.1002/cbin.10563 (2016).

130 Bear, J. E. & Gertler, F. B. Ena/VASP: towards resolving a pointed controversy at the barbed end. *J Cell Sci* **122**, 1947-1953, doi:10.1242/jcs.038125 (2009).

131 Hirata, H., Tatsumi, H. & Sokabe, M. Mechanical forces facilitate actin polymerization at focal adhesions in a zyxin-dependent manner. *J Cell Sci* **121**, 2795-2804, doi:10.1242/jcs.030320 (2008).

132 Ermolina, L. V., Martynova, N. & Zaraiskii, A. G. [The cytoskeletal protein zyxin--a universal regulator of cell adhesion and gene expression]. *Bioorg Khim* **36**, 29-37 (2010).

133 Krause, M., Dent, E. W., Bear, J. E., Loureiro, J. J. & Gertler, F. B. Ena/VASP proteins: regulators of the actin cytoskeleton and cell migration. *Annu Rev Cell Dev Biol* **19**, 541-564, doi:10.1146/annurev.cellbio.19.050103.103356 (2003).

134 Nikolopoulos, S. N. & Turner, C. E. Actopaxin, a new focal adhesion protein that binds paxillin LD motifs and actin and regulates cell adhesion. *J Cell Biol* **151**, 1435-1448 (2000).

135 Beggs, A. H. *et al.* Cloning and characterization of two human skeletal muscle alpha-actinin genes located on chromosomes 1 and 11. *J Biol Chem* **267**, 9281-9288 (1992).

136 Honda, K. *et al.* Actinin-4, a novel actin-bundling protein associated with cell motility and cancer invasion. *J Cell Biol* **140**, 1383-1393 (1998).

137 Trave, G., Pastore, A., Hyvonen, M. & Saraste, M. The C-terminal domain of alpha-spectrin is structurally related to calmodulin. *Eur J Biochem* **227**, 35-42 (1995).

138 Otey, C. A., Pavalko, F. M. & Burridge, K. An interaction between alpha-actinin and the beta 1 integrin subunit in vitro. *J Cell Biol* **111**, 721-729 (1990).

139 Hopkinson, S. B. *et al.* Focal Contact and Hemidesmosomal Proteins in Keratinocyte Migration and Wound Repair. *Adv Wound Care (New Rochelle)* **3**, 247-263, doi:10.1089/wound.2013.0489 (2014).

140 Jackson, A. L. *et al.* Position-specific chemical modification of siRNAs reduces "off-target" transcript silencing. *RNA* **12**, 1197-1205, doi:10.1261/rna.30706 (2006).

141 Schindelin, J. *et al.* Fiji: an open-source platform for biological-image analysis. *Nat Meth* **9**, 676-682, doi:http://www.nature.com/nmeth/journal/v9/n7/abs/nmeth.2019.html - supplementary-information (2012).

142 Livak, K. J. & Schmittgen, T. D. Analysis of Relative Gene Expression Data Using Real-Time Quantitative PCR and the 2−ΔΔCT Method. *Methods* **25**, 402-408, doi:http://dx.doi.org/10.1006/meth.2001.1262 (2001).

143 Preibisch, S., Saalfeld, S. & Tomancak, P. Globally optimal stitching of tiled 3D microscopic image acquisitions. *Bioinformatics* **25**, 1463-1465, doi:10.1093/bioinformatics/btp184 (2009).

144 Tinevez, J. Y. *et al.* TrackMate: An open and extensible platform for single-particle tracking. *Methods* **115**, 80-90, doi:10.1016/j.ymeth.2016.09.016 (2017).

145 Piccinini, F., Kiss, A. & Horvath, P. CellTracker (not only) for dummies. *Bioinformatics* **32**, 955-957, doi:10.1093/bioinformatics/btv686 (2016).

146 Carpenter, A. E. *et al.* CellProfiler: image analysis software for identifying and quantifying cell phenotypes. *Genome Biol* **7**, doi:10.1186/gb-2006-7-10-r100 (2006).

147 Guzman, C., Bagga, M., Kaur, A., Westermarck, J. & Abankwa, D. ColonyArea: an ImageJ plugin to automatically quantify colony formation in clonogenic assays. *PLoS One* **9**, e92444, doi:10.1371/journal.pone.0092444 (2014).

148 Munshi, A., Hobbs, M. & Meyn, R. E. Clonogenic cell survival assay. *Methods Mol Med* **110**, 21-28, doi:10.1385/1-59259-869-2:021 (2005).

149 Harizanova, J. *et al.* Highly Multiplexed Imaging Uncovers Changes in Compositional Noise within Assembling Focal Adhesions. *PLOS ONE* **11**, e0160591, doi:10.1371/journal.pone.0160591 (2016).

150 Humphries, J. D., Paul, N. R., Humphries, M. J. & Morgan, M. R. Emerging properties of adhesion complexes: what are they and what do they do? *Trends Cell Biol* **25**, 388-397, doi:10.1016/j.tcb.2015.02.008 (2015).

151 Eisenberg, J. L. *et al.* Plectin-containing, centrally localized focal adhesions exert traction forces in primary lung epithelial cells. *J Cell Sci* **126**, 3746-3755, doi:10.1242/jcs.128975 (2013).

152 Tilghman, R. W. *et al.* Focal adhesion kinase is required for the spatial organization of the leading edge in migrating cells. *J Cell Sci* **118**, 2613-2623, doi:10.1242/jcs.02380 (2005).

153 Bandyopadhyay, A., Rothschild, G., Kim, S., Calderwood, D. A. & Raghavan, S. Functional differences between kindlin-1 and kindlin-2 in keratinocytes. *J Cell Sci* **125**, 2172-2184, doi:10.1242/jcs.096214 (2012).

154 Han, E. K., McGonigal, T., Wang, J., Giranda, V. L. & Luo, Y. Functional analysis of focal adhesion kinase (FAK) reduction by small inhibitory RNAs. *Anticancer Res* **24**, 3899-3905 (2004).

155 Jung, G. Y., Park, Y. J. & Han, J. S. Mediation of Rac1 activation by kindlin-2: an essential function in osteoblast adhesion, spreading, and proliferation. *J Cell Biochem* **112**, 2541-2548, doi:10.1002/jcb.23178 (2011).

156 Ren, Y. *et al.* Kindlin-2 inhibited the growth and migration of colorectal cancer cells. *Tumour Biol* **36**, 4107-4114, doi:10.1007/s13277-015-3044-8 (2015).

157 Yano, H. *et al.* Roles played by a subset of integrin signaling molecules in cadherin-based cell-cell adhesion. *J Cell Biol* **166**, 283-295, doi:10.1083/jcb.200312013 (2004).

158 Gilmore, A. P. & Romer, L. H. Inhibition of focal adhesion kinase (FAK) signaling in focal adhesions decreases cell motility and proliferation. *Mol Biol Cell* **7**, 1209-1224 (1996).

159 Sansing, H. A. *et al.* Integrin alphabeta1, alphavbeta, alpha6beta effectors p130Cas, Src and talin regulate carcinoma invasion and chemoresistance. *Biochem Biophys Res Commun* **406**, 171-176, doi:10.1016/j.bbrc.2011.01.109 (2011).

160 Wang, P., Ballestrem, C. & Streuli, C. H. The C terminus of talin links integrins to cell cycle progression. *J Cell Biol* **195**, 499-513, doi:10.1083/jcb.201104128 (2011).

161 Wu, X. *et al.* Kindlin-2 siRNA inhibits vascular smooth muscle cell proliferation, migration and intimal hyperplasia via Wnt signaling. *Int J Mol Med* **37**, 436-444, doi:10.3892/ijmm.2015.2429 (2016).

162 Cabodi, S. *et al.* p130Cas as a new regulator of mammary epithelial cell proliferation, survival, and HER2-neu oncogene-dependent breast tumorigenesis. *Cancer Res* **66**, 4672-4680, doi:10.1158/0008-5472.CAN-05-2909 (2006).

163 Nick, A. M. *et al.* Silencing of p130cas in ovarian carcinoma: a novel mechanism for tumor cell death. *J Natl Cancer Inst* **103**, 1596-1612, doi:10.1093/jnci/djr372 (2011).

164 Kook, S. *et al.* Caspase-mediated cleavage of p130cas in etoposide-induced apoptotic Rat-1 cells. *Mol Biol Cell* **11**, 929-939 (2000).

165 Zhao, G. *et al.* Integrin-linked kinase in gastric cancer cell attachment, invasion and tumor growth. *World J Gastroenterol* **17**, 3487-3496, doi:10.3748/wjg.v17.i30.3487 (2011).

166 Troussard, A. A. *et al.* Conditional knock-out of integrin-linked kinase demonstrates an essential role in protein kinase B/Akt activation. *J Biol Chem* **278**, 22374-22378, doi:10.1074/jbc.M303083200 (2003).

167 Tao, Y., Chen, Y. C., Sang, J. R. & Xu, W. R. Phosphorylation of vasodilator stimulated phosphoprotein is correlated with cell cycle progression in HeLa cells. *Mol Med Rep* **3**, 657-662, doi:10.3892/mmr_00000312 (2010).

168 Huang, A. H. *et al.* PARVA promotes metastasis by modulating ILK signalling pathway in lung adenocarcinoma. *PLoS One* **10**, e0118530, doi:10.1371/journal.pone.0118530 (2015).

169 Craig, D. H., Zhang, J. & Basson, M. D. Cytoskeletal signaling by way of alpha-actinin-1 mediates ERK1/2 activation by repetitive deformation in human Caco2 intestinal epithelial cells. *Am J Surg* **194**, 618-622, doi:10.1016/j.amjsurg.2007.08.001 (2007).

170 Wickstrom, S. A., Lange, A., Montanez, E. & Fassler, R. The ILK/PINCH/parvin complex: the kinase is dead, long live the pseudokinase! *EMBO J* **29**, 281-291, doi:10.1038/emboj.2009.376 (2010).

171 Dixon, S. J., Costanzo, M., Baryshnikova, A., Andrews, B. & Boone, C. Systematic mapping of genetic interaction networks. *Annu Rev Genet* **43**, 601-625, doi:10.1146/annurev.genet.39.073003.114751 (2009).

172 Boucher, B. & Jenna, S. Genetic interaction networks: better understand to better predict. *Front Genet* **4**, 290, doi:10.3389/fgene.2013.00290 (2013).

173 Wong, R. P., Ng, P., Dedhar, S. & Li, G. The role of integrin-linked kinase in melanoma cell migration, invasion, and tumor growth. *Mol Cancer Ther* **6**, 1692-1700, doi:10.1158/1535-7163.MCT-07-0134 (2007).

174 Arnold, K. M., Goeckeler, Z. M. & Wysolmerski, R. B. Loss of focal adhesion kinase enhances endothelial barrier function and increases focal adhesions. *Microcirculation* **20**, 637-649, doi:10.1111/micc.12063 (2013).

175 Rahman, A. *et al.* Vinculin Regulates Directionality and Cell Polarity in 2D, 3D Matrix and 3D Microtrack Migration. *Mol Biol Cell*, doi:10.1091/mbc.E15-06-0432 (2016).

176 Ziegler, W. H., Liddington, R. C. & Critchley, D. R. The structure and regulation of vinculin. *Trends Cell Biol* **16**, 453-460, doi:10.1016/j.tcb.2006.07.004 (2006).

177 Albiges-Rizo, C., Frachet, P. & Block, M. R. Down regulation of talin alters cell adhesion and the processing of the alpha 5 beta 1 integrin. *J Cell Sci* **108 ( Pt 10)**, 3317-3329 (1995).

178 Chen, P. *et al.* Talin-1 interaction network promotes hepatocellular carcinoma progression. *Oncotarget* **8**, 13003-13014, doi:10.18632/oncotarget.14674 (2017).

179 Fukuda, K. *et al.* Molecular basis of kindlin-2 binding to integrin-linked kinase pseudokinase for regulating cell adhesion. *J Biol Chem* **289**, 28363-28375, doi:10.1074/jbc.M114.596692 (2014).

180 He, Y., Esser, P., Schacht, V., Bruckner-Tuderman, L. & Has, C. Role of kindlin-2 in fibroblast functions: implications for wound healing. *J Invest Dermatol* **131**, 245-256, doi:10.1038/jid.2010.273 (2011).

181 An, Z. *et al.* Kindlin-2 is expressed in malignant mesothelioma and is required for tumor cell adhesion and migration. *Int J Cancer* **127**, 1999-2008, doi:10.1002/ijc.25223 (2010).

182 Guo, B., Gao, J., Zhan, J. & Zhang, H. Kindlin-2 interacts with and stabilizes EGFR and is required for EGF-induced breast cancer cell migration. *Cancer Lett* **361**, 271-281, doi:10.1016/j.canlet.2015.03.011 (2015).

183 Cunningham-Edmondson, A. C. & Hanks, S. K. p130Cas substrate domain signaling promotes migration, invasion, and survival of estrogen receptor-negative breast cancer cells. *Breast Cancer (Dove Med Press)* **1**, 39-52 (2009).

184 Han, K. S. *et al.* Targeting Integrin-Linked Kinase Suppresses Invasion and Metastasis through Downregulation of Epithelial-to-Mesenchymal Transition in Renal Cell Carcinoma. *Mol Cancer Ther* **14**, 1024-1034, doi:10.1158/1535-7163.MCT-14-0771 (2015).

185 Gagne, D. *et al.* Integrin-linked kinase regulates migration and proliferation of human intestinal cells under a fibronectin-dependent mechanism. *J Cell Physiol* **222**, 387-400, doi:10.1002/jcp.21963 (2010).

186 Guo, L., Yu, W., Li, X., Zhao, G. & He, P. Targeting of integrin-linked kinase with a small interfering RNA inhibits endothelial cell migration, proliferation and tube formation in vitro. *Ophthalmic Res* **42**, 213-220, doi:10.1159/000232971 (2009).

187 Yamamura, M. *et al.* Functional analysis of Zyxin in cell migration and invasive potential of oral squamous cell carcinoma cells. *Int J Oncol* **42**, 873-880, doi:10.3892/ijo.2013.1761 (2013).

188 Choi, Y. H., McNally, B. T. & Igarashi, P. Zyxin regulates migration of renal epithelial cells through activation of hepatocyte nuclear factor-1beta. *Am J Physiol Renal Physiol* **305**, F100-110, doi:10.1152/ajprenal.00582.2012 (2013).

189 Sy, S. M. *et al.* Novel identification of zyxin upregulations in the motile phenotype of hepatocellular carcinoma. *Mod Pathol* **19**, 1108-1116, doi:10.1038/modpathol.3800626 (2006).

190 Bear, J. E. *et al.* Negative regulation of fibroblast motility by Ena/VASP proteins. *Cell* **101**, 717-728 (2000).

191 Wu, G. *et al.* Vasodilator-stimulated phosphoprotein regulates osteosarcoma cell migration. *Oncol Rep* **26**, 1609-1615, doi:10.3892/or.2011.1438 (2011).

192 Hamill, K. J. *et al.* Alpha actinin-1 regulates cell-matrix adhesion organization in keratinocytes: consequences for skin cell motility. *J Invest Dermatol* **135**, 1043-1052, doi:10.1038/jid.2014.505 (2015).

193 Friedl, P. & Wolf, K. Plasticity of cell migration: a multiscale tuning model. *The Journal of Cell Biology* **188**, 11-19, doi:10.1083/jcb.200909003 (2010).

194 Volberg, T., Romer, L., Zamir, E. & Geiger, B. pp60(c-src) and related tyrosine kinases: a role in the assembly and reorganization of matrix adhesions. *J Cell Sci* **114**, 2279-2289 (2001).

195 Clarke, J. H. *et al.* The function of phosphatidylinositol 5-phosphate 4-kinase gamma (PI5P4Kgamma) explored using a specific inhibitor that targets the PI5P-binding site. *Biochem J* **466**, 359-367, doi:10.1042/BJ20141333 (2015).

196 Bottcher, R. T., Lange, A. & Fassler, R. How ILK and kindlins cooperate to orchestrate integrin signaling. *Curr Opin Cell Biol* **21**, 670-675, doi:10.1016/j.ceb.2009.05.008 (2009).

197 Kahner, B. N. *et al.* Kindlins, integrin activation and the regulation of talin recruitment to alphaIIbbeta3. *PLoS One* **7**, e34056, doi:10.1371/journal.pone.0034056 (2012).

198 Honda, S. *et al.* Integrin-linked kinase associated with integrin activation. *Blood* **113**, 5304-5313, doi:10.1182/blood-2008-07-169136 (2009).

199 Lo, S. H. Tensin. *Int J Biochem Cell Biol* **36**, 31-34 (2004).

200 Chen, H. & Lo, S. H. Regulation of tensin-promoted cell migration by its focal adhesion binding and Src homology domain 2. *Biochem J* **370**, 1039-1045, doi:10.1042/BJ20021308 (2003).

201 Lo, S. H. Tensins. *Curr Biol* **27**, R331-R332, doi:10.1016/j.cub.2017.02.041 (2017).

202 Calderwood, D. A. *et al.* Integrin beta cytoplasmic domain interactions with phosphotyrosine-binding domains: a structural prototype for diversity in integrin signaling. *Proc Natl Acad Sci U S A* **100**, 2272-2277, doi:10.1073/pnas.262791999 (2003).

203 Legate, K. R., Wickstrom, S. A. & Fassler, R. Genetic and cell biological analysis of integrin outside-in signaling. *Genes Dev* **23**, 397-418, doi:10.1101/gad.1758709 (2009).

204 Turner, C. E. Paxillin interactions. *J Cell Sci* **113 Pt 23**, 4139-4140 (2000).

205 Izzard, C. S. & Lochner, L. R. Formation of cell-to-substrate contacts during fibroblast motility: an interference-reflexion study. *J Cell Sci* **42**, 81-116 (1980).

206 Pankov, R. *et al.* Integrin dynamics and matrix assembly: tensin-dependent translocation of alpha(5)beta(1) integrins promotes early fibronectin fibrillogenesis. *J Cell Biol* **148**, 1075-1090 (2000).

207 Izaguirre, G., Aguirre, L., Ji, P., Aneskievich, B. & Haimovich, B. Tyrosine phosphorylation of alpha-actinin in activated platelets. *J Biol Chem* **274**, 37012-37020 (1999).

208 Goss, V. L. *et al.* A common phosphotyrosine signature for the Bcr-Abl kinase. *Blood* **107**, 4888-4897, doi:10.1182/blood-2005-08-3399 (2006).

209 Crawford, A. W., Michelsen, J. W. & Beckerle, M. C. An interaction between zyxin and alpha-actinin. *J Cell Biol* **116**, 1381-1393 (1992).

210 Calderwood, D. A. *et al.* The phosphotyrosine binding-like domain of talin activates integrins. *J Biol Chem* **277**, 21749-21758, doi:10.1074/jbc.M111996200 (2002).

211 Elad, N. *et al.* The role of integrin-linked kinase in the molecular architecture of focal adhesions. *J Cell Sci* **126**, 4099-4107, doi:10.1242/jcs.120295 (2013).

212 Barnhart, E., Lee, K. C., Allen, G. M., Theriot, J. A. & Mogilner, A. Balance between cell-substrate adhesion and myosin contraction determines the frequency of motility initiation in fish keratocytes. *Proc Natl Acad Sci U S A* **112**, 5045-5050, doi:10.1073/pnas.1417257112 (2015).

213 Theisen, U., Straube, E. & Straube, A. Directional persistence of migrating cells requires Kif1C-mediated stabilization of trailing adhesions. *Dev Cell* **23**, 1153-1166, doi:10.1016/j.devcel.2012.11.005 (2012).

214 Sixt, M. Cell migration: fibroblasts find a new way to get ahead. *J Cell Biol* **197**, 347-349, doi:10.1083/jcb.201204039 (2012).

215 Stutchbury, B., Atherton, P., Tsang, R., Wang, D. Y. & Ballestrem, C. Distinct focal adhesion protein modules control different aspects of mechanotransduction. *J Cell Sci* **130**, 1612-1624, doi:10.1242/jcs.195362 (2017).

216 Akhshi, T. K., Wernike, D. & Piekny, A. Microtubules and actin crosstalk in cell migration and division. *Cytoskeleton (Hoboken)* **71**, 1-23, doi:10.1002/cm.21150 (2014).

# 6. Supplementary information

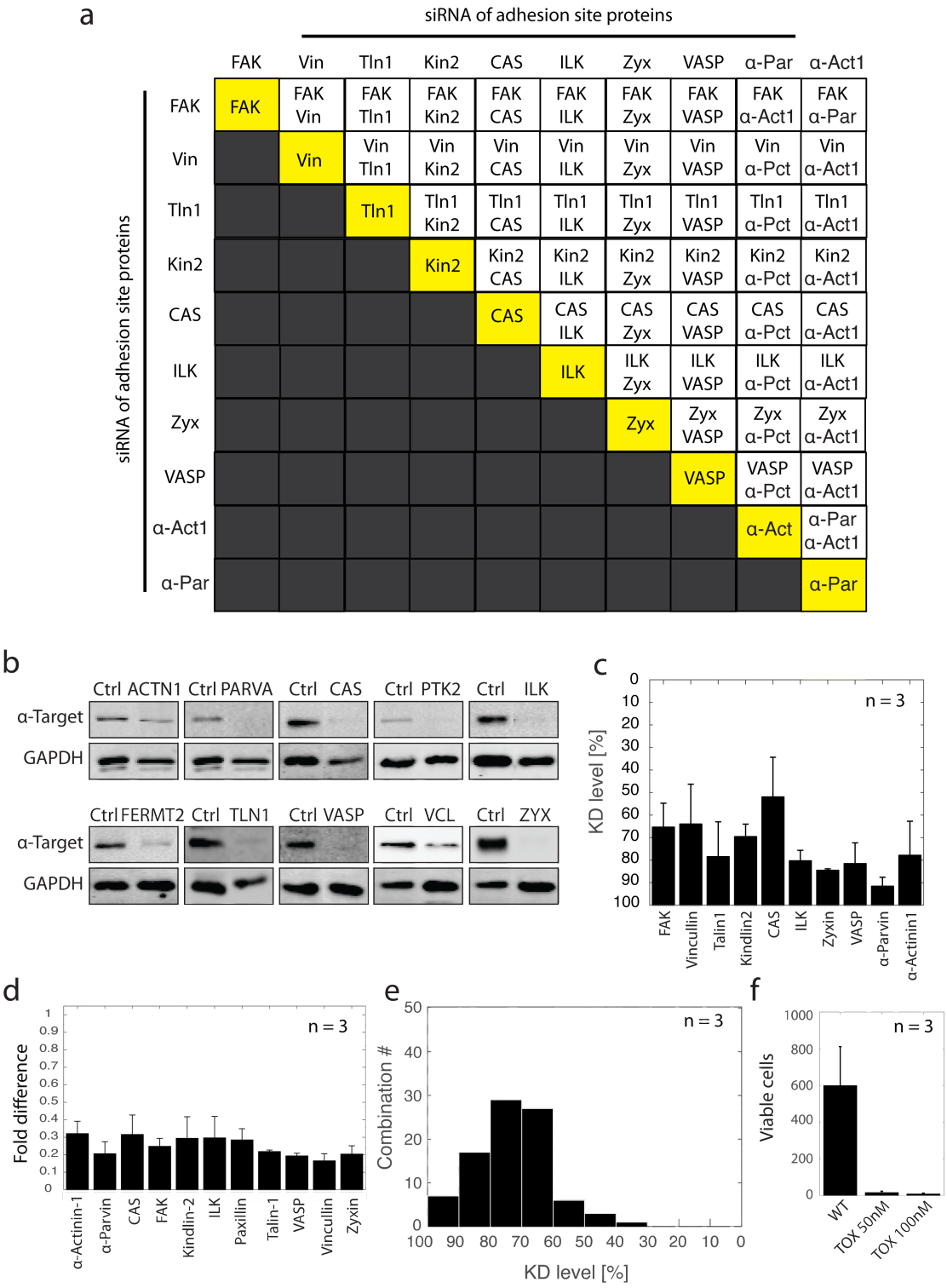


**Figure S1 Matrix of individual and pairwise combination of proteins and quantification of individual protein knockdown using western blot and RT-qPCR.** The diagonal of the matrix represent 10 adhesion site proteins (yellow color boxes) for indivudal siRNA

perturbations. Ten siRNA gave rise to 45 pairwise siRNA combinations (white boxes). Grey highlighted boxes included complimentary order of the 45 pairs (not included). (b) REF52 cells were transfected with siRNA for each protein individually, immuno-blotted with respective antibodies, as indicated. GAPDH was used as loading control. (c) Bar plot showing quantification of KD for each protein. Error bars represent SD. (d) REF52 cells were transfected with individual siRNAs, post 48 h RNA extracts were prepared and used for the quantification of mRNA level by RT-qPCR. Error bars represent SD. (e) REF52 cells were transfected with 45 pairwise combinations of siRNAs followed by RNA extraction. Level of mRNA was estimated for both proteins in each combination using RT-qPCR. Plots represents the number of combinations showing % of KD. (f) REF52 cells transfected with TOX siRNA and control cells were trypsinized counted using trypan blue.

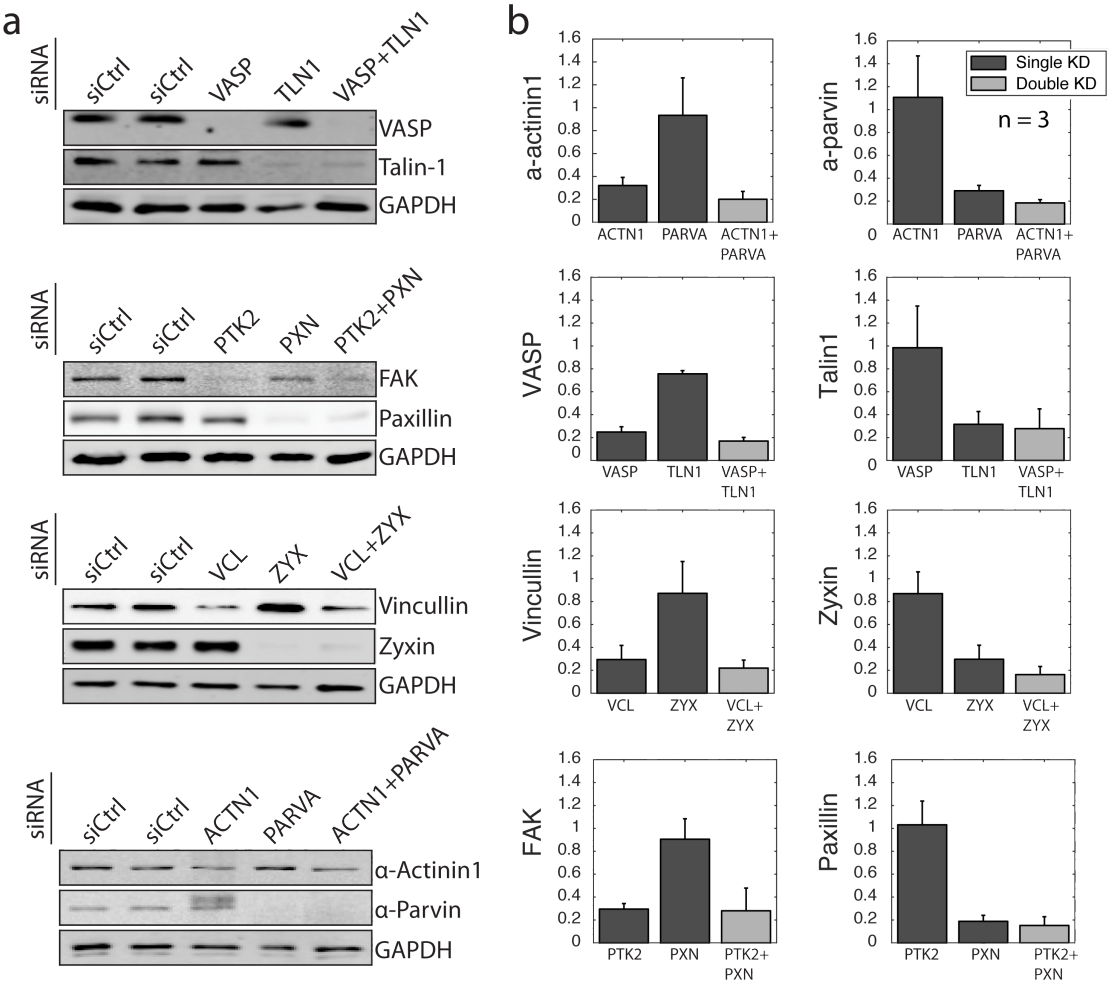


**Figure S2 Quantification of combined protein knockdown using western blot and RT-qPCR.** (a) REF52 cells were transfected with individual siRNA as well as with siRNA combinations for four different pairs. Lysates were prepared for each KD condition and examined by SDS-gel electrophoresis. Immunoblotting was done with respective antibodies, as indicated, to evaluate the expression level of the proteins. GAPDH was used as loading control. (b) Bar plots showing quantification of KD for each protein pair. Error bars represent SD.

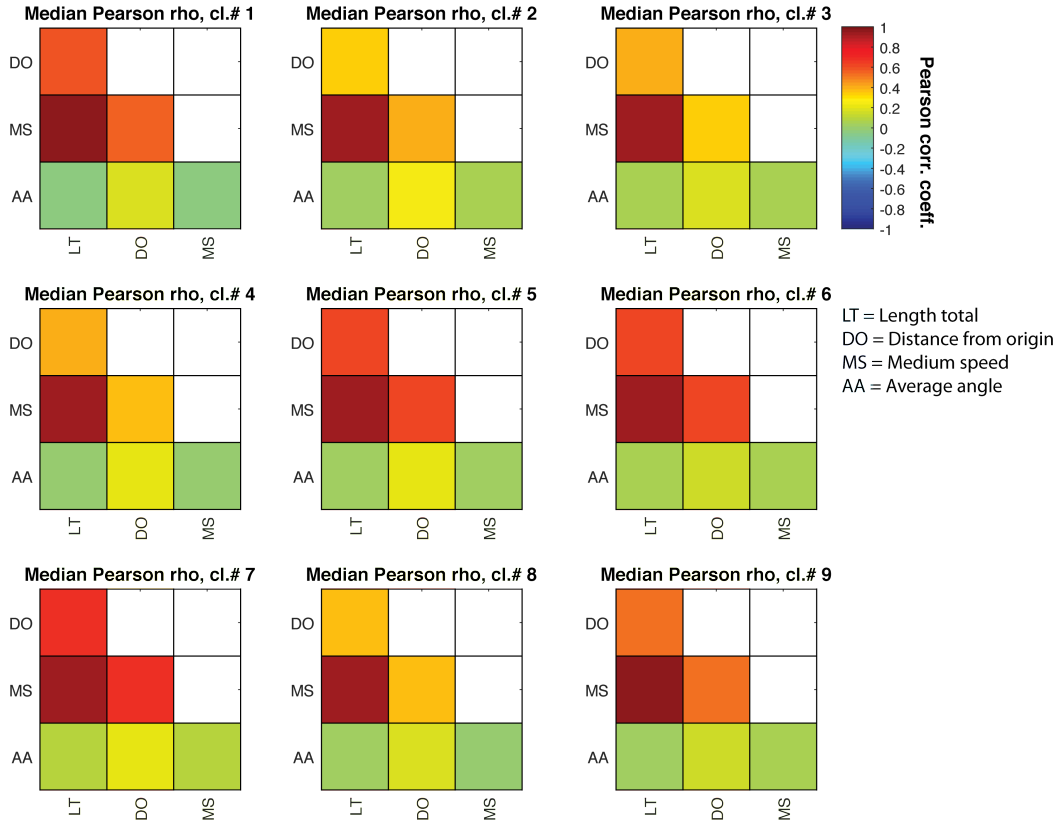


**Figure S3 Pearson correlation between the five parameters related to cell migration.** Only median speed and total track length were correlated in all pairwise combination. Other parameters were orthogonal (not correlated).

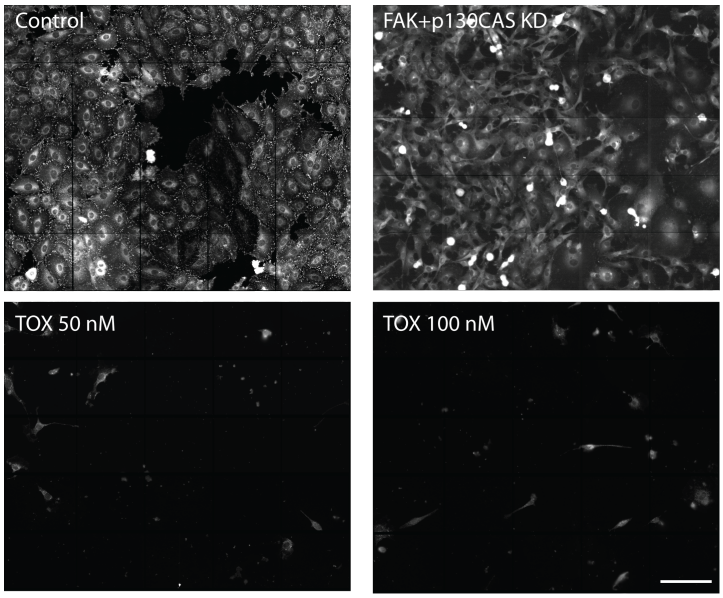


**Figure S4 Images from control wells and siRNA treated well.** Montage of 5x5 images from untransfected REF52 cells, cells co-transfected with FAK and CAS siRNA, cells transfected with 50 nM and 100 nM TOX siRNA. Scale bar is 100 µm.

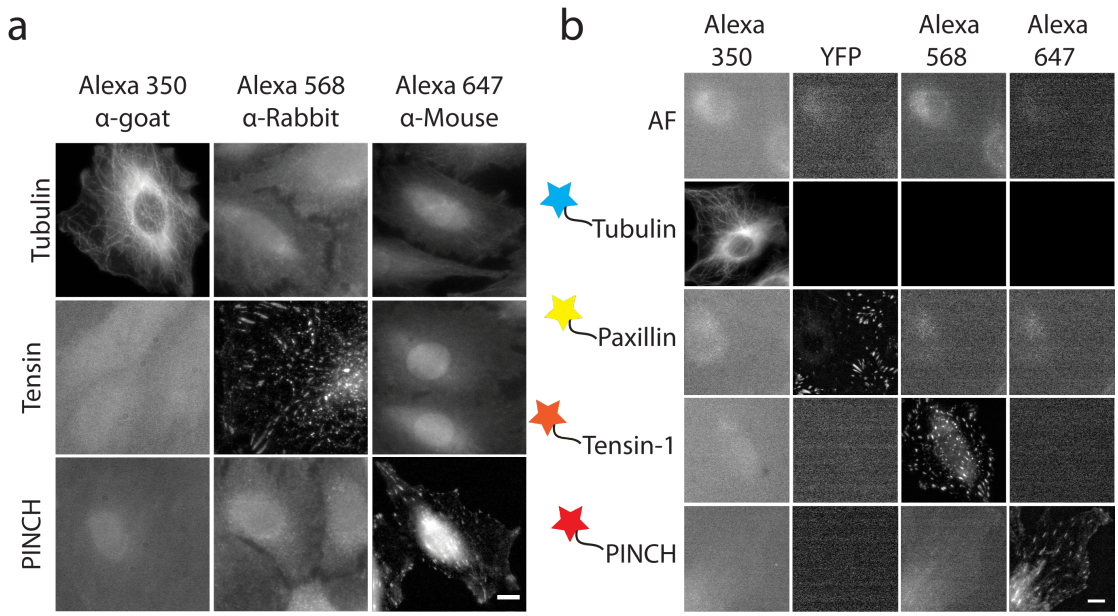


**Figure S5 Optimization of antibodies and imaging setup for fixed-cells imaging screen.** (a) Cross reactivity of the secondary antibodies tested against primary antibodies, as indicated. The diagonal represents the specific signal of each secondary antibody whereas other images indicate non-specific signal from secondary antibodies. (b) Bleed-through matrix of the four-color imaging of tubulin, paxillin, tensin-1 and PINCH. REF52 cells were immunostained with primary and secondary antibodies as indicated and subjected to four-color imaging acquisition. Scale bar is 10 μm.

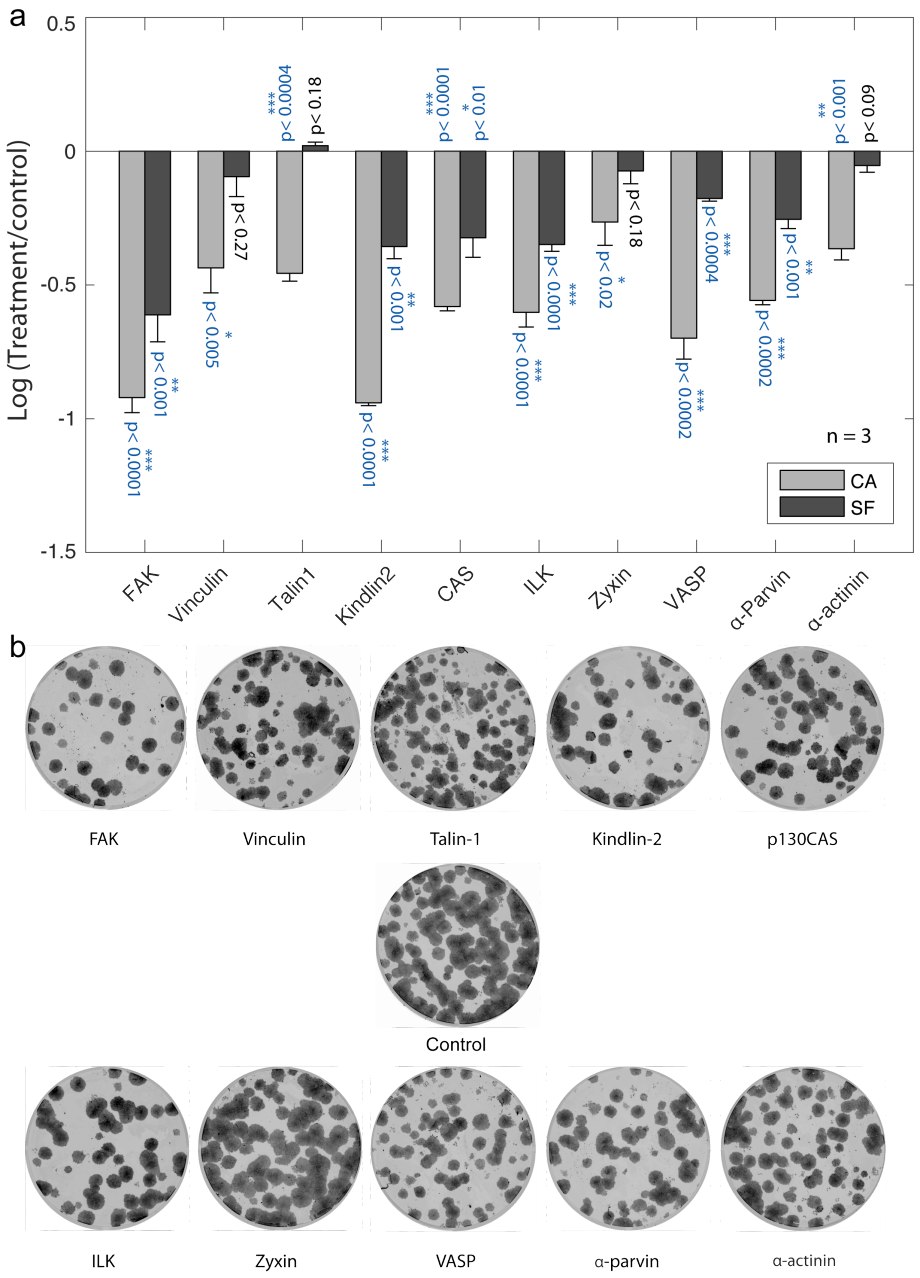


**Figure S6 Effect of individual knockdown of focal adhesion proteins on colony area and survival fraction.** (a) Bar plots comparing the KD effect of the 10 proteins on colony area (CA) and survival fraction (SF). The values were normalized to the control and represented in log scale. Values close to zero indicate KD effect similar to the control. All single KDs cause significant decline in colony area especially in case of FAK and kindlin-2. Survival fraction showed different trend from colony area with the significant decrease in some of the combinations (FAK, kindlin-2, CAS, ILK, VASP and α-parvin) and no significant change in others (talin-1, α-actinin and zyxin) as compared to control. Error bars represent standard error of mean (SEM). (b) Representative images from the clonogenic assay show the effects of single KDs and control sample. All the images are presented under same brightness and contrast settings.

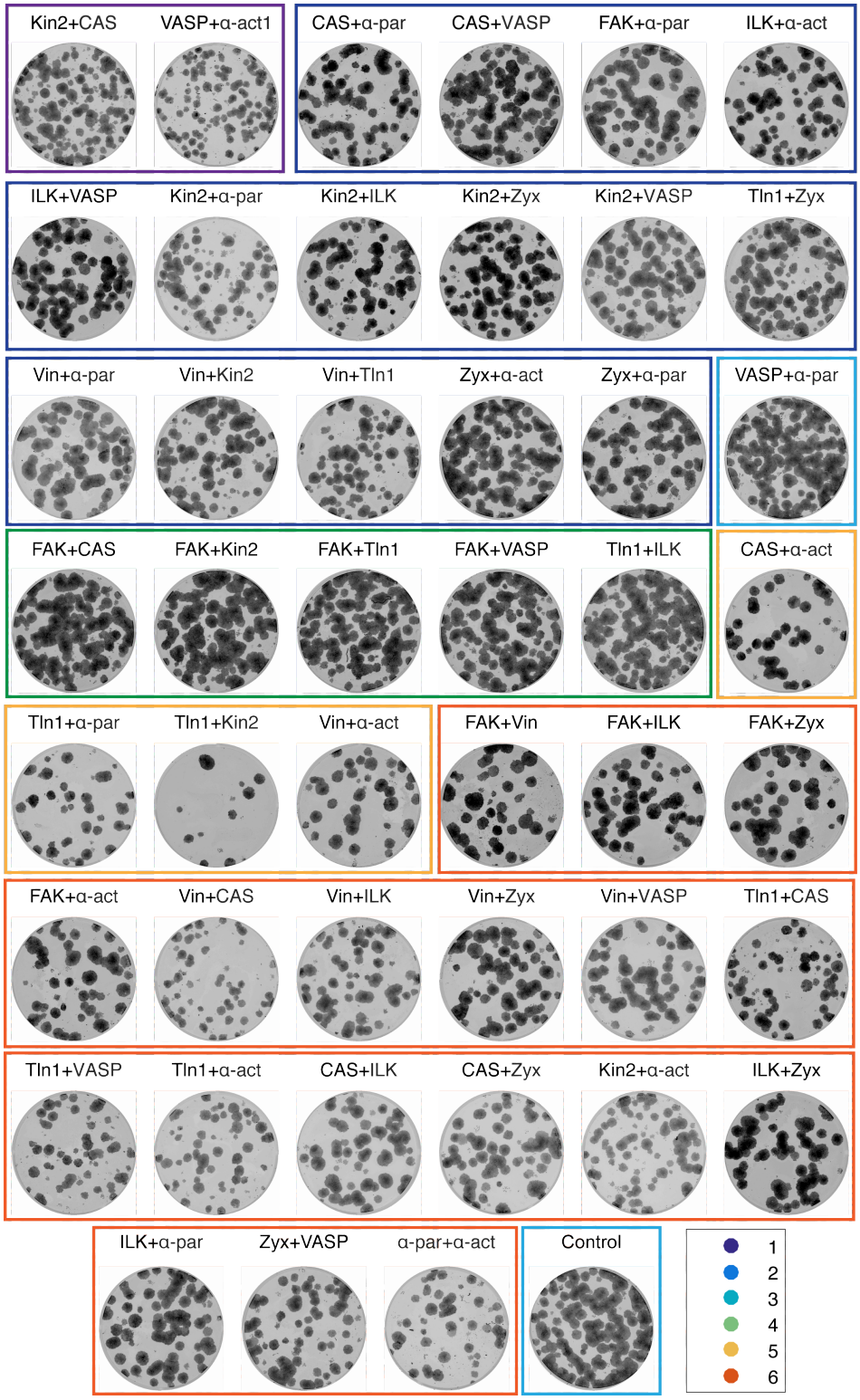


**Figure S7 Representative colony images of combined KD conditions from each cluster.** Representative images of the colony formation assay for 45 KD conditions identified in six different clusters. The boxes around the images are color coded according to the corresponding cluster color as shown in the legend. All the images are presented under same brightness and contrast settings.

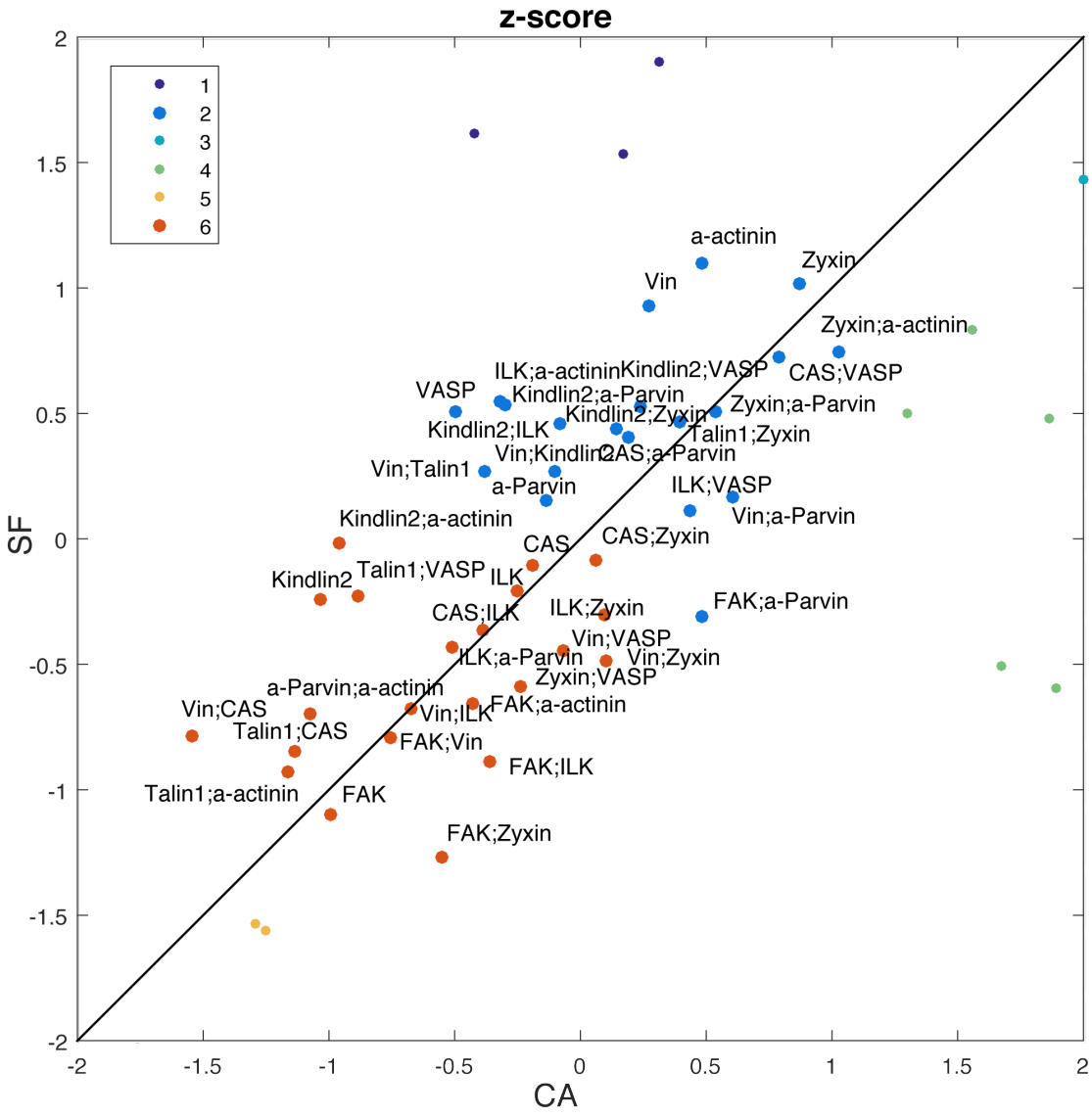


**Figure S8 Knockdown conditions belonging to survival and proliferation cluster 2 and 6.** The names of the proteins are mentioned for cluster 2 and 6. Z-score for CA and SF were computed for each condition including single and double knockdowns. The clustering unified the KD conditions into six groups symbolized with different colors.

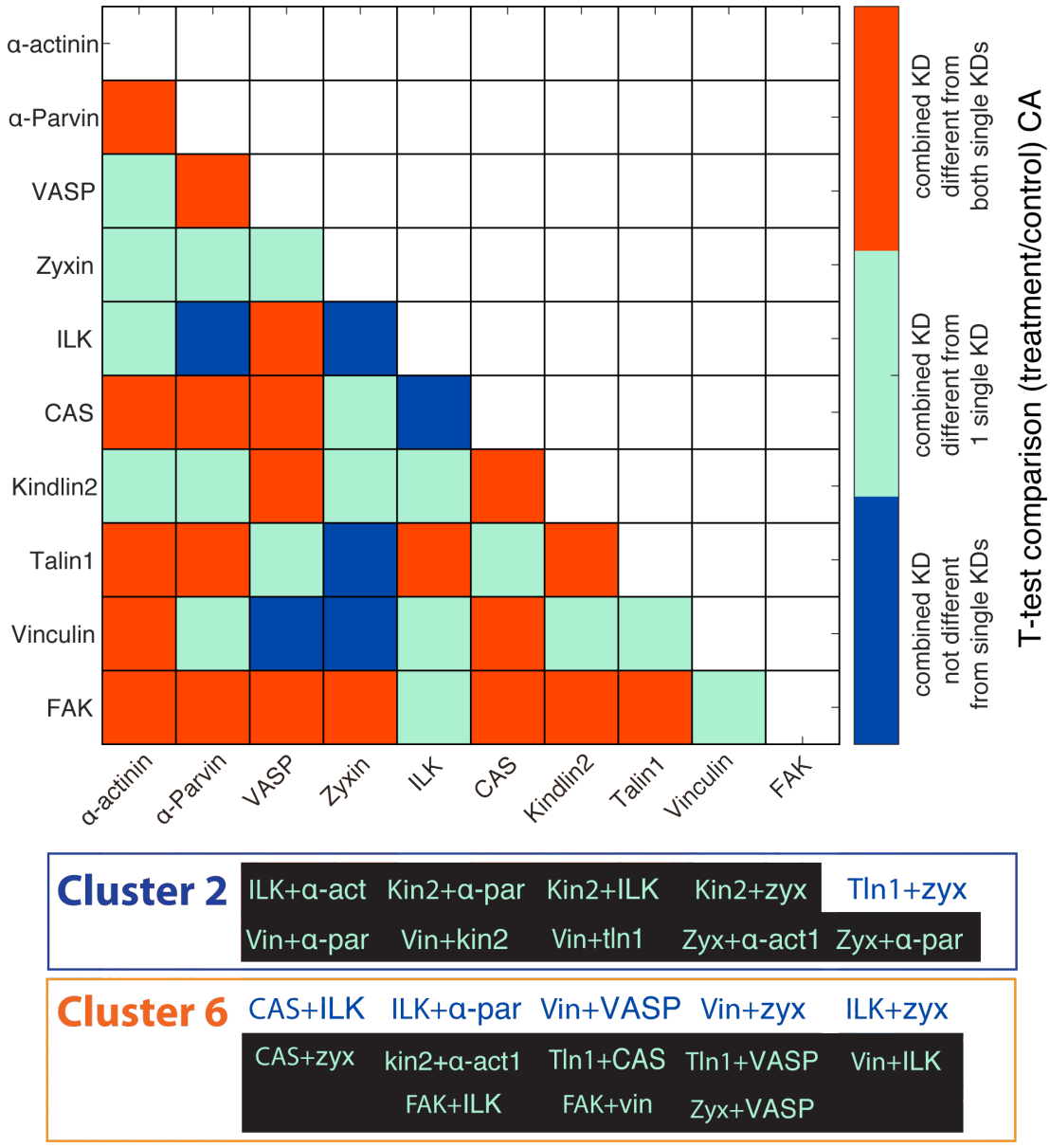


**Figure S9 Comparison of colony area for each combined KD with corresponding individual KD conditions.** The heatmap matrix summarizes t-test comparison for colony area that identified three different cases. In the first case combined KD not significantly different from individual KDs (6 combinations, represented as blue colored boxes). In the second case combined KD was significantly different from one of the single KDs (18 combinations, represented as green colored boxes). In the third case combined KD was significantly different from both single KDs (21 combinations, represented as red colored boxes). Highlighted KD pairs of cluster 2 and 6 (bottom) are those in which CA was similar to one of the contributing protein (cyan color) or both contributing proteins (blue color).

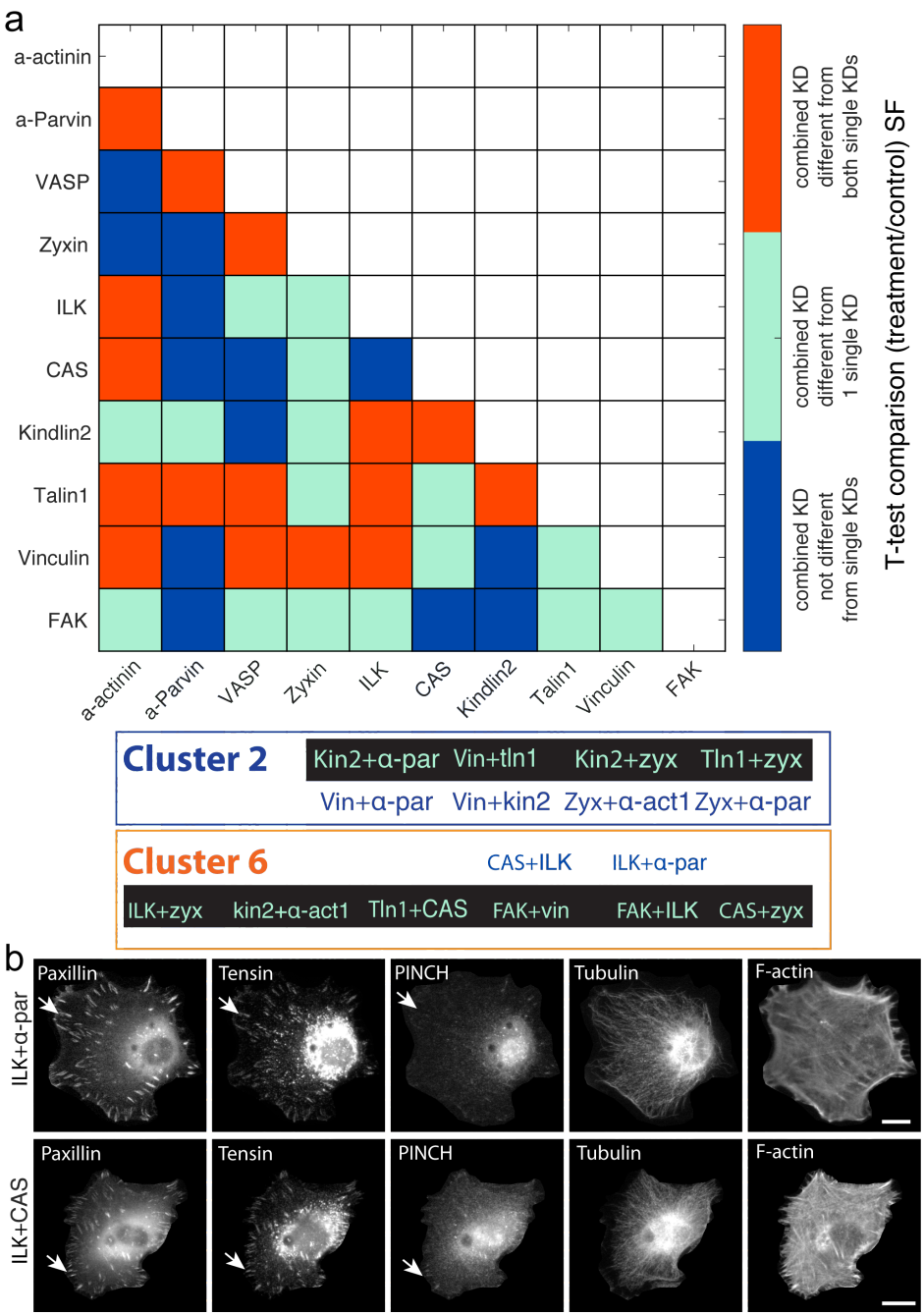


**Figure S10 Comparison of survival fraction for each combined KD with corresponding individual KD conditions and immunostaining images of ILK+α-par and ILK+CAS KD.** (a) The heatmap matrix summarized the outcome of the t-test comparison for survival fraction that identified three different cases. In the first case combined KD not significantly different from individual KDs (13 combinations, represented as blue colored boxes). In the second case combined KD was significantly different from one of the single KDs (16 combinations, represented as green colored boxes). In the third case combined KD was significantly different from both single KDs (16 combinations, represented as red colored boxes). Scale bar is 10 μm. Highlighted KD pairs of cluster 2 and 6 (bottom) are those in which CA was similar to one of the contributing protein (cyan color) or both contributing proteins (blue color). (b) Immunostaining of REF52 cells transfected with indicated KD conditions for indicated readout proteins. Scale bar is 10 μm.

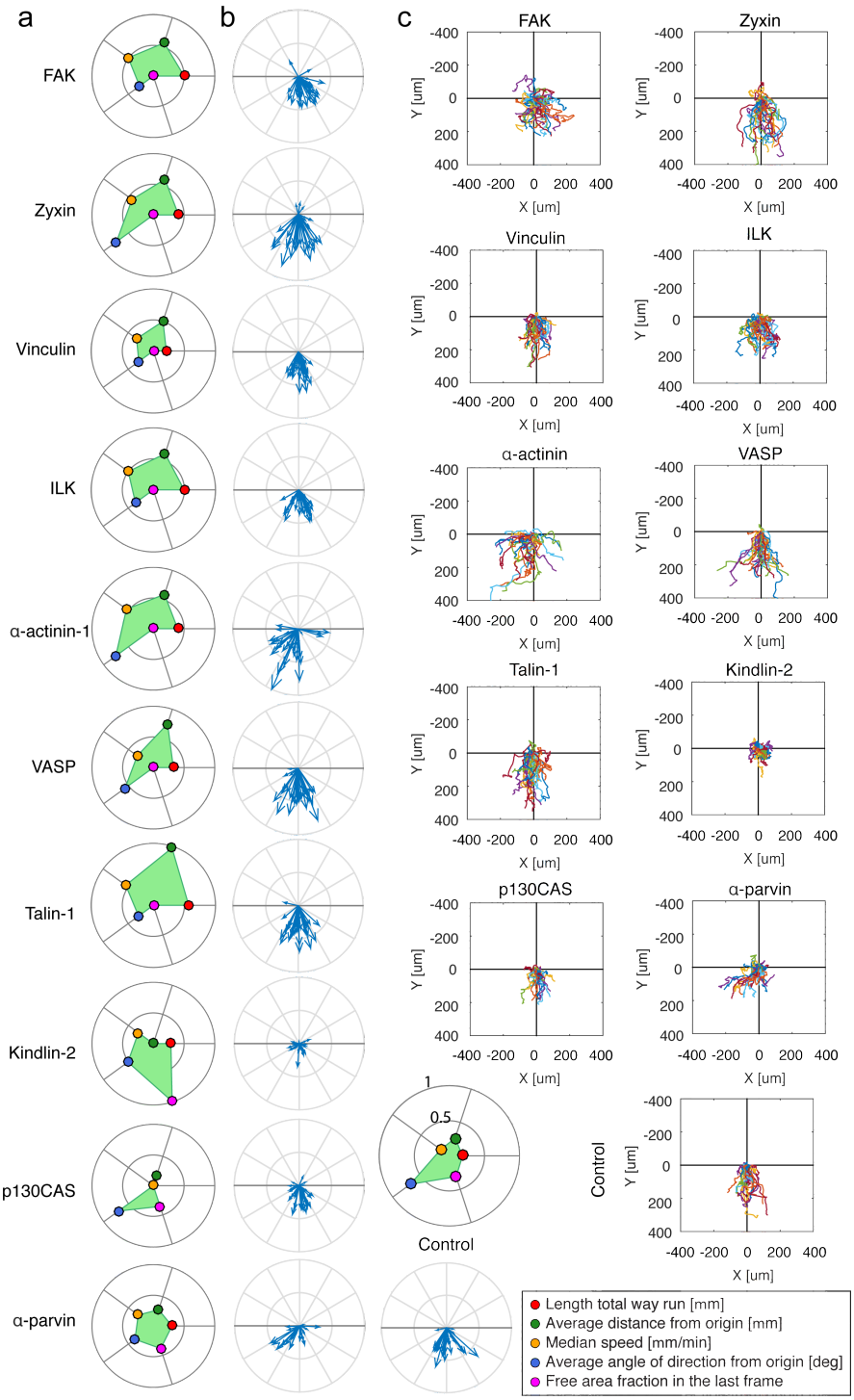


**Figure S11 Single siRNA perturbations regulate migration.** (a) Multiparameteric migration profiles for each single KD. (b) Compass plots indicated the angle of the migrating cells (randomly selected 30 cells for each condition). (c) Individual cell tracks were plotted to visualize the directionality and track of migrating cells (randomly selected 30 cells for each condition).

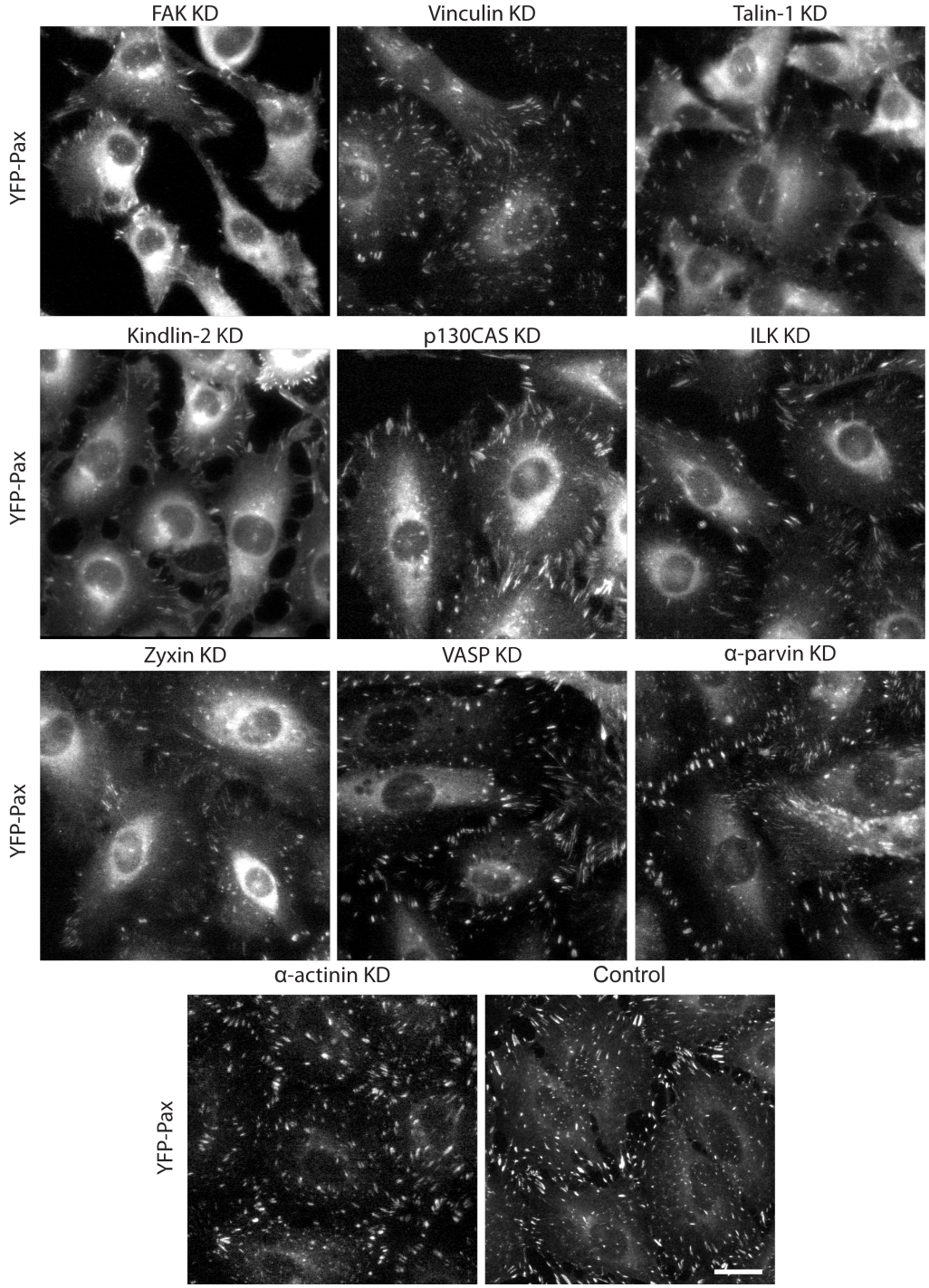


**Figure S12 Individually depleted FA proteins effect on FA formation.** REF52 cells were transfected with respective siRNA for each protein indicated in the figure. Cells were fixed and imaged for YFP-paxillin to evaluate the formation of focal adhesions. Scale bar is 10 μm.

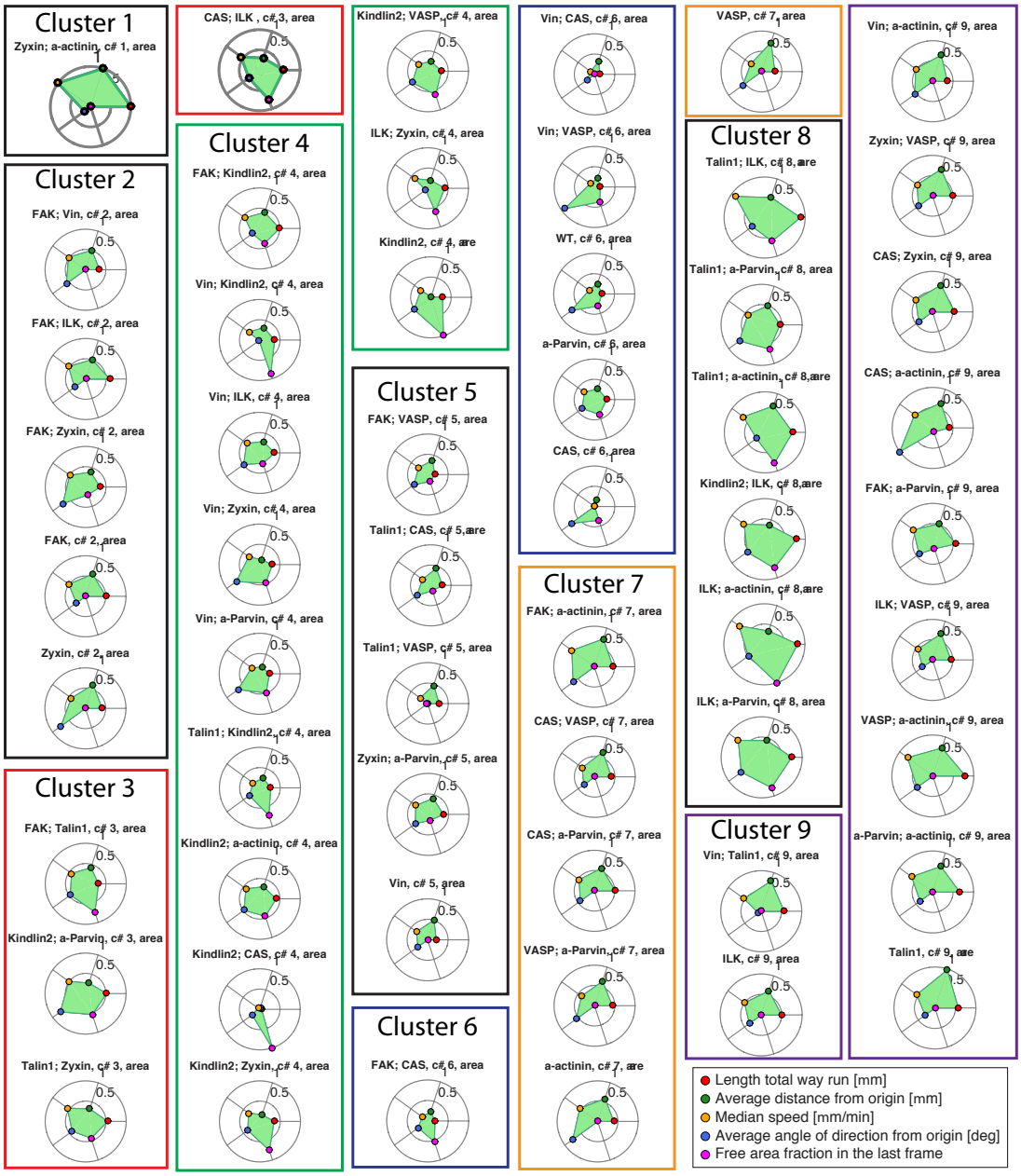


**Figure S13 Migration profiles of the KD conditions belonging to each cluster.** Multiparameteric migration profiles for 45 KD conditions in clusters 1-9. The colored outlines are used to distinguish the KD conditions corresponding to each cluster.

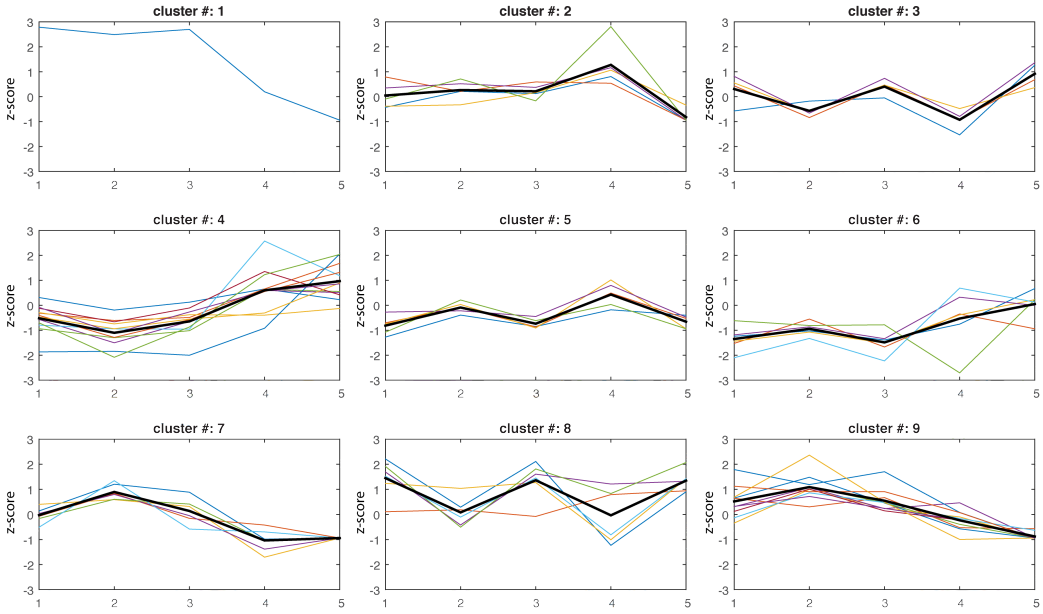


**Figure S14 Line profiles of the KD conditions in each cluster.** Line profiles of for each KD condition in clusters 1-9, based on the calculated z-scores. On x-axis are the multiple extracted parameters from time-lapse images. 1 – Total track length (mm), 2 – Average distance from origin (mm), 3 – Average speed (mm/min), 4 – Average angle of the direction from origin (deg) and 5 – Free area fraction in the last frame.

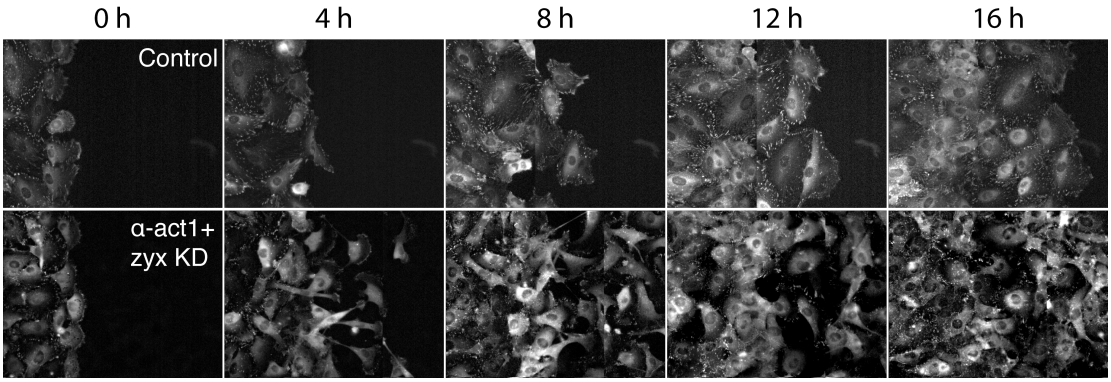


**Figure S15 Time-lapse images of REF52 cells transfected with α-act1+zyx and α-act1+FAK.** All fields were cropped at the same position from images collected at 0, 4, 8, 12 and 16 h after the initiation of live cell imaging. Cells were imaged with 20x objective.

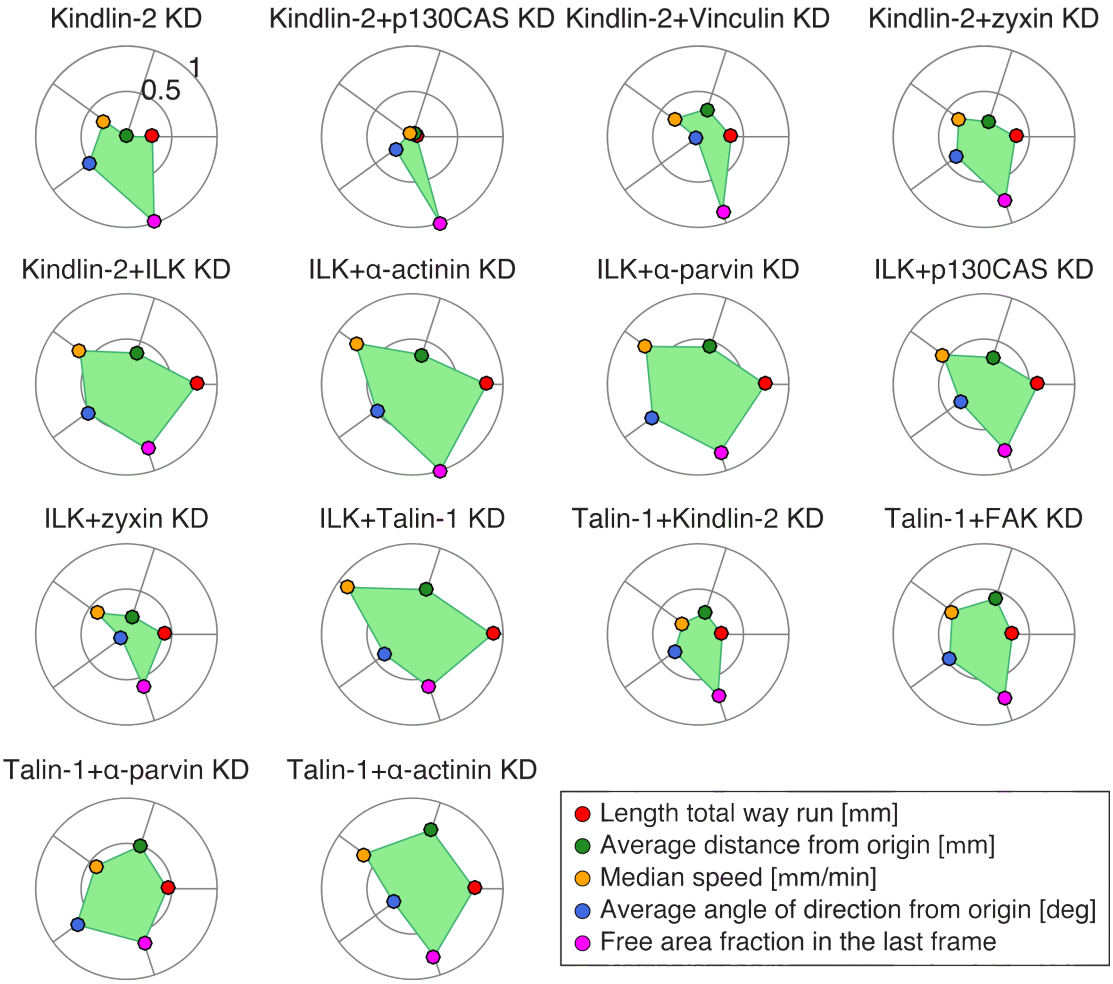


**Figure S16 Combinations that impaired cell migration.** Multiparameteric migration profiles of each KD condition that showed impaired migration indicated by the free area fraction (pink color circle).

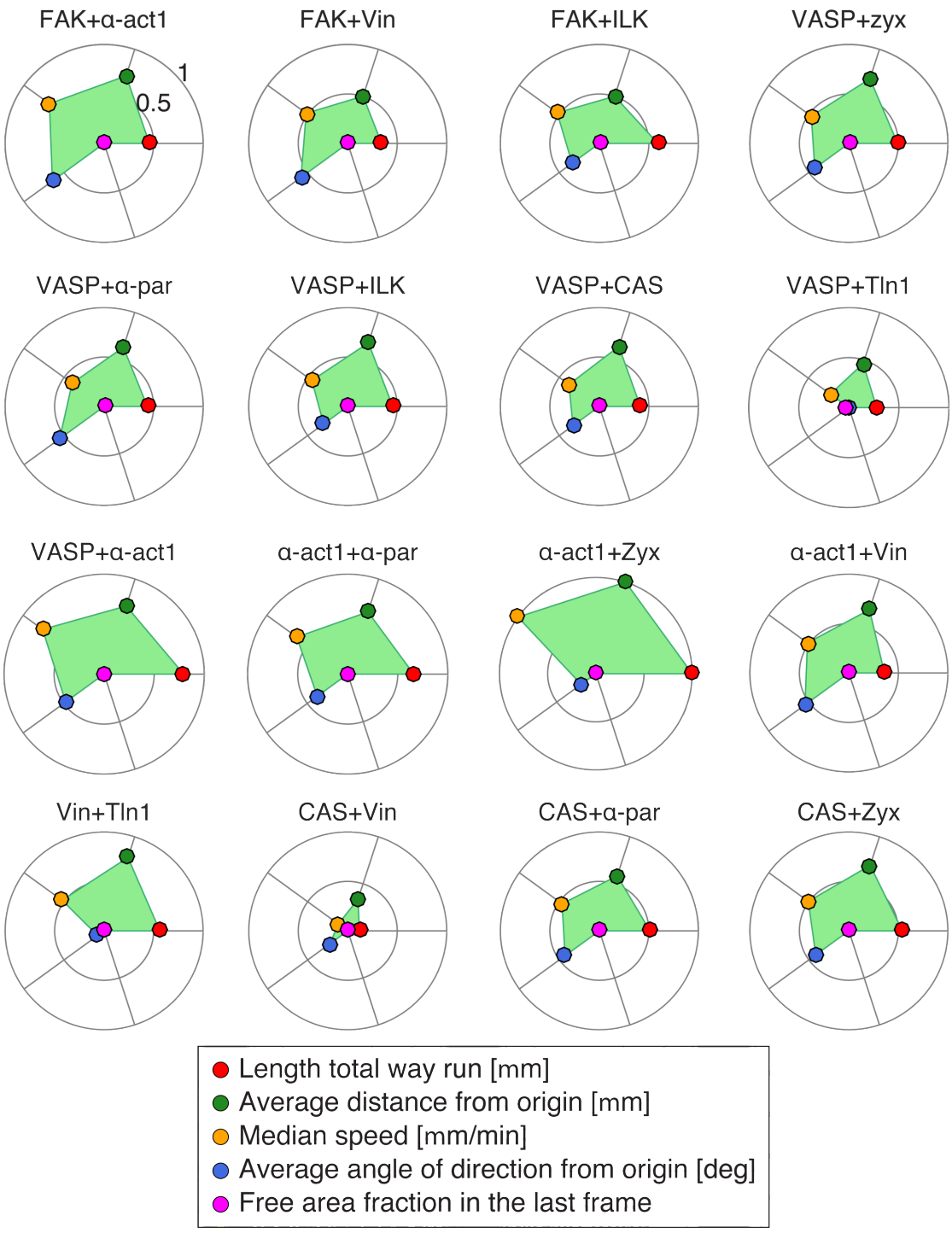


**Figure S17 Combinations that enhanced cell migration.** Multiparameteric migration profiles for each KD condition in that showed enhanced migration indicated by the free area fraction (pink color circle).

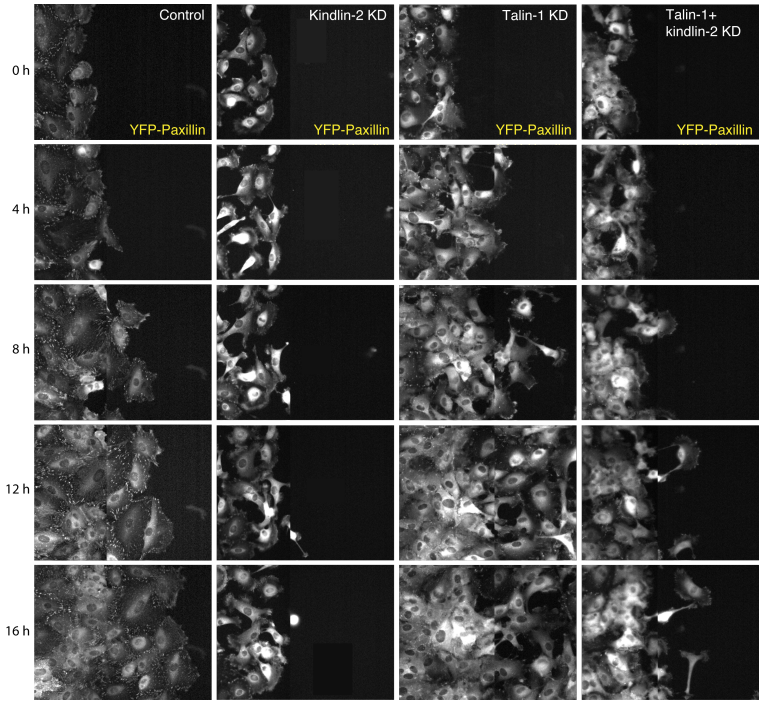


**Figure S18 Time-lapse images of REF52 cells transfected with tln1 and kin2.** REF52 cells were transfected with tln1, kin2 and combination of tln1 and kin2. The fields were cropped at the same position from time points 0, 4, 8, 12 and 16 h after the initiation of imaging. Cells were imaged with x20 objective.

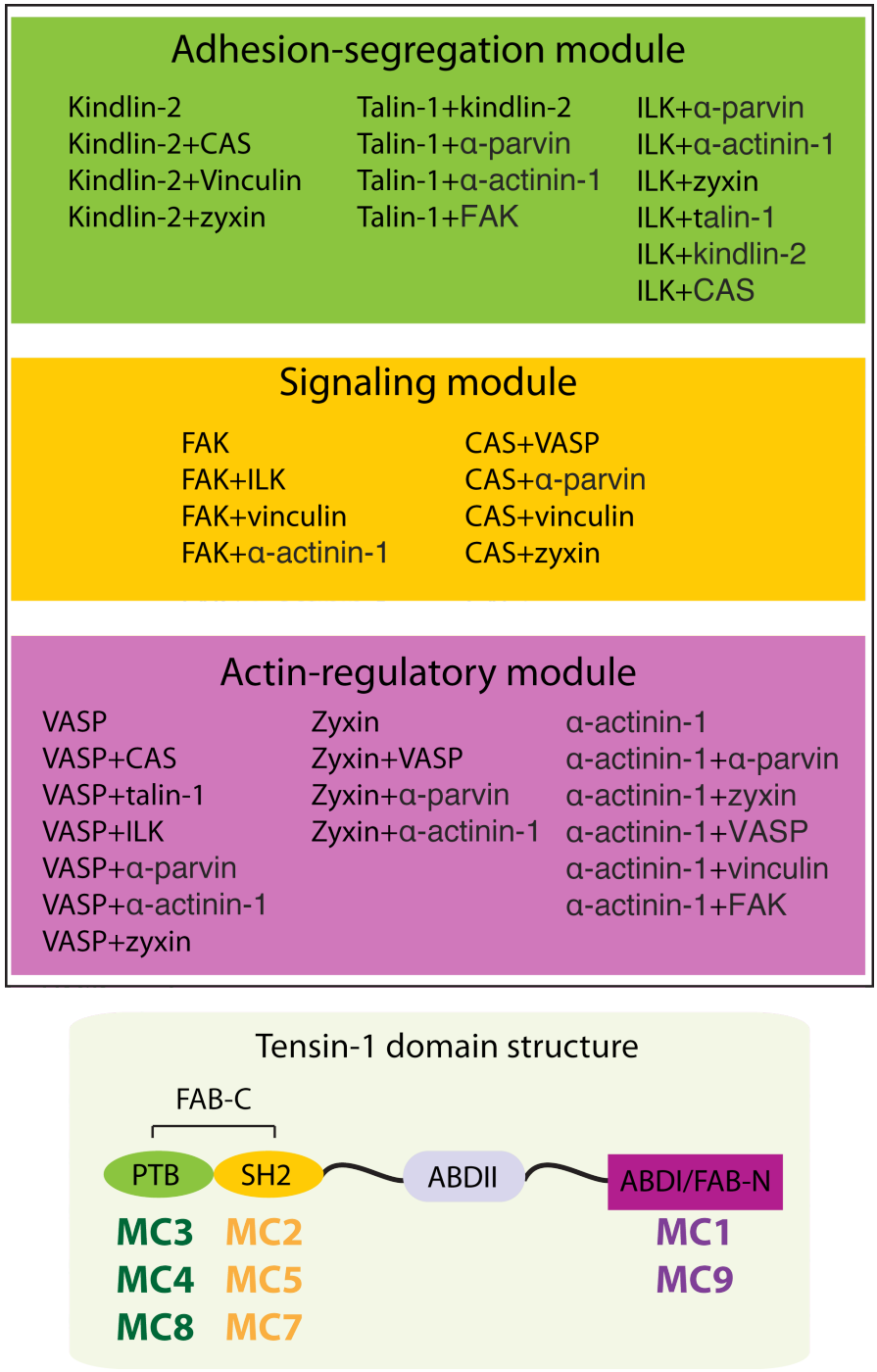


**Figure S19 KD conditions included in each functional modules.** Integrin-segregation module includes individual depletion of kin-2 and three common nodes ILK, kindlin-2, talin-1 (large green circles) that were depleted with designated proteins (small green circles), which led to the impaired migration and caused arrest of tensin-1 in FA. In signaling module two common nodes are CAS, FAK (big yellow circles) depleted with indicated proteins (small brown circles) caused mislocalization of tensin-1 and enhanced migration. In actin-regulatory module common nodes are α-actinin-1, zyxin, VASP (big purple circles) depleted with indicated proteins (small purple circles), which led to enhanced migration and tensin-1 dislocation.

# List of movies

**Movie 3.1 REF52 cells stably expressing YFP-paxillin and transfected with zyx+α-act1 siRNA. Images were collected every 20 min for 16 h, and the display rate is 7 frames/s. Scale bar is 10 µm.**

**Movie 3.2 REF52 control cells stably expressing YFP-paxillin. Images were collected every 20 min for 16 h, and the display rate is 7 frames/s. Scale bar is 10 µm.**

**Movie 3.3 REF52 cells stably expressing YFP-paxillin and transfected with FAK+vin siRNA. Images were collected every 20 min for 16 h, and the display rate is 7 frames/s. Scale bar is 10 µm.**

**Movie 3.4 REF52 cells stably expressing YFP-paxillin and transfected with FAK+tln1 siRNA. Images were collected every 20 min for 16 h, and the display rate is 7 frames/s. The movie shows confined mode of migration. Scale bar is 10 µm.**

**Movie 3.5 REF52 cells stably expressing YFP-paxillin and transfected with FAK+tln1 siRNA. Images were collected every 20 min for 16 h, and the display rate is 7 frames/s. The movie shows discontinuous mode of migration. Scale bar is 10 µm.**

**Movie 3.6 REF52 cells stably expressing YFP-paxillin and transfected with kin2+vin siRNA. Images were collected every 20 min for 16 h, and the display rate is 7 frames/s. Scale bar is 10 µm.**

**Movie 3.7 REF52 cells stably expressing YFP-paxillin and transfected with kin2+CAS siRNA. Images were collected every 20 min for 16 h, and the display rate is 7 frames/s. Scale bar is 10 µm.**

**Movie 3.8 REF52 cells stably expressing YFP-paxillin and transfected with FAK+VASP siRNA. Images were collected every 20 min for 16 h, and the display rate is 7 frames/s. Scale bar is 10 µm.**

**Movie 3.9 REF52 cells stably expressing YFP-paxillin and transfected with Vin+CAS siRNA. Images were collected every 20 min for 16 h, and the display rate is 7 frames/s. Scale bar is 10 µm.**

**Movie 3.10 REF52 cells stably expressing YFP-paxillin and transfected with VASP+CAS siRNA. Images were collected every 20 min for 16 h, and the display rate is 7 frames/s. Scale bar is 10 µm.**

**Movie 3.11 REF52 cells stably expressing YFP-paxillin and transfected with ILK+tln1 siRNA. Images were collected every 20 min for 16 h, and the display rate is 7 frames/s. The movie shows confined mode of migration. Scale bar is 10 µm.**

**Movie 3.12 REF52 cells stably expressing YFP-paxillin and transfected with ILK+tln1 siRNA. Images were collected every 20 min for 16 h, and the display rate is 7 frames/s. The movie shows sporadic mode of migration. Scale bar is 10 µm.**

**Movie 3.13 REF52 cells stably expressing YFP-paxillin and transfected with ILK+kin2 siRNA. Images were collected every 20 min for 16 h, and the display rate is 7 frames/s. The movie shows confined mode of migration. Scale bar is 10 µm.**

**Movie 3.14 REF52 cells stably expressing YFP-paxillin and transfected with ILK+kin2 siRNA. Images were collected every 20 min for 16 h, and the display rate is 7 frames/s. The movie shows undirected-sporadic mode of migration. Scale bar is 10 µm.**

**Movie 3.15 REF52 cells stably expressing YFP-paxillin and transfected with ILK+α-act1 siRNA. Images were collected every 20 min for 16 h, and the display rate is 7 frames/s. The movie shows confined mode of migration. Scale bar is 10 µm.**

**Movie 3.16 REF52 cells stably expressing YFP-paxillin and transfected with ILK+α-act1 siRNA. Images were collected every 20 min for 16 h, and the display rate is 7 frames/s. The movie shows sporadic mode of migration. Scale bar is 10 µm.**

**Movie 3.17 REF52 cells stably expressing YFP-paxillin and transfected with ILK+α-par siRNA. Images were collected every 20 min for 16 h, and the display rate is 7 frames/s. The movie shows confined mode of migration. Scale bar is 10 µm.**

**Movie 3.18 REF52 cells stably expressing YFP-paxillin and transfected with ILK+α-par siRNA. Images were collected every 20 min for 16 h, and the display rate is 7 frames/s. The movie shows sporadic mode of migration. Scale bar is 10 µm.**

**Movie 3.19 REF52 cells stably expressing YFP-paxillin and transfected with Tln1+vin siRNA. Images were collected every 20 min for 16 h, and the display rate is 7 frames/s. Scale bar is 10 µm.**

**Movie 3.20 REF52 cells stably expressing YFP-paxillin and transfected with tln1 siRNA. Images were collected every 20 min for 16 h, and the display rate is 7 frames/s. Scale bar is 10 µm.**

**Movie 3.21 REF52 cells stably expressing YFP-paxillin and transfected with kin2 siRNA. Images were collected every 20 min for 16 h, and the display rate is 7 frames/s. Scale bar is 10 µm.**

**Movie 3.22 REF52 cells stably expressing YFP-paxillin and transfected with tln1+kin2 siRNA. Images were collected every 20 min for 16 h, and the display rate is 7 frames/s. Scale bar is 10 µm.**

# List of figures

# List of tables

# List of abbreviations

| | |
|---|---|
| 2D culture | 2 dimensional culture |
| Arp2/3 | Seven protein subunit comples |
| AS | Adhesion sites |
| BCAR1 | p130 Crk-Associated Substrate |
| CAS | p130 Crk-Associated Substrate |
| Cdc42 | Cell division cycle 42 |
| CDKs | Cyclin-dependent kinases |
| $CO_2$ | Carbon dioxide |
| DMEM | Dulbecco's modified eagle's medium |
| ECM | Extra cellular matrix |
| EGTA | Ethylene glycol-bis(β-aminoethyl ether)-N,N,N',N'-tetraacetic acid |
| Em. | Emission |
| Ex. | Excitation |
| FA | Focal adhesions |
| FAK | Focal adhesion kinase |
| FAT | Focal-adhesion-targeting |
| FB | Fibrillar adhesions |
| FERMT2 | Kindlin-2 |
| FN | Fibronectin |
| GAPDH | Glycelaldehyde phosphate dehydrogenase |
| H | Hour |
| IgG | Immunoglobulin G |
| ILK | Integrin link kinase |
| KD | Knockdown |
| kDa | Kilo-dalton |
| kin2 | Kindlin-2 |
| LDHA | Lactate dehydrogenase A |
| MAR | Migration associated parameters |
| MAPK | Mitogen-activated protein kinase |
| MC | Migration cluster |
| Ml | Milliter |

| | |
|---|---|
| Min | minutes |
| NA | Nascent adhesions |
| $Na_2EDTA$ | Sodium Ethylenediaminetetraacetic acid |
| NaCl | Sodium chloride |
| PARVA | α-parvin |
| PI3K | Phosphoinositide 3-kinase |
| PTK2 | FAK |
| Rac1 | Ras-related C3 botulinum toxin strate 1 |
| REF52 | Rat embryonic fibroblasts |
| RIPA | Radioimmunoprecipitation assay buffer |
| ROCK | Rho-associated protein kinase |
| RT | Room temperature |
| SDS | Sodium dodecyl sulfate |
| TEMED | N,N,N,N- (Tetramethylethylendiamine) |
| tln1 | Talin-1 |
| TP | Time point |
| Tris-HCl | Tris hydrochloride |
| VASP | Enabled/Vasodilator Stimulated Phosphoprotein |
| Vin | Vinculin |
| YFP | Yellow fluorescent protein |
| Zyx | Zyxin |
| α-act1 | α-actinin1 |
| α-par | α-parvin |
| Ml | Microliter |
| Mm | Micrometer |

# Acknowledgement

I am indebted to many people, without them this dissertation would literally have not been accomplished. The research work presented in this thesis is greatly inspired by a gifted scholar Prof. Dr. Philippe Bastiaens. It is my great pleasure to express my humblest gratitude for his scientific guidance, constructive criticism and patience during the time of carrying out these studies.

I would also like to particularly thank PD Dr. Leif Dehmelt for valuable suggestions to shape my thesis and for accepting my request to be my second supervisor. My special thanks to Dr. Eli Zamir who introduced me to the research field of focal adhesions and for the supervision in initial years of my PhD studies. I am thankful to Dr. Astrid Krämer and Tanja Forck who has been always there to listen my problems and suggest the best solutions.

I would have not been able to excel through PhD without the scientific support and helpful discussion of my good friend Dr. Jana Harizanova. Jana without your keen observations, valuable suggestions and data analysis, this work would have not become to what it is now.

It would be unfair if the wonderful attitude of my lab fellows is not acknowledged. I would like to express my gratitude to Dr. Sven Müller to facilitate me in conducting the microscopy experiments. I am highly grateful to Dr. Aneta Koseska, Dr. Ola Sabet, Dr. Christian Klaus Schuermann and Dr. Illaria Visco for their benevolent attitude in the lab and for reading my thesis. I appreciate the assistance from technical staff of our department; especially Ms. Lisaweta Rossmannek and Mr. Michael Riechl for cell culture. I cherish all my memorable moments with my colleagues.

Finally, I would like to thank my family members: my mother Rukhsana Masood, my father Masood-ul-Haq, my brothers Dawood Masood, Yahya Masood and my sister Javaria Masood for their endless love and encouragement throughout my life. Last but not the least, I am obliged for tremendous patience of my husband Dr. Imtiaz Ali and daughters Ayesha & Haniah. Without their love and support, this work would have not been accomplished.

*Sarah Imtiaz*